Towards a standardized statistical correction between RANSe-based full-scale CFD and sea trial measurement

B.J.H. Vendeloo

Thesis Report

TU Delft Delft University of Technology

Ship Hydromechanics

Towards a standardized statistical correction between RANSe-based full-scale CFD and sea trial measurement

Thesis Report

B.J.H. Vendeloo

October 19, 2021

Faculty of Mechanical, Maritime and Materials Engineering (3mE) · Delft University of Technology


TU Delft
Delft
University of
Technology

Thesis for the degree of MSc in Marine Technology in the specialization of hydromechnis

Towards a standardized statistical correction between RANSe-based full-scale CFD and sea trial measurements

By

Bauke Johan Herman Vendeloo

Performed at

Damen Shipyards

This thesis MT.21.003.m. is classified as confidential in accordance with the general conditions for projects performed by the TUDelft.

27-10-2021

Company supervisors
Responsible supervisor: Antoine Reverberi

Daily Supervisor(s): Antoine Reverberi

Thesis exam committee
Chair/Responsible Professor: Tom van Terwisga
Staff Member: Cornell Thill
Staff Member: Andrea Coraddu
Company Member: Antoine Reverberi

Author Details
Studynumber: 4379365

Abstract

With the increase of computational power the usage of CFD grew as well. CFD can be used for various tasks in ship design, one of them is computing the resistance of a ship sailing through water. Together with the corresponding ship speed, the required power can be derived. It is the task of a ship designer to determine the required power as accurate as possible. All software that includes CFD must be validated before the results can be used. Usually, CFD is validated against extrapolated towing tank test results. Since the last decade, more research is conducted into the possibilities of full-scale CFD validated against sea trial data. Sea trial is the event where the ship is tested if it complies to the design requirements. The sea trial results can be affected by, amongst others, environmental conditions, such as wind, waves, current or shallow water, and methods have been developed to correct for them. Nevertheless, uncertainties arise when validating full-scale CFD results against sea trial data. The research to these uncertainties is presented in this report with the following main-research question: "How can the uncertainty of the statistical $C_{F,\,CFD}$ be quantified and reduced, and to what extent can it be used to predict the power-speed relationship?"

This research considers Amels LE and SX super yachts. Bare hull, appended hull, and actuator disk simulations were performed using CFD, and compared to sea trial results. The results of the CFD are unique because they were generated after the sea trials were conducted, resulting in the ship speed in CFD and sea trial being similar. The results were compared using $C_{F,\,CFD}$, the relative error between measured sea trial and CFD computed resistance. The uncertainty was defined as a function of accuracy of precision, represented by the mean μ and standard deviation σ of $C_{F,\,CFD}$. First, it was investigated if the uncertainty of $C_{F,\,CFD}$ could be reduced by including more physics in the simulations and what the impact of more variety in ship dimensions was. Subsequently, an investigation to the driving factors behind the uncertainty was conducted by performing a linear regression. After which it was investigated if the total uncertainty can be reduced by replacing experimental uncertainty by numerical uncertainty. Finally, a statistical correction to adjust the resistance was used to predict the power-speed relationship. Two correction factors were investigated. The first is based on the sample mean $\overline{X}$ of $C_{F,\,CFD}$, and the second is $C_{F,\,CFD}$ derived from a CDF.

It was seen that including more physics reduced the uncertainty of $C_{F,\,CFD}$. The uncertainty decreased whilst comparing bare hull to appended hull simulations, and it increased whilst comparing appended hull to actuator disk simulations. Thus, it was concluded that the actuator disk does not lead to a more realistic simulation of the flow. More variety in the ship dimensions lead to a larger uncertainty of $C_{F,\,CFD}$, which was expected. The variance was found to be caused by the ship speed, the mean wave height and mean wind speed, and also by the block coefficient if different ship types are considered. By computing the hull efficiency η_H numerically instead of experimentally, the total uncertainty of $C_{F,\,CFD}$ was reduced. The power-speed relationship can be predicted accurately, but not precise with $C_{F,\,CFD}$ based on $\overline{X}$. While the prediction with a $C_{F,\,CFD}$ derived from a CDF is not accurate and not precise.

It was concluded that the uncertainty of $C_{F,\,CFD}$ can be quantified by representing it as a function of μ and σ. It can be reduced by including more physics, and by replacing experimental uncertainty for numerical uncertainty. Finally, the power-speed relationship can be predicted accurately, but not precisely using $C_{F,\,CFD}$ based on $\overline{X}$.

Table of Contents

List of Figures

List of Tables

Acknowledgement

As many see writing a thesis as an individual process, I have not experienced it this way. I was given the opportunity to gather a group of experts around me who could give advice. First of all, I would like to thank Antoine Reverberi for being my daily supervisor from Damen Shipyards. The time you took to guide me through the process is well appreciated. Next, I want to thank Tom van Terwisga for not only being the chair of my graduation committee, but also for providing the opportunity to receive help from knowledgeable employees from Marin. The spar sessions on my graduation topic were beneficial, for which I thank Thomas Schulz and Thijs Hasselaar. Cornel Thill, also professor from the TU Delft, was involved since my midterm meeting. I would like to thank him for the time he took to give feedback on my work, and for the valuable suggestions. A special thanks also is given to Sebastian Sigmund, Scott Terry and Renske Marijnisse, other team members from the Hydromechanics team of Damen for participating in discussions about my results. At last but not least, I would like to thank Gert-Jan Vendeloo, who is my dad, for providing feedback on the readability of my report.

Chapter 1

Introduction

The research present in this report was performed at Damen. Damen is an international shipbuilding company based in the Netherlands. Damen builds a wide variety of vessels, but for almost all vessels it holds that they are standardized and can be build in series. This research was performed on the Amels LE and SX series. The LE series have a comparable shape but different size, and the same holds for the SX series. Compared to each other, they differ in shape and size. Because the vessels are constructed serial, the information available on all these individual vessels is comparable, making it valuable for research.

1-1 The reason of research

Almost every vessel needs a propulsion system driven by an engine. The power that can be delivered by the engine determines the speed that the vessel can sail. Usually, the design speed of the vessel is contractually defined. So, it is the task of a naval architect to design a vessel that meets this contract requirement. The power required to sail at that speed can be determined with power prediction methods, and for almost all methods it holds that the basis of the method is to determine the resistance of a vessel at that certain ship speed. With these two quantities known the required power can be determined. the resistance prediction methods can be divided into empirical, experimental, and numerical methods. Also, every method is in model-scale or full-scale. Every power prediction method has a level of uncertainty, which can be expressed in terms of accuracy and precision. The uncertainty of the power prediction methods also results in the usage of design margins.

At Damen, multiple prediction methods are used in different design phases. In early design phases the method developed by Holtrop and Mennen in 1982 [4], later revised by Holtrop in 1984 [5], is used. This is an empirical power prediction method which has as advantage that only basic hull geometry, propeller properties, and efficiencies must be known. Next, towing-tank testing of vessels in model scale is an example of an experimental power prediction method that can be used by Damen. Typically, they are used in later design phases when it is unlikely that the design of the vessel will change drastically. An advantage of this method is that not only the resistance of the vessel can be determined, but it can also give insights in other ship performances in a well controlled environment. A disadvantage is that the experimental results must be extrapolated to full-scale, which introduces the scaling problem. Finally, numerical methods are used at Damen as well. Damen uses RANSe-based Computational Fluid Dynamics (CFD) to determine the resistance of a vessel with which the

required power can be determined. Before the results of numerical methods can be used for purposes such as resistance determination of a vessel sailing in water, they must be verified and validated. At Damen this was done for simulations in full-scale and the results were validated against extrapolated towing tank results. The numerical power prediction methods can be used in all design phases, as long as the general shape of the vessel is known.

It is believed that the currently used power prediction methods introduce design margins that are too conservative. The design margins are caused by the uncertainty of the power prediction methods, thus the aim is to develop a power prediction method with a smaller uncertainty than the currently used power prediction methods. Therefore, the uncertainty of validating full-scale RANSe-based CFD against sea trial results were investigated.

1-2 Literature review

Research on the effects of scaling ship resistance accelerated the developments of full-scale CFD. Scale effects arise when model-scale testing results are extrapolated to full-scale. The total resistance of a ship can be decomposed into viscous resistance and wave resistance [6]. The viscous resistance is scale dependent and the wave making resistance is assumed to be independent of scale. However, several studies showed that this is an incorrect assumption. For example Raven et al. [7] conducted research on the effects of scaling in ship resistance and concluded that the wave resistance coefficient was 20% larger at full-scale than at model-scale. The directly computed total resistance was 10% larger than the extrapolated model-scale results. Although the correlation allowance compensates for this effect, it was suggested that a better understanding of the scaling could reduce it and its variability which results in an increase of the reliability of the prediction. The research by Terzieve et al. [8] in 2019 also proved the findings that the wave resistance is scale dependent. They performed bare hull simulations on three different scales and the Froude number was kept constant. Large changes in Reynolds number showed that the wave resistance is not scale independent.

Nowadays, the whole maritime industry is putting effort into the development of full-scale CFD. Already in 2011 Castro et al. [9] conducted research to full-scale CFD, where they performed both towed resistance and self-propulsion simulations and compared them with extrapolated model-scale results. It was concluded that they were in good agreement, the full-scale CFD towed resistance coefficient C_T was 5.1% larger compared to the extrapolated test results, and almost all self-propulsion factors were within the 2% of the experimentally computed values. It was concluded that these results showed the possibilities of full-scale CFD. Then in 2014 Ponkratov and Zegos [10] also performed full-scale CFD self-propulsion simulations, but compared their results with full-scale sea trial data to eliminate the effect of scaling. The environmental conditions that were encountered during the sea trial were simulated as well. It was concluded that the agreement of thrust and torque between CFD and sea trial measurements was very good. For K_Q the difference was less than 2%, and for K_T the difference was 2% for one of the gauges and 7% for the other. They also explained that it is very challenging to measure the propeller thrust which could be a reason for the larger error of one of the gauges. Ever since the work by Ponkratov and Zegos [10], more research was conducted into full-scale CFD self-propulsion simulations which was validated against sea trial results. For example by Jasak et al. [11], Mikkelsen et al. [12], [13] and Sun et al. [14] where the possibilities of full-scale CFD were proved but also that more research is needed to the uncertainty of sea trial results.

To accelerate the developments in this area of research Joint Industry Projects (JIP) were set up. One of them is the Lloyd's Register (LR) test case. Several parties participated by comparing their full-scale CFD results with sea trial data provided by LR. The proceedings were described by Ponkratov [15]. All participants received a 3D scan of the vessel that was made during docking and after cleaning of the hull. The scan was then used as a model for the CFD simulations. Participants used different methods to computed self-propulsion simulation, but it was concluded that all gave reasonable results for the speed and power. Another project is JoRes [16] where five main tasks can be distinguished. The first is to review current guidelines and recommendations regarding ship performance predictions. Second, full-scale measurements will be performed on the flow field around the ship, the speed and power, environmental influences, the vessel's condition and propeller cavitation. Third, model test will be performed where the conditions are identical as with the full-scale measurements. Fourth, a CFD workshop similar to the LR case is organized. At last, the findings will be discussed with ITTC.

Since the Virtual Towing Tank (VTT) project was completed in 2018, full-scale CFD is used at Damen for various topics including resistance simulations. The VTT was a project where CFD results were validated against extrapolated towing tank results. Currently, the first steps are taken in a new project: the Virtual Sea Trial (VST). In the VST the CFD results will be validated against sea trial measurement results. The first steps were taken by van Dijk during his master thesis [2]. A sea trial dataset of Amels LE super yachts was provided to him, and he performed RANSe-based CFD based on this dataset to have a better match on speed and displacement. The two main topics of this research were a grid sensitivity study and the derivation of a correction factor between the CFD method and sea trial results. The grid sensitivity study was performed for inviscid and viscid flow. The correction factor was derived statistically. Afterwards it was parameterized using a Lasso regression and it was concluded that the parameters it depends on are the trim, draught, speed and wetted surface.

When validating full-scale CFD results with sea trial measurement there are two types of uncertainty. The first is the computational uncertainty in the full-scale CFD power prediction method. According to Larsson et al. [1] the computational uncertainty is caused by modelling and numerical errors. The second is the experimental uncertainty in sea trial data.

1-3 Problem statement

Because it is assumed that the currently used design margins are too conservative, there is the desire to reduce them. The VTT project proved that full-scale RANSe-based CFD can predict the ship resistance already accurate and precise. In combination with the developments in the area of research to full-scale RANSe-based CFD this lead to the belief that that full-scale RANSe-based validated against sea trial data can predict the ship resistance even better. The differences between full-scale RANSe-based CFD and sea trial results are captured in the CFD correction factor $C_{F,CFD}$. In order to use this power prediction method correctly, the uncertainty of $C_{F,CFD}$ and its driving factors must be determined. The following main-research question will be answered to tackle the problem:

> How can the uncertainty of the statistical $C_{F,CFD}$ be quantified and to what extent can it be used to predict the power-speed relationship?

Because the main research question consists of multiple aspects which are more convenient to answer separately, it was divided into five sub-reserach questions:

1. What is the effect of including more physical effects in the simulations on the uncertainty of $C_{F,\,CFD}$?
2. What is the effect of increasing variety in ship dimensions on the uncertainty of $C_{F,\,CFD}$?
3. What are the driving factors behind the variance in $C_{F,\,CFD}$?
4. What is the impact of replacing experimental uncertainty by numerical uncertainty on the total uncertainty of $C_{F,\,CFD}$?
5. To what extent can a statistical $C_{F,\,CFD}$ be used to predict the power-speed relationship?

1-4 Research goals and scope

Two goals were set for this research. The first goal is to develop a better understanding of the uncertainty in the comparison between full-scale RANSe-based CFD and sea trial measurements. The aim is to quantify and discover the sources of the uncertainty. After this is achieved it is investigated how the magnitude can be reduced. The second goal is to develop a statistical correction factor between full-scale RANSe-based CFD and sea trial measurements and subsequently investigate how well it performs in terms of predicting the power-speed relationship.

The scope of this research is bounded by the provided databases. Two databases were provided, one contains sea trial measurement results the other contains the results of CFD simulations. In both databases several yacht types are present. The CFD database is built after sea trial such that the vessel speeds match with the speed encountered during trial.

1-5 Thesis outline

The research to the uncertainty in comparing full-scale CFD results with sea trial data is presented in this report. In chapter 2 required background knowledge to better understand the research and its approach is provided. In chapter 3 the approach to answer the main-research and sub-research questions is explained. Subsequently, in chapter 4 the results of quantifying and reducing the uncertainty are presented. Chapter 5 presents the outcome of the research to the driving factors behind the variance in $C_{F,\,CFD}$. Next, in chapter 6 the effect of replacing experimental uncertainty by numerical uncertainty on the total uncertainty of $C_{F,\,CFD}$ is presented. Then, in chapter 7 it is explained how the power prediction method performs. Seventh, in chapter 8 the final conclusions are presented. The report is finished with the recommendations, presented in chapter 9.

Chapter 2

Background

The required knowledge to understand the problem and its solution is explained in this chapter. First, the vessels that are considered are elucidated. Followed by the decomposition of the ship's resistance. Next, the procedure of sea trials and the used CFD method are explained. The fifth section describes the used databases in detail. In the sixth section the usage of non-dimensional numbers is explained. Afterwards, the scaling problem is explained. Which occurs when scaling the results of ship testing in model-scale to full-scale. Subsequently, the used definition of uncertainty is elaborated. Finally, the usage of margins was explained

2-1 Vessel descriptions

In this research, two types of Amels super yachts were considered. The first is the Amels Limited Edition series and the other is the Amels SeaXplorer series. Within the series the vessels differ in size but are of comparable shape. The Amels LE is a range of super yachts with custom interior. The design is a balance between full custom and semi-custom, which results in a reduced delivery time [17]. The Amels SeaXplorer is an expedition yacht that can be of a length up to 105 meters. It combines luxury and exploring possibilities [18]. A summary of the main design parameters can be found in table 2-1. Because there are some minor differences in measured main dimensions the averages are presented.

Table 2-1: Main Design Parameters

	LE180	LE199	LE212	LE242	LE272	SX65	SX75
Installed power [kW]	1050	1500	2000	2000	2350	1000	2000
Average ∇ [ton]	683.4	1060	1218.5	1591	2203	1478.5	2041
Average L_{wl} [m]	49.81	59.65	59.1	67.53	76.7	61.85	76.7
Average B_{wl} [m]	9	10.15	11.64	11.76	13.98	12.56	13.81
Average D_{wl} [m]	3.18	3.38	3.68	3.64	3.64	3.37	3.5

In figure 2-1 an impression of a LE series super yacht is presented, and in figure 2-2 an impression of a SX series super yacht is presented.

Figure 2-1: Impression of a LE series super yacht

Figure 2-2: Impression of a SX series super yacht

2-2 The resistance of a ship

Every vessel that sails through water is subject to resistance. The total resistance can be determined with equation 2-1, where c_T represent the frictional component and c_W the wave-making component of the resistance. The frictional resistance is due to the viscosity of the water. The sailing of the ship through water causes waves which contribute to the total resistance as wave-making resistance [6]. ρ is the water density in [kg/^{3}, S the surface area of the hull in [m^2, and v the ship speed in [m/s]

$$R_T = [(1+k)c_T + c_W] \cdot \frac{1}{2}\rho S v^2 \tag{2-1}$$

2-3 Sea trials

The main goal of sea trials is to determine the performance of the vessel in terms of ship speed and power, and propeller shaft speed with an accuracy of 2% for the shaft power and 0.1 *knots* for the ship speed. Publication of ISO15016:2015 [3] describes the standard guidelines for the assessment of speed and power performance during sea trial. It is written by the International Organization for Standardization (ISO) and the International Towing Tank Conference (ITTC). The sea trial have to take place in prescribed conditions for both the vessel and environmental conditions. This means that the hull and propeller surfaces must be smooth, because growth of fouling may lead to added resistance. The conditions for the environmental conditions are: no wind, no waves, no current and deep water of a temperature of 15 $°C$. These ideal environmental conditions are unlikely to comply with in reality, therefore, correction methods are developed. All parameters that are needed for the analysis of the performance of the vessel are listed in tables in appendix D. Table D-1 presents the parameters that need to be measured every trial run and table D-2 presents the parameters that need to be measured once at the trial location. With the draft readings, the length, beam and displacement can be determined.

2-4 CFD

At Damen CFD calculations are made with FINE/Marine software by Numeca. The Equipe Modélisation Numérique (EMN) developed the ISIS-CFD solver and it uses the incompressible unsteady Reynolds-Averaged Navier-Stokes equations (RANSe). The solver uses the finite volume method to spatially discretize the transport equations into a system of algebraic

equations which can be solved iteratively. The velocity field is obtained from the momentum equations and the pressure field from the mass conservation constraint converted to the pressure equation. For turbulent flows, additional transport equations are necessary for closure. [19]

2-4-1 Governing equations

The governing equations are split into the conservation equations: momentum and mass, and into turbulence equations which are necessary for closure.

Equations for momentum and mass conservation

The generalized form of Gauss' theorem is used for the mass, momentum and volume fraction conservation equations. In the equations V represent the control volume bounded by the closed surface S. $\vec{U}$ represents the velocity field and p the pressure field. τ_{ij} and g_i are components of the viscous stress tensor and the gravity vector respectively. I_j is reduced to only the j component which is unity. The volume fractions are represented by c_i and a distinction between fluid and non-fluid is made by assigning $c_i = 1$ or $c_i = 0$ and a mixture is assigned with $c_i = \frac{1}{2}$. The total density ρ and viscosity μ are defined as follows: $\rho = \sum_i c_i \rho_i$, $\mu = \sum_i c_i \mu_i$ and $1 = \sum_i c_i$.

$$\frac{\partial}{\partial t}\int_V \rho \mathrm{d}V + \int_S \rho(\vec{U} - \vec{U}_d)\cdot\vec{n}\mathrm{d}S = 0 \tag{2-2}$$

$$\frac{\partial}{\partial t}\int_V \rho U_i \mathrm{d}V + \int_S \rho U_i(\vec{U} - \vec{U}_d)\cdot\vec{n}\mathrm{d}S = \int_S (\tau_{ij} I_j - pI_i)\cdot\vec{n}\mathrm{d}S + \int_V \rho g_i \mathrm{d}V \tag{2-3}$$

$$\frac{\partial}{\partial t}\int_V c_i \mathrm{d}V + \int_S c_i(\vec{U} - \vec{U}_d)\cdot\vec{n}\mathrm{d}S = 0 \tag{2-4}$$

Turbulence equations

To close the RANS equations, the turbulent Reynolds stresses need to be determined. All the used models are based on the Boussinesq hypothesis in terms of the eddy viscosity.

$$\tau_{ij} = \tau_{t_{ij}} + \tau_{l_{ij}} \tag{2-5}$$

$$\tau_{l_{ij}} = 2\mu S_{ij} \tag{2-6}$$

$$\tau_{t_{ij}} = 2\mu_t S_{ij} - \frac{2}{3}\rho K \delta_{ij} \tag{2-7}$$

Actuator disk

Initially, the idea of an actuator disk as a model for a propeller was invented by W.J.M. Rankine (1865), A.G. Greenwood (1888) and R.E. Froude (1888), and was further developed afterwards. The idea is that a control volume can be used to determine the difference in flow velocity V and pressure P, with the actuator disk area A_{Disk} and radius R the thrust T and torque Q can be determined [20]. In the ISIS-CFD code by FINE/Marine three options can be used in order to determine the propeller characteristics: via body drag, open water data or a propeller code. Only the first two options are used and thus described.

When the option *body drag* is chosen, thrust T and torque Q are computed iteratively with the equations 2-8 and 2-9. In here f_{bx} and $f_b\theta$ are the axial and tangential body forces respectively, which in turn are computed with equations 2-10 and 2-11. Furthermore, all other parameters that are necessary can be found in appendix A. T and Q are solved iteratively, so an initial value must be provided, and the simulation continues until it converges to the solution where $T = \sum F_{ext} - F_{drag}$.

$$T = \rho L^2 U^2 \iiint_A f_{bx} \mathrm{d}A \qquad (2\text{-}8)$$

$$Q = \rho L^3 U^2 \iiint_A r f_{b\theta} \mathrm{d}A \qquad (2\text{-}9)$$

$$f_{bx} = A_x r^* \sqrt{1 - r^*} \qquad (2\text{-}10)$$

$$f_{b\theta} = A_\theta \frac{r^* \sqrt{1 - r^*}}{r^*(1 - r_h^{'} + r_h^{'}} \qquad (2\text{-}11)$$

When the option *open water data* is selected, the thrust T and torque Q will also be solved iteratively. In this case K_T, K_Q and J are provided externally by the open water propeller data. Again, the simulations are continued until the solution converges to $T = \sum F_{ext} - F_{drag}$.

2-5 Databases

Damen provided two databases for this research. The first is a database containing the results of sea trials. The second database contains the results of CFD computations of three different procedures: bare hull, appended hull and actuator disk. The CFD simulations were performed by Joris van Dijk during his thesis [2].

2-5-1 Sea trial database

At Damen an in-house developed sea trial analysis tool (TAT) is used to process and analyze the sea trial measurements. The resistance is derived from the measured speed, shaft speed and shaft power. Figure 2-3 [21] shows the process schematically. The used shaft efficiency η_S is equal to 0.99 and the used relative rotative efficiency η_R is equal to 1.0. The open water efficiency is read from the propeller curves. Finally, the hull efficiency is calculated with the thrust deduction factor and wake factor. Currently, the thrust deduction factor is assumed to be constant and equal to 0.11 and the wake factor can be determined with sea trial results. In chapter 6 a numerical estimate of η_H is presented and compared with the original η_H.

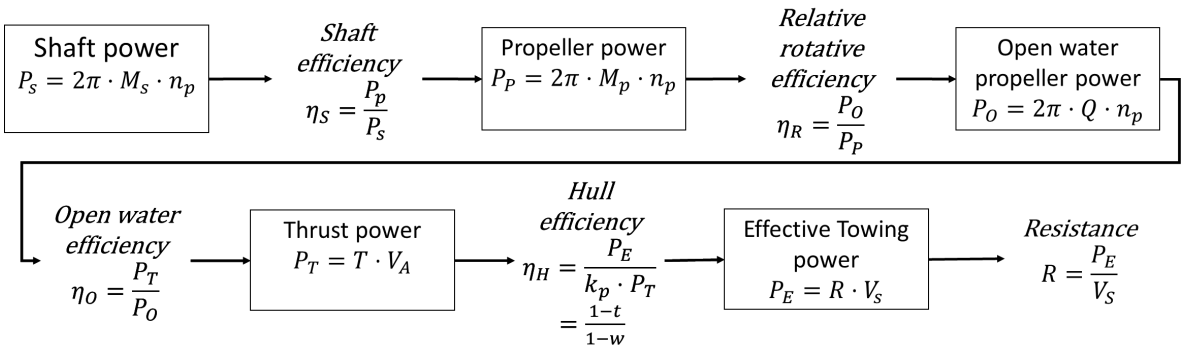

Figure 2-3: Deriving the power from the measured ship speed, shaft speed and power

In the trial analysis tool the correction methods for environmental conditions are implemented. The added resistance due to reflected waves is calculated with equation 2-12. Where R_{AWL} is the mean resistance increase in [N], ρ_s the water density in [kg/m^3], g the gravitational acceleration in [m/s^2], B the beam in [m], $H_{1/3}$ the significant wave height in [m] and L_{BWL} is the distance from the bow to 95% of the maximum beam at the waterline [3]. The following restrictions are set to allow that the waves do not induce motions: the $H_{1/3} \leq 2.25\sqrt{L_{PP}/100}$, the vertical acceleration at the bow may not exceed $0.05g$ and the wave direction is from ahead. At the moment the added resistance due to motion induced waves is not implemented [3].

$$R_{AWL} = \frac{1}{16}\rho_s g H_{1/3}^2 B\sqrt{\frac{B}{L_{BWL}}} \tag{2-12}$$

The added resistance due to wind is computed with equation 2-13. Where R_{AA} is the resistance increase due to relative wind in [N], A_{XV} is the projected area above the waterline in [m^2], C_{AA} the wind resistance coefficient, V_G the measured ship speed over ground in [m/s], V_{WRef} is the relative wind velocity at reference height in [m/s], ψ_{WRef} is the relative wind direction at reference height in [°] and ρ_A is the density of air in [kg/m^3] [3].

$$R_{AA} = \frac{1}{2}\rho_A \cdot C_{AA}(\psi_{WREF}) \cdot A_{XV} \cdot V_{WRef}^2 - \frac{1}{2}\rho_A \cdot C_{AA}(0) \cdot A_{XV} \cdot V_G^2 \tag{2-13}$$

The speed of vessels decreases when it sails through shallow water, equation 2-14 is used to compensate for this effect. Where ΔV is the decrease in speed due to shallow water in [m/s], V_s the ship speed through water in [m/s], h the water depth in [m], A_M the midship section area underwater in [m^2] and g the gravitational acceleration in [m/s^2] [3].

$$\frac{\Delta V}{V_S} = 0.1242\left(\frac{A_M}{h^2} - 0.05\right) + 1 - \left(tanh\frac{gh}{V_s^2}\right)^{1/2} \tag{2-14}$$

The current present at the sea trial location also causes a change in ship speed. The current speed is calculated with the 'mean of means' method [3]. In order to use this method, at least two double runs must be performed. It is assumed that the current varies parabolically over time and the ship speed trough water can be calculated with equation 2-15. Where V_S is the ship speed in [m/s], V_{G1}, V_{G2}, V_{G3} and V_{G4} are the measured ship speeds over ground during the first, second, third and fourth run respectively in [m] [3].

$$V_S = \frac{V_{G1} + 3V_{G2} + 3V_{G3} + V_{G4}}{8} \tag{2-15}$$

The sea trial database is created during the thesis research by J.M. van Dijk [2]. The parameters that are needed to analyze the sea trial results are shown as column names. During sea trial, four engine speeds are tested, which results in four different ship speed measurements per vessel. In the sea trial database there are 14 different LE180 yachts, 3 different LE199 yachts, 3 different LE212 yachts, 3 different LE242 yachts, 1 LE272 yacht, 1 SX66 yacht and 1 SX75 yacht. Every vessel itself has a unique yard number.

2-5-2 CFD Database

The used CFD database contains the numerical prediction of the considered vessels and was created during the research by J.M. van Dijk [2]. The CFD simulations were run on approximately similar ship speeds that were encountered during sea trials. The CAD models of the ships were simplified thus features as annodes, cooling fins, welds and other hull imperfections are not included. Yaw, roll, sway and surge motions are fixed because the simulations were performed for half a ship. The domain was set on $10L \times 3L \times 3L$ (X × Y × Z), where L is the ship length in [m]. Artificial damping was applied to the rear field. The free surface and the kelvin wake were refined. Damen uses the Numeca Fine/Marine solver for CFD simulations, it is optimized for maritime applications. The incompressible unsteady RANSe are solved with the finite volume method, and multiphase flows and moving grids can be dealt with. The choice was made to use the $k - \omega$ turbulence model because no complicated flows were expected.

In the thesis by J.M. van Dijk [2] three types of simulations were run: bare hull, appended hull and actuator disk. In bare hull simulations the hull is modeled without any appendages. Also, no propulsion force is applied, so it is the towed resistance that is computed. In appended hull simulations appendages such as the rudder and other smaller details are modeled, which results in a more realistic simulation. Again, the towed resistance is computed. The actuator disk simulation is an appended hull simulation, and an actuator disk is added such that the propulsion force can be determined. The bare hull simulations are the less costly, actuator disk simulations are the most expensive and appended hull falls in between. In all simulations the roughness of the hull is excluded.

2-6 Non-dimensional numbers

There are two important non-dimensional numbers in the analysis of the performance of ships. The first is the Froude number F_n and the second is the Reynolds number R_e. The Froude number represents the relationship between inertial forces and gravitational forces. It is also used to represent the ship's velocity non-dimensional. It is a function of the ship speed v, the gravitational constant g and the ship's length L as shown in the equation below.

$$F_n = \frac{v}{\sqrt{gL}} \tag{2-16}$$

The Reynolds number is used to determine if a flow is turbulent or laminar. High values represent a turbulent flow and low numbers a laminar flow. The Reynolds number is a function of the ship's speed v, length L, and the kinematic viscosity of the water ν. This is shown in equation 2-17

$$R_e = \frac{vL}{\nu} \tag{2-17}$$

2-7 Scaling problem

When extrapolating a model-scale ship to full-scale three similarities must be achieved. First, geometrical similarity ensures that the ratio of the geometry of the full-scale ship to model-scale ship is constant with λ. The length, areas and volume scale as follows: $L_s = \lambda \cdot L_m$, $A_s = \lambda^2 \cdot A_m$ and $V_s = \lambda^3 \cdot V_m$. Second, kinematic similarity involves time thus it ensures

that the ratio of full-scale to model-scale time is constant: $t_s = \tau \cdot t_s$. Third, dynamical similarity holds that the ratio of acting forces is constant, which are hydrodynamic or inertial forces κ, gravitation forces κ_g and friction forces κ_f. To achieve dynamic similarity the scaling constants of the hydrodynamic and the gravitation forces, and the hydrodynamic and the friction forces must be equal. The Froude number F_n and Reynolds number R_n are dimensionless numbers representing the ratio of inertial and gravitational forces, and inertial and frictional forces respectively. To achieve dynamic similarity on all forces is practically impossible, because to achieve F_n similarity the model-scale ship speed must be smaller than in full-scale while for R_n it holds that the model-scale ship speed must be larger than in full-scale with a constant kinematic viscosity. Therefore, model-scale testing is usually performed on Fn similarity, resulting in a R_n that differs by two orders of magnitude compared to full-scale. [22]

2-8 Uncertainty

The data in both provided database is subject to uncertainty. The CFD based resistance is subject to computational uncertainty which is present in all numerical methods. The trial bases resistance is subject to experimental uncertainty because the data is gathered by means of measurements during sea trials. Uncertainty can be seen as a combination of accuracy and precision. Bureau International des Poids et Measured (BIPM) provided a definition for these three terms [23]:

> Accuracy is the closeness of agreements between a measured quantity value and a true quantity value of a measurand. [23, p. 37]
>
> Precision is the closeness of agreement between indications or measured quantity values obtained by replicate measurements on the same or similar objects under specified conditions. [23, p. 38]
>
> Uncertainty is a non-negative parameter characterizing the dispersion of the quantity values being attributed to a measurand, based on the information used. [23, p. 41]

2-8-1 Uncertainty in CFD database

In the book Principles of Naval Architecture by Larsson et al. [1] an explanation is given of the different errors that can be distinguished in computational methods, this is schematically presented in figure 2-4. Within the computational errors, they made a distinction between modelling and numerical errors. These two categories are even further divided into sub-categories.

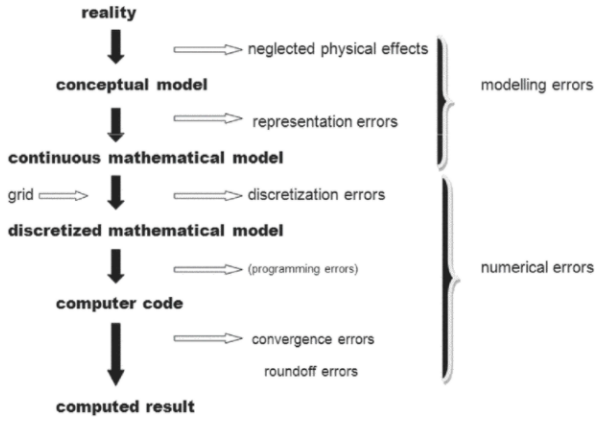

Figure 2-4: Computational errors as proposed by Larsson et al. [1]

Usually, a numerical model is a simplification of reality, which introduces modelling errors. First, some physical effects are neglected because they are unimportant or it is impossible to model them. This step results in the development of the conceptual model. Secondly, the conceptual model is further developed into a mathematical model. Often this mathematical model consists of a set of differential or integral equations, in order to solve these, approximations such as linearizations are introduced. The errors due to this are called representation errors.

The numerical errors consist of discretization errors, convergence errors and round-off errors. The discretization errors arise because the continuous numerical equations need to be discretized. Examples of discretizations are using differences for derivatives or sums for integrals. Next, The convergence error, or iterative error, follow from the numerical method that is used to solve the model. Most methods use an iterative solution strategy, where the difference between two consecutive iterations becomes smaller and smaller until it reaches the convergence criterion after which the process is terminated, and thus the solution is reached. But, this criterion is not zero and therefore a convergence error is present. Finally, the round off error is present because a computer internally stores values up to a certain number of decimals.

A grid refinement study was performed and a mesh uncertainty of 1.43% was determined. The convergence error was computed as follows. For computational reasons the simulations were started at a ship speed of 0 [m/s] and raised to the desired ship speed. The resistance showed an overshoot and slowly converged afterwards, which is shown in figure B-1 in Appendix B. The resistance was computed as a mean over the last 250 time steps where the standard deviation was less than 1% [2]. The round-off error is of the order 10^{-14}.

2-8-2 Uncertainty in sea trial database

The uncertainty in the sea trial dataset is experimental uncertainty. The data is either measured or computed based on measured input data. As explained in section 2-3 during sea trials the ship and propeller shaft speed, and the propeller shaft power are measured. The accuracy of the shaft measurements is 2% and the accuracy of the ship speed is 0.1 $[kts]$.

2-9 Design margins

In general, margins are added to a solution to cope with uncertainty. Eckert and Isakson [24] defined two types of margins. Safety margins to deal with known risks and design margins to deal with uncertainty in the design parameters. However, it was concluded that the two are often used interchangeably and sometimes even used both.

At Damen, the mentioned safety factor are called correction factors and design margins are used to cope with uncertainty. It is assumed that the Holtrop-Mennen predicted resistance curve is an underestimate of the actual resistance curve because a model is not a perfect representation of reality. This underestimation is dealt with by reducing the speed associated with a predicted resistance curve by a certain percentage. In other words, it implies that the actual resistance is higher than the predicted resistance at a given speed. Also, a margin on the speed results in the margin being multiplied by a factor of three for the installed power. Because the power is a function of speed to the power three.

Chapter 3

Methodology

In this chapter all the applied methods to answer the research questions are discussed. First, the treatment of ship resistance is explained. In the second section the definition of the uncertainty of $C_{F,CFD}$ is explained. Section 3-3 elaborates on the data processing that was required. After which the used statistics are explained. Subsequently, the method to determine the driving factors behind the uncertainty of $C_{F,CFD}$ is explained, which was a multivariate linear regression. In the sixth section it is explained how the uncertainty can be reduced by replacing experimental uncertainty by numerical uncertainty. Finally, the derivation of power from resistance is presented.

3-1 Non-dimensional resistance

The resistance of a ship determines in combination with the desired ship speed what the required power is to sail at that speed. In subsection 2-5-1 it was explained how the resistance can be derived from sea trial measurements, and how it can be predicted with CFD. Comparing the sea trial and CFD resistance is more convenient when it is non-dimensionalized, which is done with equation 3-1. In here C_T represents the non-dimensional resistance coefficient, R the resistance, ρ the water density, v the ship speed and A_{ws} the area of the underwater surface of the ship.

$$C_T = \frac{R}{\frac{1}{2}\rho v^2 A_{ws}} \tag{3-1}$$

There are also actuator disk simulations present, with similar resistance as appended hull. Therefore, the thrust based on sea trial measurements and actuator disk simulations is compared. The thrust is non-dimensionalized similar to the procedure as for the resistance, in equation 3-1 the resistance R is replaced by thrust T.

3-1-1 Townsin roughness

Roughness is not directly considered in the CFD simulations, but there are methods to add roughness indirectly. According to the 1978 ITTC performance prediction method [25] the roughness can be included as an allowance factor presented in equation 3-2. Where k_s is the average hull roughness and in this report a value of 1.5×10^{-4} [m] is used, L_{WL} is the length of the waterline in [m] and Re is the Reynolds number.

$$\Delta C_F = 0.044 \left[\left(\frac{k_s}{L_{WL}} \right) - 10 \cdot Re^{-\frac{1}{3}} \right] + 0.000125 \tag{3-2}$$

The Townsin resistance coefficient ΔC_F is added to C_T. But, because it is an added resistance it cannot be added to the thrust coefficient which was used in the analysis of the actuator disk performance. The resistance coefficient C_T with including roughness is expresses as follows:

$$C_{T_{CFD,\,Townsin}} = C_{T_{CFD}} + \Delta C_F \tag{3-3}$$

3-1-2 The CFD correction factor $C_{F,\,CFD}$

The gap between CFD and sea trial results is defined as the CFD correction factor $C_{F,\,CFD}$. The gap is caused by modelling aspects such as the minimal difference in ship speed between sea trial and CFD, roughness of the hull, propeller and appendages, the simplified propeller model, the absence of the environmental conditions and other physics that are not captured with the CFD simulations. So, $C_{F,\,CFD}$ is the difference between the resistance derived during sea trial and the resistance calculated with CFD. In the case of the actuator disk simulations the resistance is replaced by the propeller thrust. $C_{F,\,CFD}$ is mathematically represented by equation 3-4. Where $C_{T_{Trial}}$ is the non-dimensional sea trial resistance and $C_{T_{CFD}}$ the non-dimensional CFD resistance. When Townsin roughness is included it transforms to equation 3-5.

$$C_{F,\,CFD} = \frac{C_{T_{Trial}} - C_{T_{CFD}}}{C_{T_{CFD}}} \tag{3-4}$$

$$C_{F,\,CFD_{Townsin}} = \frac{C_{T_{trial}} - C_{T_{CFD,Townsin}}}{C_{T_{CFD,Townsin}}} \tag{3-5}$$

3-2 Uncertainty of $C_{F,\,CFD}$

In section 2-8 it was explained that the CFD database is subject to computational uncertainty and the sea trial dataset to experimental uncertainty. This leads to the uncertainty of $C_{F,\,CFD}$ being a combination of both. In order to quantify the uncertainty of $C_{F,\,CFD}$ the description by the BIPM presented in section 2-8 was used. In this case the measurand is the $C_{F,\,CFD}$ and the accuracy is represented by the mean μ and the precision by the standard deviation σ. Equation 3-6 and 3-7 are the mathematical representations of μ and σ, where n represent the population size.

$$\mu = \frac{1}{n} \left(\sum_{i=1}^{n} x_i \right) \tag{3-6}$$

$$\sigma = \sqrt{\frac{1}{n} \sum_{i=1}^{n} (x_i - \mu)^2} \tag{3-7}$$

Figure 3-1 [26] illustrates how μ and σ can represent the accuracy and precision respectively. As described in section 3-1-2 $C_{F,\,CFD}$ is a relative error, which means that the accuracy increases as its mean value gets closer to zero and the precision improves as the standard deviation closer to zero.

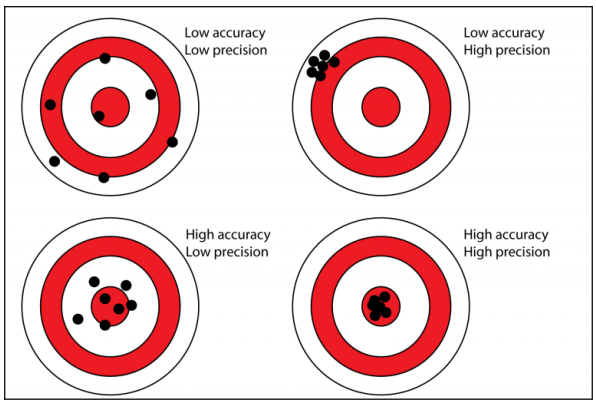

Figure 3-1: Accuracy and precision

Because the uncertainty in $C_{F,CFD}$ is a function of μ and σ it can be represented as a confidence interval according to Vrijdag [27] and such a 95% confidence interval is presented below. Logically, the smaller the interval, the smaller the uncertainty of the parameter of interest.

$$[\mu_{C_{CFD}} - 2\sigma_{C_{CFD}},\ \mu_{C_{CFD}} + 2\sigma_{C_{CFD}}]$$

To represent the uncertainty of a curve or function a confidence band is used. A Cumulative Density Function (CDF) was used to represent $C_{F,CFD}$ statistically. Around the CDF a confidence band with various levels of uncertainty can be plotted. The method to compute the uncertainty band is explained in section 3-4-2.

3-3 Data processing

As described in section 2-5 two databases were provided containing CFD and sea trial measurement results respectively. These two databases were aggregated to one database. The whole method of processing the data can be described in six steps which are listed below.

1. Data collection; raw data was collected in the form of the sea trial and CFD database provided by Damen. The data within these databases is collected by van Dijk [2] as described in section 2-5.

2. Data preparation; the raw data must be prepared before it could be processed. First, data rows needed to be removed because it consisted of NaN values only. Second, variables needed to be added. Third, some variables needed to be converted. Fourth, the CFD data had to be sorted. Finally, the sea trial and CFD databases had to be aggregated.

3. Data input; the aggregated sea trial and CFD dataset.

4. Data processing; the data is statistically treated. The mean and standard deviation of the $C_{F,CFD}$ were used to determine the accuracy and precision of the CFD method and to generate a normal distribution. Also, a regression is performed to investigate which parameters are of influence on $C_{F,CFD}$. These steps are explained in more detail in sections 3-4 and 3-5

5. Data output; in the form of graphs and tables.
6. Data storage; as CSV files.

3-3-1 Data preparation

The CFD database contains rows that have NaN values for the speed. These values are not useful in the data processing. Therefore, the rows that contain such values are deleted. The column *Fx* represents the exerted force on the hull in x-direction and is equal to the resistance of the ship. However, the value of the force is stored negative and was converted to positive. The Reynolds number and block coefficient are not included in the CFD database. Thus, these are computed and added to the database. Next, the ship type is extracted from the *processedhulls* column and added as a new column. As described in section 2-5-2 three types of simulations are present in the database. The CFD database is split into a bare hull, appended hull, and actuator disk database. Next it is further split into ship type: LE180, LE199, LE212, LE242, LE272 and SX. In the sea trial database the speed is only given in knots, but for the analysis the unit of speed is [m/s]. So, a new column is added with speed given in [m/s].

The CFD and sea trial database had to be aggregated to facilitate the data processing. The yard number was the leading parameter in the aggregation: vessels with equal yard number are paired, because these are the same vessel. A maximum difference between ship speed of sea trial and CFD of 0.05 [m/s] was used as a second restriction to reduce uncertainty. Three aggregated databases were created: bare hull with trial, appended hull with trial and actuator disk with trial. All three databases are similar and the parameters of interest are presented as column names.

3-4 Statistical data treatment

The statistical treatment of $C_{F,\,CFD}$ consists of three parts. First, μ and σ were determined in order to investigate the uncertainty of $C_{F,\,CFD}$ as described in section 3-2. Second, an investigation to the distribution of the $C_{F,\,CFD}$ was performed to determine if it was normally distributed. A more detailed explanation is provided in section 3-4-1. At last, a CDF is generated based on the μ and σ of $C_{F,\,CFD}$. The CDF will be used as a predictor for $C_{F,\,CFD}$ with a certain level of risk. Around the CDF a confidence band is plotted such that uncertainty is taken into account. The confidence band was build with a bootstrap method. The whole method is further elaborated in section 3-4-2.

3-4-1 Pre-investigation on distribution of $C_{F,\,CFD}$

A distribution can be assumed for any random variable and an investigation to the distribution of $C_{F,\,CFD}$ was performed. The distribution function or cumulative density function (CDF) F is defined by F: $\mathbb{R} \rightarrow [0, 1]$ which is mathematically represented by equation 3-8. It describes the chance that variable X takes a value larger than a. [28]

$$F(a) = P(X \leq a) \text{ for } -\infty < a < \infty \tag{3-8}$$

Random variable X is considered continuous if f: $\mathbb{R} \rightarrow \mathbb{R}$ for a and b with $a \leq b$, described by equation 3-9, where f represents the probability density function (PDF) of X and has to satisfy $f(x) \geq 0$ for all x and $\int_{-\infty}^{\infty} f(x)\mathrm{d}x = 1$ [28].

$$P(a \leq X \leq b) = \int_b^a f(x)\mathrm{d}x \tag{3-9}$$

Both the CDF F and PDF f contain all the probabilistic information of a real random variable X. The relation between them follows from integral calculus [28]:

$$F(b) = \int_{-\infty}^{b} f(x)\mathrm{d}x \text{ and } f(x) = \frac{\mathrm{d}}{\mathrm{d}x}F(x)$$

A well-known PDF is the normal distribution, which is mathematically represented by equation 3-10 with parameters μ and $\sigma^2 \geq 0$. The distribution is denoted by $\mathrm{N}(\mu, \sigma^2)$. As explained the CDF can be determined by integrating the PDF, resulting in equation 3-11. Both equations hold for $-\infty \leq x \leq \infty$. Because any normal distribution $N(\mu, \sigma^2)$ can be transformed to $N(0, 1)$ the PDF transforms to equation 3-12 and the CDF to equation 3-13 [28]. The graphs corresponding to equations 3-12 and 3-13 are presented in figures 3-2 and 3-3.

$$f(x) = \frac{1}{\sigma\sqrt{2\pi}} e^{-\frac{1}{2}\left(\frac{x-\mu}{\sigma}\right)^2} \tag{3-10}$$

$$F(a) = \int_{-\infty}^{a} \frac{1}{\sigma\sqrt{2\pi}} e^{-\frac{1}{2}\left(\frac{x-\mu}{\sigma}\right)^2} \mathrm{d}x \tag{3-11}$$

$$\phi(x) = \frac{1}{\sqrt{2\pi}} e^{-\frac{1}{2}x^2} \tag{3-12}$$

$$\Phi(a) = \frac{1}{\sqrt{2\pi}} \int_{-\infty}^{a} e^{-\frac{1}{2}x^2} \mathrm{d}x \tag{3-13}$$

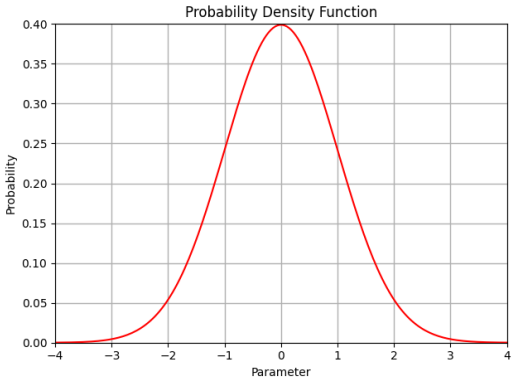

Figure 3-2: A PDF with $\mu = 0$ and $\sigma = 1$

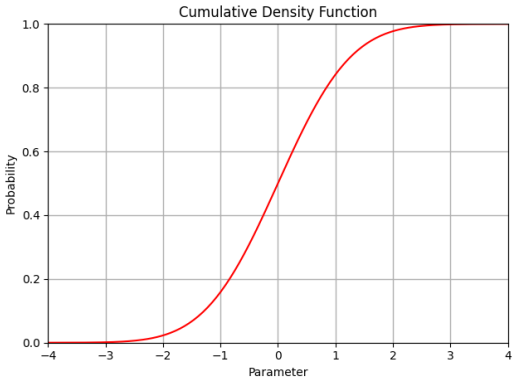

Figure 3-3: A CDF with $\mu = 0$ and $\sigma = 1$

A Gaussian KDE plot is used to inspect if the data is normally distributed. It forms a PDF based on the input. The Gaussian KDE plot is compared to a theoretical normal PDF based on μ and σ of that dataset. Subsequently, histogram plots were used to explain deviations the Gaussian KDE plot has from the theoretical PDF. The number of bins m in the histogram was determined with Sturges' Rule [29] presented in equation 3-14 where n is the number of data points. Although it was already presented in 1926, Sturges' Rule is still being used today. The probability distribution function PDF corresponding to the sample mean and standard deviation is plotted next to the histogram.

$$m = 1 + 3.22 \log_{10}(n) \tag{3-14}$$

3-4-2 Statistical prediction method for $C_{F,\,CFD}$

A CDF was developed as a statistical prediction method for $C_{F,\,CFD}$, and the CDF is mathematically represented by 3-11. Around the CDF a 95% confidence band was plotted to represent the uncertainty of the CDF. The confidence band was created with a bootstrapping method.

The CDF can be used to derive $C_{F,\,CFD}$ for new build yachts. The probability that $C_{F,\,CFD}$ has a specific value can be read from the graph. With the confidence band, a lower and upper bound for that specific value can be read as well. $C_{F,\,CFD}$ is derived at a probability of 95%. Which means that for 95% of the cases the $C_{F,\,CFD}$ is sufficient. Or in other words, a risk of 5% is taken.

Bootstrapping is a random resampling with replacement procedure to create a bootstrap dataset. A number of samples n will be drawn from the original population with replacement. Thus, the size of the bootstrap dataset is not bounded by the size of the original dataset. There are two types of bootstrap methods. First, a non-parametric bootstrap where the samples are directly drawn from the population to create a bootstrap sample for random variable X. Second, a parametric bootstrap where the samples are drawn from a distribution that describes the random variable X. Bootstrap databases were used to form the lower and upper bound of the 95% confidence band around the PDF. An example of a non-parametric and parametric CDF with 95% confidence band are shown in figures 3-4 and 3-5.

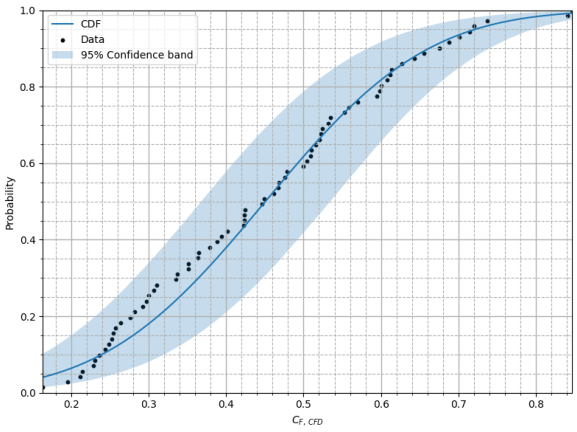

Figure 3-4: Parametric CDF with bootstrap confidence band

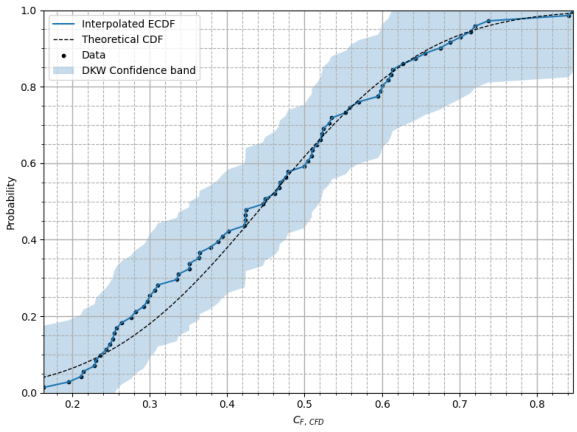

Figure 3-5: Non-parametric CDF with bootstrap confidence band

A number of 10000 bootstrap databases were generated. Every dataset is sorted and added to a larger database. In this database the columns represent every single bootstrap dataset and the rows represent the percentiles. The sample mean and standard deviation are determined for every percentile, and the 2.5^{th} and 97.5^{th} are used as lower and upper bound of the 95% confidence band.

The samples of the non-parametric bootstrap were directly drawn from the data itself; thus the sample size is equal to the population size. The samples of the parametric bootstrap were drawn from a normal distribution based on the population mean and standard deviation. An

equally spaced array with a length of 250 was created to draw from:

$$[\textit{begin};\ \textit{end};\ \#\ \textit{of steps}]$$
$$[\mu - 4 \cdot \sigma;\ \mu + 4 \cdot \sigma;\ 250]$$

3-5 Regression on $C_{F,\,CFD}$

Regression is used to discover the sources of the uncertainty. Regression techniques can be used to understand the relationship between independent and dependent variables and also to predict future outcomes. There are various different regression methods, such as linear, polynomial and quantile.

Linear regression distinguishes between simple and multivariate linear regression. Simple linear regression shows the relation between a continuous response variables y and one predictor variable x, which is mathematically represented by equation 3-15. Multivariate linear regression shows the linear relation between a continuous response variables y and multiple predictor variables x_n, with n the number of variables. This is represented by equation 3-16. A polynomial regression is comparable with linear regression, it can also be simple and multivariate, but it can deal with higher order relations. In equation 3-17 the multivariate polynomial regression is shown. [30]

$$y = \beta_0 + \beta_1 x X + \epsilon \tag{3-15}$$
$$y = \beta_0 + \beta_1 x_1 + \beta_2 x_2 + ... + \beta_n x_n + \epsilon \tag{3-16}$$
$$y = \beta_0 + \beta_1 x_1 + \beta_2 x_2 + \beta_1 x_1^2 + \beta_2 x_2^2 + \beta_1 \beta_2 x_1 x_2 + \epsilon \tag{3-17}$$

In this research multivariate linear regression is applied on response variable $C_{F,\,CFD}$, but not all available variables were included into the regression. There are several methods available to determine the predictor variables, such as shrinkage methods or subset selections. In this research first a list of expected predictor variables x_n was established where two types were distinguished: design and environmental condition parameters. Subsequently, the independence, or collinearity, of the predictor variables was investigated. It is important that the predictor variables are not collinear to obtain proper results in a multivariate regression. A pair plot can be used to visualize if there is any collinearity between two predictor variables. Predictor variable a is shown on the x-axis and predictor variable b on the y-axis, collinearity can be discovered in this way. The strength of the collinearity was determined with Pearson's correlation coefficient, see equation 3-18.

$$\rho_{a,b} = cor(a,b) \equiv \frac{cov(a,b)}{\sigma_a \sigma_b} \tag{3-18}$$

In here σ_a and σ_b represent the standard deviation of the variables a and b and $cov(a,b)$ represents the covariance [31]. The sign of $\rho_{a,b}$ defines the direction of the trend and the strength of the correlation is divided into three categories:

1. Weak: $|\rho_{a,b}| \leq 0.3$
2. Moderate: $0.3 \leq |\rho_{a,b}| \leq 0.7$

3. Strong: $0.7 < |\rho_{a,b}| \leq 1.0$

The dependent variables x_n are normalized by a max/min normalization before the multivariate regression is performed. A max/min normalization ensures that the range of all input variables lies between 0 and 1, resulting in that the absolute value of the regression coefficient also lies between this range. The sign, indicates the direction of the relationship. Equation 3-19 mathematically presents the used normalization. Where $\overline{x}$ represents the entire vector of the predictor variable, x_i the original value, and $x_i^{'}$ the normalized value.

$$x_i^{'} = \frac{x_i - min(\overline{x})}{max(\overline{x}) - min(\overline{x})} \tag{3-19}$$

Besides the regression is evaluated on the magnitudes and directions of the correlation coefficient, the statistical significance of the predictor variables is assessed. Which is done by evaluating the P-value. The P-value tests the null-hypothesis that the independent variable has no correlation with the dependent variable. When change in the independent variable does not result in change in the dependent variable, there is no correlation. The P-value of an independent variable must be below the significance level to reject the null-hypothesis. In general, a significance level of 0.05 is used. So, the P-values must be below 0.05 to be significant.

3-6 Estimate of numerical hull efficiency

The hull efficiency η_H is a function of the thrust deduction factor t and wake factor w. Mathematically, t is the relative difference between the required thrust T and the resistance R, and w is the relative difference between the ship speed v_s and advance velocity v_a. ηH in place, is a ratio between them. This is mathematically represented by equations 3-20, 3-21 and 3-22. Physically, t compensates for the added resistance due to suction of the propeller, and w compensates for the effect of the ship being in the way of the propeller. Usually, the used hull efficiency in analysis of ship performance is not determined numerically. It is either computed with sea trial results, based on sister ships or extrapolated from model test results. With CFD the t and w can be determined numerically.

$$t = \frac{T - R}{T} \tag{3-20}$$

$$w = \frac{v_s - v_a}{v_s} \tag{3-21}$$

$$\eta_H = \frac{1 - t}{1 - w} \tag{3-22}$$

To determine t, the CFD-based appended hull resistance R and actuator disk thrust T are inserted in equation 3-20. Currently, the t is assumed to be speed-independent and equal to 0.11 for all LE vessels. It was investigated if this assumption is correct. Because there are no actuator disk simulations available for the SX series, these vessels are not considered.

In order to determine w numerically, v_A must be computed. This was done by coupling the CFD solver to an open water data file, as explained in section 2-4. As J is known, v_A can be determined as follows: $v_a = J \cdot n \cdot D_p$. With n the propeller speed in [rps] and D_p the propeller diameter in [m].

3-7 Resistance to power

The goal of using full-scale RANSe based CFD is to make a more accurate and precise prediction of the power-speed relationship such that the design margins can be reduced. With CFD the ship resistance R is determined, and by multiplying the resistance with the ship speed the effective power P_{eff} is computed. Subsequently, the required break power P_B can be derived by multiplying the P_{eff} with η_H, η_O, η_R, η_S and η_{GB} as presented in figure 3-6.

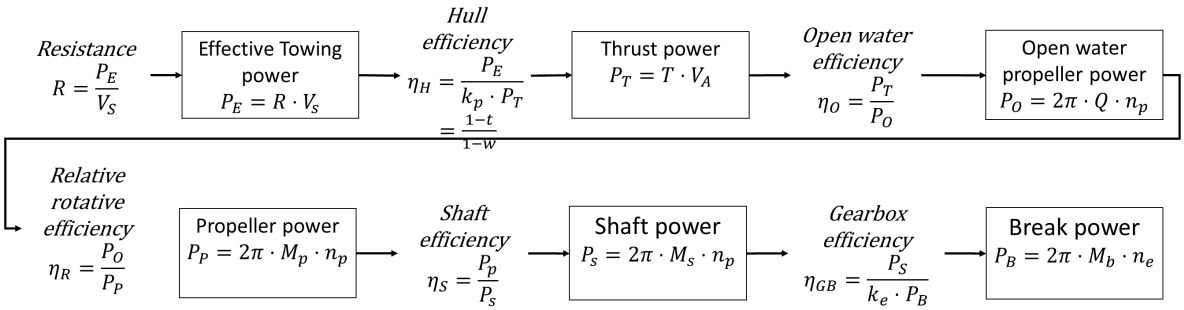

Figure 3-6: Deriving break power P_B from resistance R

Chapter 4

Accuracy and precision of full-scale RANSe based CFD simulations

In section 3-2 it is explained that the accuracy and precision of the CFD based resistance prediction can be expressed in terms of the mean μ and the standard deviation σ of $C_{F,\,CFD}$. A small value of μ and σ represents high accuracy and precision respectively. A positive μ indicates an underprediction and a negative μX an overprediction by the CFD simulations. This chapter presents the research to the effect of including more physical effects in the simulations and to the effect of data variety on the accuracy and precision. The study is divided into three stages. First, the LE180 series was investigated because the larges amount of the database is about this yacht. Another advantage is that the differences in main dimensions and hull form are minimal. Second, the results for entire LE series were analyzed and also compared to the LE180 results only. At last the SX series was included, and a similar analysis was made as for the LE180 and the entire LE series.

4-1 Accuracy and Precision for the LE180, entire LE series and entire LE and SX series

The μ and σ of $C_{F,\,CFD}$ of the Amels LE180 are presented in table 4-1. It holds that μ decreases as more physical effects are included in the simulations. First, this is showed by comparing the three simulation types with and without Townsin roughness separately. For the results without roughness μ decreases, and a similar trend is seen for the results where the roughness is included. The roughness was not included for the actuator disk simulation results because the comparison was made on thrust instead of resistance. Second, the effect of Townsin roughness on the accuracy was also investigated by comparing the simulations types with each other. The results of the bare and appended hull simulations show that including roughness leads to a higher accuracy indicated by μ being closer to zero.

The impact of including more physical effects on σ is less significant. Only whilst comparing bare hull to appended hull simulations σ decreases significantly, and it even increases whilst comparing appended hull to actuator disk simulations.

Table 4-1: Development of μ and σ whilst comparing the CFD simulations of the Amels LE180

	Without Townsin Roughness			With Townsin Roughness		
	Bare Hull	Appended Hull	Actuator Disk	Bare Hull	Appended Hull	Actuator Disk
n	40	39	36	40	39	36
μ	0.5516	0.0729	0.0694	0.5227	0.0566	-
σ	0.1498	0.0789	0.0897	0.1528	0.0795	-

The μ and σ of the entire Amels LE series are presented in table 4-2. The results for the accuracy and precision of the entire LE series were analyzed on three aspects. First, the results of the three simulation types were compared with and without Townsin roughness. Second, the effect of the Townsin roughness itself was investigated. Third, they were compared with the results of the LE180. When considering μ for the results without roughness, the accuracy of the simulation increases when bare hull and appended hull simulations are compared, but it slightly decreases whilst appended hull to actuator disk simulations are compared. A similar trend is seen in the results where the roughness is included. μ of the entire LE series is smaller compared to the LE180, indicating that an increase of variety in the ship's main dimensions does not directly lead to a decrease in accuracy of $C_{F,CFD}$.

Next, it can be seen that σ decreases when comparing bare hull to appended hull simulations, considering both the results with and without roughness. While it increases slightly in the between appended hull and actuator disk simulations. Also, including Townsin roughness leads to a slightly larger σ. Finally, when comparing σ of the entire LE series with the LE180, it can be seen that the precision is less for the entire series LE-series for all three simulation types and also considering Townsin roughness.

Table 4-2: Development of μ and σ whilst comparing the CFD simulations of the entire Amels LE series

	Without Townsin Roughness			With Townsin Roughness		
	Bare Hull	Appended Hull	Actuator Disk	Bare Hull	Appended Hull	Actuator Disk
n	63	48	45	63	48	45
μ	0.4900	0.0544	0.0568	0.4582	0.0375	-
σ	0.1662	0.0823	0.0861	0.1671	0.0833	-

At last, μ and σ of the entire Amels LE and SX series combined are presented in table 4-3. Since only bare hull simulations of the SX series were available, these are also the only simulation types of the LE series included. The effect of roughness is analyzed, and the results are also compared with the entire LE series. The roughness led to a decrease of μ and an increase in σ. The same tendency is seen for both μ and σ when they are compared to the results of the entire LE series only.

Table 4-3: Development of μ and σ whilst comparing the CFD simulations of the entire Amels LE and SX series combined

	Without Townsin Roughness			With Townsin Roughness		
	Bare Hull	Appended Hull	Actuator Disk	Bare Hull	Appended Hull	Actuator Disk
n	71	-	-	71	-	-
μ	0.4824	-	-	0.4508	-	-
σ	0.1646	-	-	0.1647	-	-

4-2 Analysis of the accuracy

In general, it was seen that including more physical effects in the simulations leads to a higher accuracy. The improvement of the accuracy was visualized by presenting the data in a bar chart, shown in figure 4-1. The largest improvement of accuracy can be seen whilst comparing the bare hull simulations to the appended hull simulations, for both the LE180 and entire LE series. The accuracy of the appended hull simulations is higher because more hull details are modelled which results in a more realistic simulation of the flow around the ship. For the LE180 it holds that the accuracy also slightly improves when comparing appended hull to actuator disk simulations, and for the entire LE series it slightly decreases.

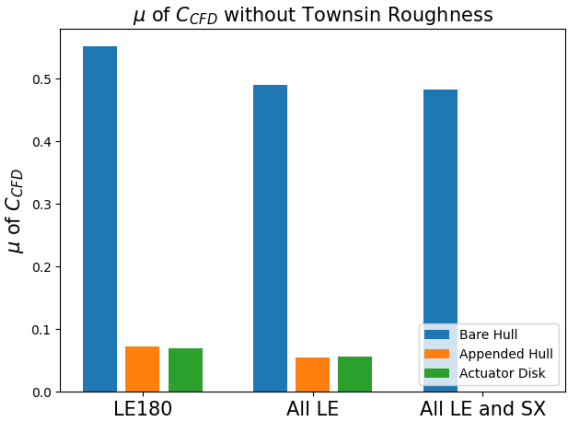

Figure 4-1: Change of accuracy whilst comparing simulation types per vessel series

There are three possible explanations for the marginal improvement and decrease in accuracy whilst comparing appended hull to actuator disk simulations. First, the actuator disk is a simplification of a real propeller, it allows a thrust to be determined, but it does not provide a more realistic simulation of the flow. Thus, the accuracy does not improve as much as was observed between the bare hull and appended hull simulations. Second, the $C_{F,CFD}$ for the appended hull simulations is based on the resistance while it is based on the thrust for the actuator disk simulations. Thus, the thrust deduction factor t is only considered in the appended hull simulations. Currently, the thrust deduction factor t is assumed to be independent of speed and equal to 0.11. If this assumption is incorrect it could lead to an incorrect derivation of the resistance. At last, the corrections for environmental conditions

are performed on the resistance, so they are not incorporated in the $C_{F,CFD}$ of the actuator disk simulations.

The effect of including roughness via the Townsin equation, see equation 3-2, was evaluated by comparing the simulations types with and without the roughness. The results are visualized in figures 4-2 and 4-3. It was seen that the effect of roughness is minimal for the bare hull simulations. The accuracy of the simulations of the LE180 improves with approximately 5%, of the entire LE series with approximately 6%, and of the entire LE and SX series with approximately 7%. The percentual effect is larger for the appended hull simulations. It increases for the LE180 with approximately 22 % and for all LEs with 31%.

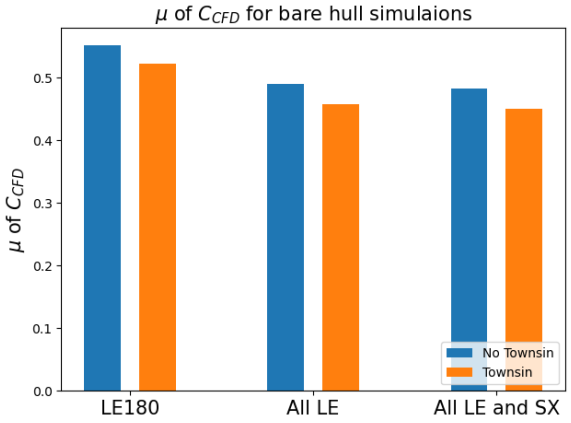

Figure 4-2: Change of accuracy considering roughness in the bare hull simulations per vessel series

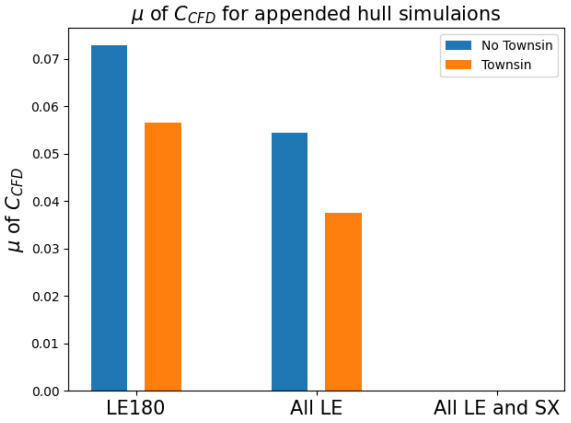

Figure 4-3: Change of accuracy considering roughness in the appended hull simulations per vessel series

The correction by Townsin is a function of the average hull roughness factor k, the ship's waterline L_{WL} and ship speed in R_e, thus the correction is independent of simulation type. Because the appended hull resistance already predicts the resistance more accurately, μ of $C_{F,CFD}$ is closer to zero, results in the effect of Townsin roughness being relatively larger.

The effect of increasing the variety in the data, by including more ship types, leads to a decrease of the μ of $C_{F,CFD}$ and the size of the reduction differs per simulation type. The trends are presented in figures 4-4 and 4-5. It was seen that for the bare hull simulations the accuracy improves with approximately 11% when comparing LE180 dataset to the entire LE dataset without Townsin roughness and it improves with 12 % with Townsin Roughness. The improvement is much less when comparing the entire LE series with the entire LE and SX combined, namely 2% for both with and without Townsin. For the appended hull simulations without roughness the accuracy improved with 25% and with Townsin with 34 %. And for the actuator disk simulations the μ decreases with 18% comparing LE180 to all LE's.

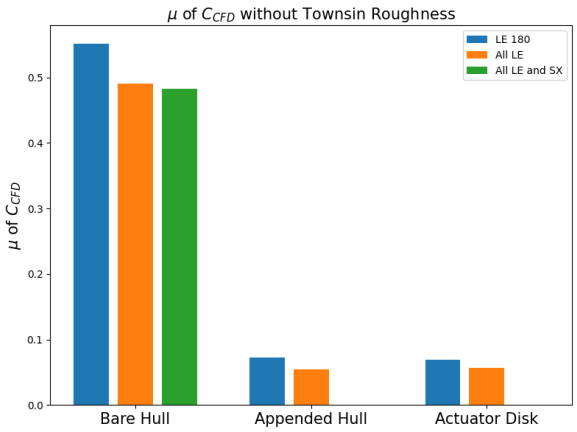

Figure 4-4: Change of accuracy whilst comparing vessel series per simulation type

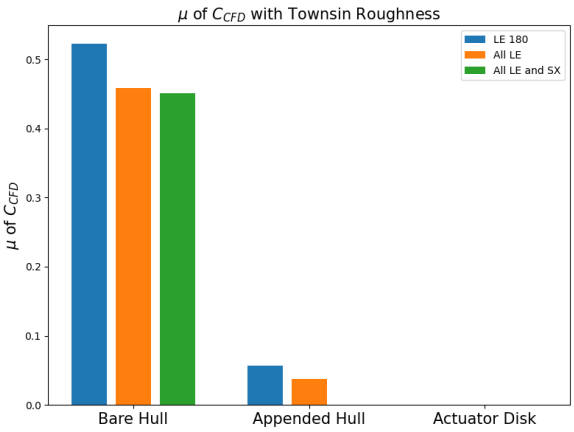

Figure 4-5: Change of accuracy whilst comparing vessel series per simulation type

There can be several causes that the accuracy improves as the variety in the data increases. First, the vessels other than the LE180 are larger. As explained in section 2-5-1, the correction method for waves only corrects for reflected waves, so not for motion induced waves. If this assumption is incorrect for the LE180, the gap between CFD results and trial is larger. Which leads to a larger μ. Second, there is fewer data present for other ship types than the LE180 especially for the appended and actuator disk simulations. Thus, it is harder to draw conclusions over the entire LE series.

Summarizing, the accuracy of $C_{F,\,CFD}$ increases by including more physical effects. Especially whilst comparing bare hull and appended hull simulations, while the effect is less significant when comparing appended hull to actuator disk simulations. The effect of Townsin was only evaluated for the bare hull and appended hull simulations. For bare hull simulations the effect was relatively less compared to the appended hull simulations. Which is caused by that the magnitude of the Townsin correction is equal at both simulations. At last, including more different ship types has a positive effect on the accuracy for these datasets.

4-3 Analysis of the precision

The standard deviation of $C_{F,\,CFD}$ is considered is too large. To find the driving factors, linear regression was applied to $C_{F,\,CFD}$ and the results are presented in chapter 5. For the appended hull and actuator disk simulations the σ is even larger than μ.

The trend of σ is visualized with bar charts in figure 4-6. The largest improvement is seen between the bare hull and appended hull simulations, for both the LE180 and the entire LE series. When comparing appended hull to actuator disk simulations the precision decreases, for both the LE180 only and the entire LE series.

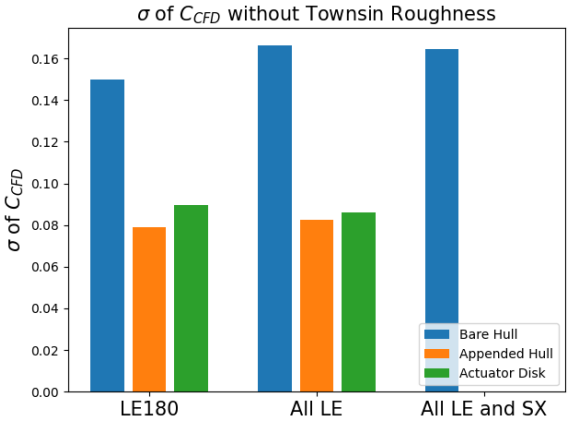

Figure 4-6: Change of precision whilst comparing simulation types per vessel series

Again, the improvement between bare and appended hull simulations was assumed to be caused by a more realistic simulation of the flow. The reduction between appended hull and actuator disk simulations may be due to two reasons. First, the flow was simulated well already in the appended hull simulations, and now the addition of a simplified propeller model leads to a decrease in precision. The other explanation is that the corrections for environmental conditions are performed on the resistance, and not on the thrust. The absence of correction for the environmental conditions could introduce a larger σ.

Figures 4-7 and 4-8 show the effect of Townsin roughness on the σ of $C_{F,CFD}$ based on the bare hull and appended hull simulations. The effect of roughness via Townsin on the precision is minimal, but negative. When considering bare hull simulations the precision decreases with approximately 2% for the LE180 series, with approximately 1% for the entire LE series and remains almost equal when the SX data is included as well. For the appended hull simulations the precision decreases with 1% for the LE180 series, as for the entire LE series.

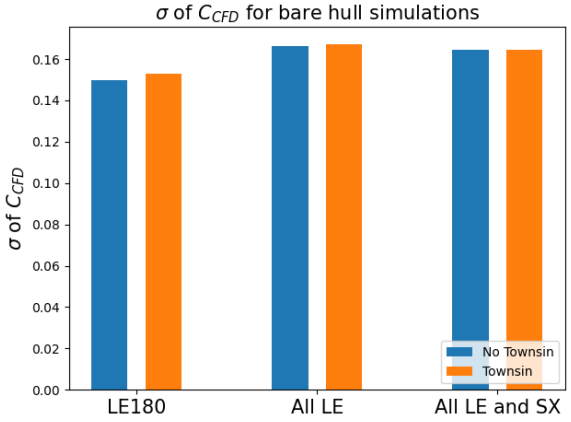

Figure 4-7: Change of accuracy considering roughness in the bare hull simulations per vessel series

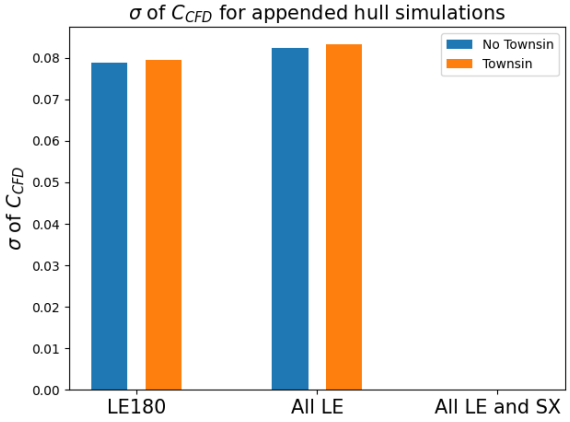

Figure 4-8: Change of accuracy considering roughness in the bare hull simulations per vessel series

The behavior of σ due to roughness were unexpected. Two hypotheses have been developed.

Because there are small differences in speed the correction by Townsin is not constant. Another aspect could be that the used average hull roughness k is not correct. Now, it is assumed equal for every ship. But it could differ between the ships because there can be some time between launch and trial, resulting in more fouling on the hull.

The effect of variety in the data was investigated by comparing the results of the LE180 series to the entire LE series and by comparing the results of the entire LE series with the entire LE and SX series, which was visualized with bar charts as presented in figures 4-9 and 4-10. First, the bare hull simulations are considered. The precision decreases with 11% when comparing the LE180 series to the entire LE series without Townsin, and with 12% when Townsin is incorporated. Then, it slightly improves with 1% when comparing the entire LE series to the entire LE and SX series, for both with and without Townsin. Second, the appended hull simulations were investigated. The precision decreases with 4% when Townsin is not considered whilst comparing the LE180 series to the entire LE series, and it decreases with 5% when Townsin is considered. At last, the effect on the precision of the actuator disk simulations was investigated. The precision improves with 4% when the LE180 series is compared to the entire LE series.

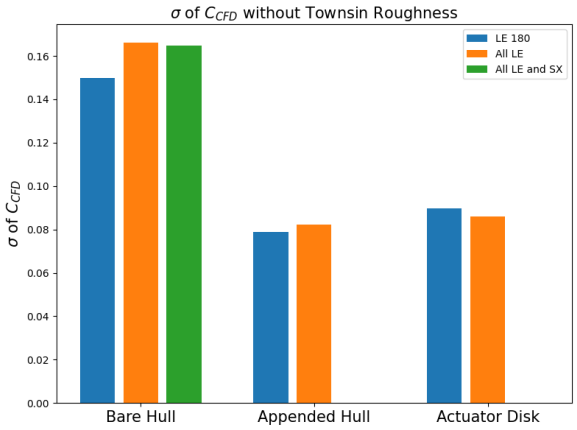

Figure 4-9: Change of accuracy between vessel series per simulation type

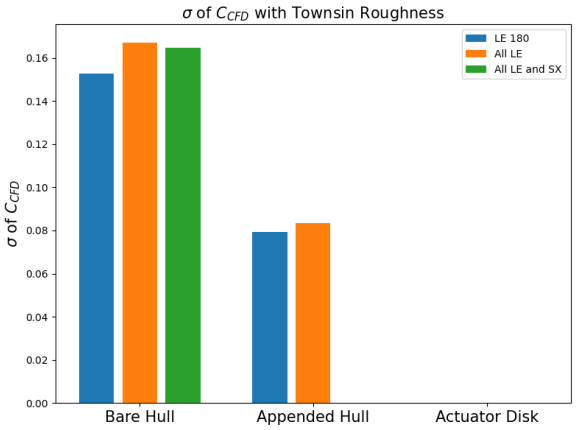

Figure 4-10: Change of accuracy between vessel series per simulation type

As presented in section 4-2 the accuracy slightly improved when comparing the entire LE to the entire LE and SX series for the bare hull simulations and also when comparing LE180 series to the entire LE series for the actuator disk simulations. The standard deviation is mathematically represented by equation 3-7, it can be seen that it is a function of μ, thus a change in μ could result in a change of the σ.

Altogether, the effect of more physics in the simulations on $C_{F,\,CFD}$ is positive when comparing bare hull to appended hull simulations, but is negative when comparing appended hull to actuator disk simulations. The effect of the Townsin roughness is minimal, but negative.

4-4 Chapter conclusion

The uncertainty of $C_{F,CFD}$ was defined as a function of the accuracy and precision. The accuracy is represented by mean μ, and the precision by the standard deviation σ of $C_{F,CFD}$. Two possible causes for the uncertainty of $C_{F,CFD}$ were examined. The first cause is the effect of more physics in the simulations. To investigate the effect on the uncertainty of $C_{F,CFD}$, two methods are considered. First, by comparing the bare hull with appended hull simulations, and appended hull with actuator disk simulations. Second, by including roughness via Townsin's equation for roughness. The second cause is the effect of variety in the data on the accuracy and precision, which was investigated by including more different ship types. The different ship types had other main dimensions which introduces variety in the data.

The largest improvement of accuracy and precision was seen between bare hull and appended hull simulations, for both the LE180 series and the entire LE series. Subsequently, the accuracy only slightly improves between appended hull and actuator disk simulations of the LE180 series, and it slightly decreases considering the entire LE series. The precision worsens for both the LE180 series and the entire LE series. Three possible explanations of the reduction of accuracy were presented. First, the actuator disk is a simplification of a real propeller, and thus does not lead to a more realistic simulation of the flow. Second, t is assumed constant which may introduce an incorrect derivation of the resistance, and thus an incorrect $C_{F,CFD}$ for the bare hull and appended hull simulations. Third, the corrections for environmental conditions are performed on the resistance rather than thrust, creating a larger gap between the CFD and sea trial results. The effect of Townsin roughness is positive on the accuracy, and it is relatively larger for appended hull simulations. The precision worsens by the addition of Townsin roughness, and in combination with the minimal effect of Townsin roughness this lead to the decision to not include it in further analysis. Summarizing, the total uncertainty decreased whilst comparing bare hull to appended hull simulations, and it increased whilst comparing the appended hull to the actuator disk simulations. It can be concluded that including more physical effects has a positive effect on the uncertainty in $C_{F,CFD}$, and the actuator disk model should be revised.

The impact of variety in the data is positive on the accuracy of the bare hull, appended hull, and the actuator disk simulations. More variety has a negative impact on the precision as this is represented by the standard deviation which is an indicator of the variance in a dataset. The improvement of accuracy when more ship types are considered was explained by the way added resistance due to waves is implemented. The correction only includes reflected waves and not motion induced waves, this could introduce an incorrect added resistance by waves for the LE180 series. The ship types other than the LE180 are larger, so the added resistance is likely to be more accurate. In some situations the precision also slightly improved. This was explained by the fact that σ is a function of μ, and when μ decreases σ could decrease as well. Because the accuracy was influenced positively, but the precision negatively, it was concluded that the effect of variety in ship dimensions on the uncertainty of $C_{F,CFD}$ is negative.

Chapter 5

Multivariate linear regression on $C_{F,CFD}$

A multivariate linear regression was used to investigate the cause of the variance in $C_{F,CFD}$. Three steps were taken to determine which variables could be used in the regression. First, a list of possible dependent variables was set up, consisting of the following parameters: ship speed V_s in [m/s] or as F_n measured during trial, C_b, ∇ or L_{wl} to describe differences in the hull, and finally mean wave height H_w and mean wind speed V_w to take the influence of environmental conditions into account. Next, pair plots were used to investigate if there was any linear relationship between the independent variables and dependent variable $C_{F,CFD}$. Finally, collinearity matrices were used to determine if the independent variables were not collinear. When there is collinearity between independent parameters, they are not independent and cannot be used in the regression.

5-1 Preliminary list of dependent variables

The variation in $C_{F,CFD}$ is caused by two aspects. First, there are differences within the same yard number, and second, there are differences between yard numbers. The variation within the same yard number, is believed to be due to the different test speeds during sea trial measurements. The variation between yard numbers which is not only due to that the test speeds are not exactly equal, but also due to differences in hull size, differences in the hull due to ship building and due to environmental conditions. Since there is no parameter available that describes small construction differences between the hulls, this is not included in the regression. The preliminary list of dependent variables consists of the following parameters:

1. Ship speed represented by:
   (a) The measured ship speed during trial V_s in [m/s] or,
   (b) The non-dimensional measured ship speed during trial F_n
2. Difference in hull shape represented by:
   (a) The block coefficient C_b or,
   (b) The volume of the ship ∇ in [m^3] or,
   (c) The length of the water line L_{wl} in [m]
3. Impact of environmental conditions during trial:
   (a) The mean wave height H_w in [m] and/or,
   (b) The mean wind speed V_w in [m]

5-2 Pair plots

Pair plots were used to investigate if there is a linear relationship between a single dependent variable and independent variable $C_{F,\,CFD}$. Seven pair plots were created, one for every dataset. The trends between the independent variables and dependent variable $C_{F,\,CFD}$ are comparable in all seven datasets. A linear trend line is fitted over the data to aid in discovering any linear relationship. The quality of the linear fit is assessed with the R^2 value. R^2 is a statistical measure that shows the part of variance of the dependent variable that can be explained by an independent variable. The value always lies between zero and one. A value of zero means that there is no linear relationship, and a value of one means that there is a perfect linear relationship.

5-2-1 Pair plots of the LE180 series bare hull simulations

In figure 5-1 the pair plots for the bare hull simulations of LE180 are shown and the corresponding R^2 values are presented in table 5-1. Only the R^2 values of the linear fit between the ship speed and $C_{F,\,CFD}$ are not approaching zero.

Table 5-1: R^2 of the bare hull simulation for LE180 series

	F_n	V_s	C_b	∇	L_{wl}	H_w	V_w
$C_{F,\,CFD}$	0.599891	0.620564	0.031136	0.04995	0.048334	0.081894	0.006595

The trend of the relation between $C_{F,\,CFD}$ and ship speed is negative. Which means that the relative error $C_{F,\,CFD}$ decreases as the ship speed increases. A trend in the relationship between $C_{F,\,CFD}$ and all three of the hull parameters was difficult to find without the aid of the trend line. The absence of a clear trend is also confirmed by the values of R^2 approaching zero. The reason that there is not a trend between the parameters describing hull differences and $C_{F,\,CFD}$ can be explained by the fact that the hull sizes are comparable within the LE180 series. Nevertheless, the trend line indicates a negative relationship. The trend in environmental conditions is also difficult to discover without the trend lines. The linear relationship between H_w and $C_{F,\,CFD}$ is slightly positive, and between V_w and $C_{F,\,CFD}$ slightly negative. However, both R^2 values are approaching zero, indicating that there is no linear dependency.

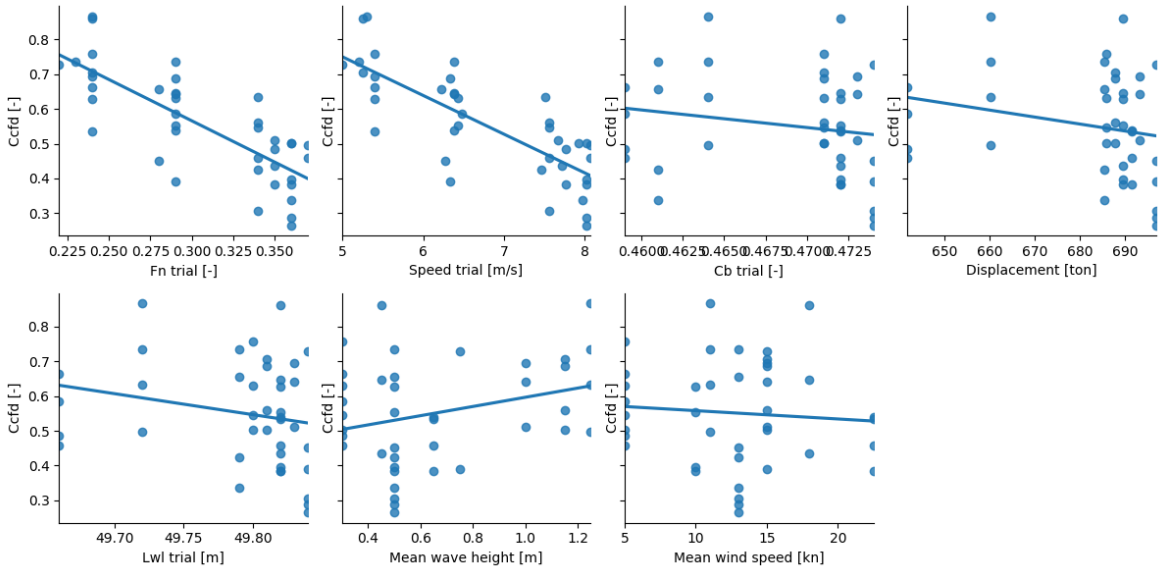

Figure 5-1: Pair plots for bare hull simulations of the LE180 series

5-2-2 Pair plots of the LE180 series appended hull simulations

The pair plots for the appended hull simulations of the LE180 series are presented in figure 5-2, and the corresponding R^2 values are presented in table 5-2. The R^2 values changed compared to the bare hull results, they decreased for the ship speed and $C_{F,CFD}$, and for all other the values increased. Because all R^2 values are small, the linear fitted trend lines do not represent the data very well, but they can still be used to discover the direction of the trends. The size of the appended hull dataset is smaller compared to the bare hull dataset, which could be a cause of the reduction of the R^2 values.

Table 5-2: R^2 of the appended hull simulation for LE180 series

	F_n	V_s	C_b	∇	L_{wl}	H_w	V_w
$C_{F,CFD}$	0.211846	0.22867	0.098999	0.168483	0.166069	0.187574	0.071048

Similar trends were observed as in the bare-hull simulations. There is a negative relationship between variables describing the ship speed and $C_{F,CFD}$, and between C_b, ∇, and L_{wl} and $C_{F,CFD}$. Between the mean wave height and $C_{F,CFD}$ a positive relationship was discovered. The relationship between mean wind speed and $C_{F,CFD}$ is negative but the R^2 value is approaching zero, which means that the fit is not good.

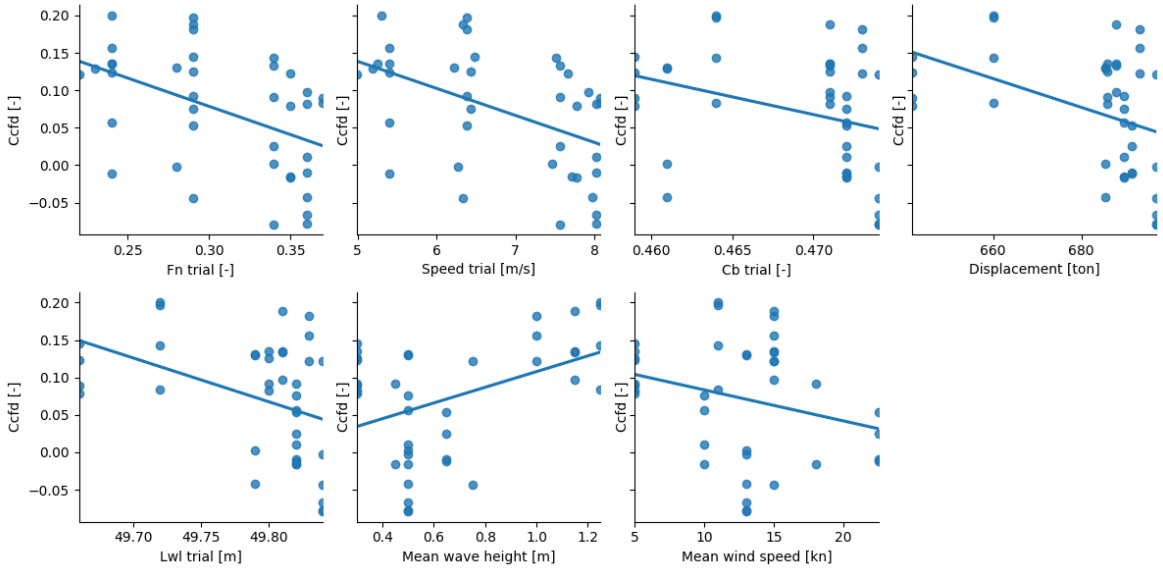

Figure 5-2: Pair plots for appended hull simulations for the LE180

5-2-3 Pair plots of the LE180 series actuator disk simulations

Figure 5-3 presents the pair plots that belong to the actuator disk results of the LE180 are shown, and table 5-3 shows the corresponding R^2. This dataset is the smallest of all considered datasets. The values of R^2 between ship speed and $C_{F,\,CFD}$ increased again compared to the appended hull results, while the changes of the R^2 values of the others are marginal.

Table 5-3: R^2 of the actuator disk simulation for LE180 series

	F_n	V_s	C_b	∇	L_{wl}	H_w	V_w
$C_{F,\,CFD}$	0.374639	0.395241	0.081825	0.147487	0.14334	0.160089	0.027788

Despite the small size of the dataset, trends in the data were discovered with the aid of the linear fitted trend lines. Similar relationships are present between the independent variables and dependent variable $C_{F,\,CFD}$ of the actuator disk results as for the bare hull and appended hull results. However, one should not lose sight of the fact that the R^2 values are small, indicating that the linear fit is not good.

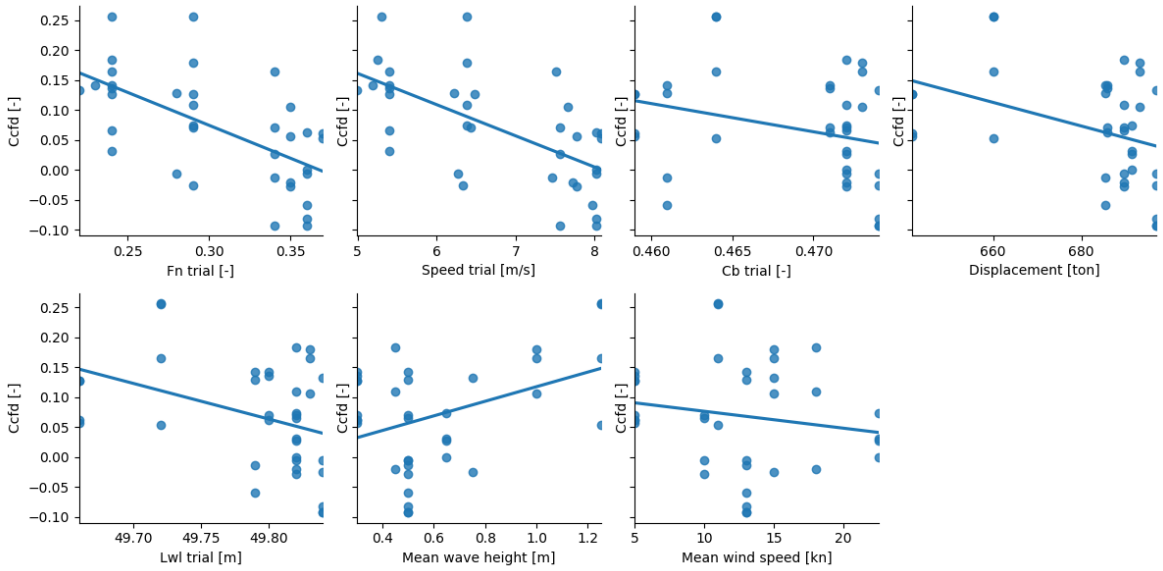

Figure 5-3: Pair plots for actuator disk simulations for the LE180 series

5-2-4 Pair plots of the entire LE series bare hull simulations

The pair plots of the bare hull simulations for the entire LE series are shown in figure 5-4, and the corresponding R^2 values are presented in table 5-4. Compared to the bare hull results of the LE180 series, the R^2 values of F_n and V_s decreased, the R^2 values of C_b increased while it decreased for the other two parameters describing the differences in hull size. Also, the R^2 value of the linear fit between C_b and $C_{F,\,CFD}$ is bigger than for the other two variables describing the hull, which is because C_b is dimensionless.

Table 5-4: R^2 of the bare hull simulation for the entire LE series

	F_n	V_s	C_b	∇	L_{wl}	H_w	V_w
$C_{F,\,CFD}$	0.270552	0.351599	0.089788	0.022531	0.035678	0.109023	0.016757

The trend between the variables representing the ship speed and $C_{F,\,CFD}$, and between the variables representing the differences in hull size is negative. The trend between C_b is more pronounced than in the results for the LE180 series because the differences in the hull sizes are larger. Between H_w and $C_{F,\,CFD}$ the trend is positive, which was also seen in all other cases. Finally, the trend between V_w and $C_{F,\,CFD}$ was practically impossible to discover without the linear fit but it is slightly negative. There is actually hardly any trend, which is represented by the value of R^2 being close to zero.

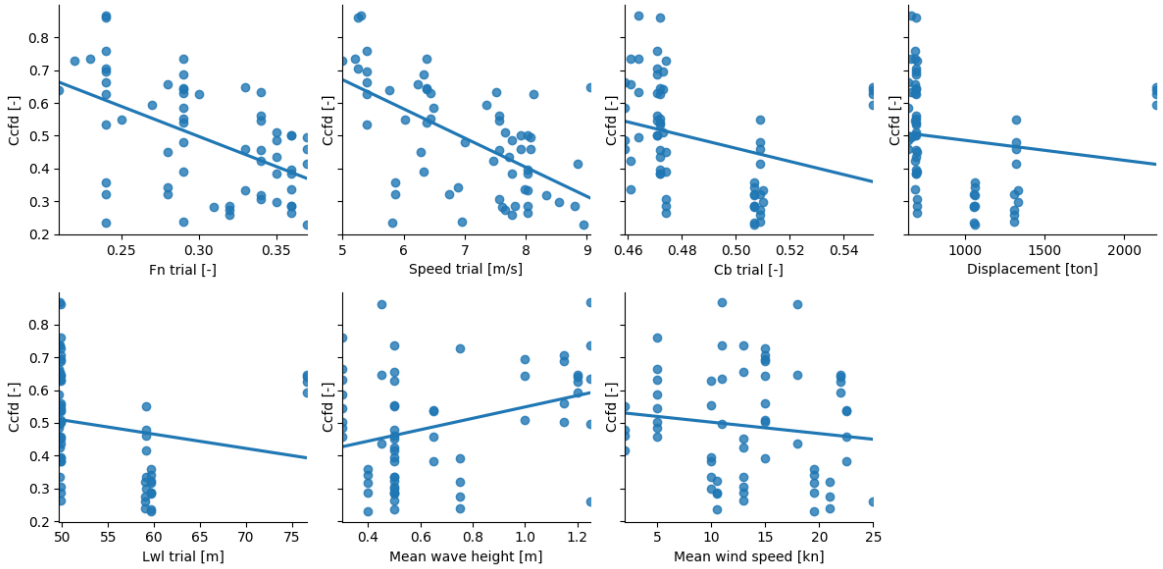

Figure 5-4: Pair plot for the bare hull simulation for the entire LE series

5-2-5 Pair plots of the entire LE series appended hull simulations

The pair plots corresponding to the appended hull simulation of all LE are presented in figure 5-5, and the corresponding values of R^2 can be found in table 5-5. The R^2 values of the linear fit between the variables describing the ship speed and $C_{F,\,CFD}$ decreased compared to the bare hull simulations. Then, it increased for C_b, ∇ and L_{wl}. This is believed to be due that only the LE180 and LE199 are present in this dataset, thus the variance in hull sizes is less.

Table 5-5: R^2 of the appended hull simulation for the entire LE series

	F_n	V_s	C_b	∇	L_{wl}	H_w	V_w
$C_{F,\,CFD}$	0.119391	0.205723	0.277452	0.24996	0.221552	0.23627	0.085792

Despite the fact that only the LE180 and LE199 are present in the appended hull simulations, the relationships between the independent variables and dependent variable $C_{F,\,CFD}$ are comparable as for the bare hull simulations. The relation between speed and $C_{F,\,CFD}$, ship size and $C_{F,\,CFD}$ and, mean wind speed and $C_{F,\,CFD}$ is negative. While, the relation between mean wave height and $C_{F,\,CFD}$ is positive.

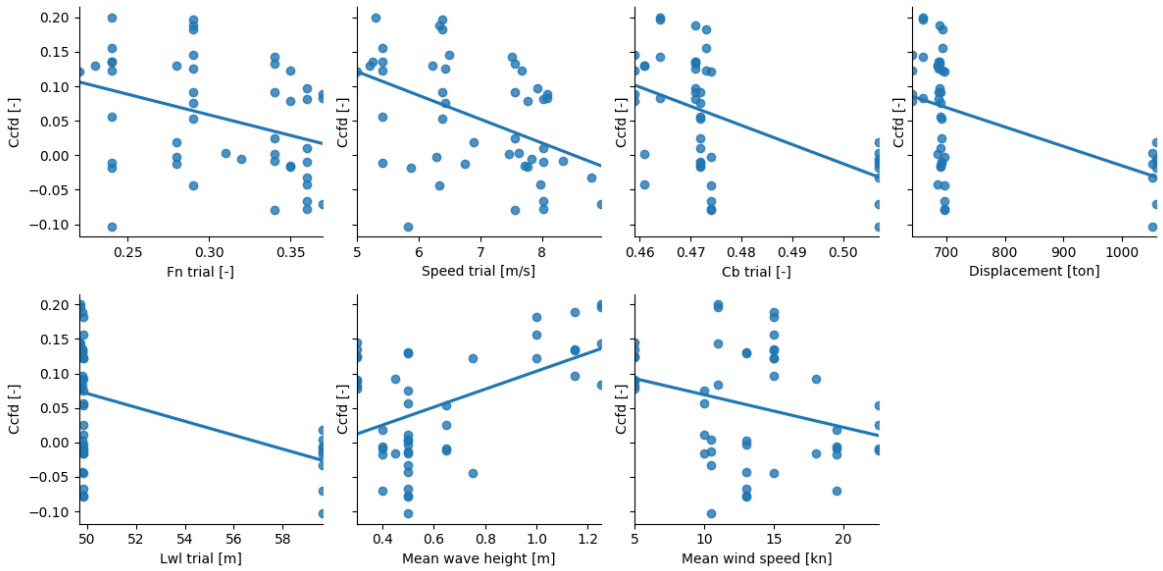

Figure 5-5: Pair plot for the appended hull simulation for the entire LE series

5-2-6 Pair plots of the entire LE series actuator disk simulations

The pair plots of the actuator disk simulations for all LE are shown in figure 5-6, and the corresponding R^2 values are presented in table 5-6. The R^2 of the linear fits between V_s, F_n and $C_{F,CFD}$ increased again, while it decreased for all other parameters. This was also seen in the LE180 series. This dataset is smaller, which could be a reason that the variance can be described less.

Table 5-6: R^2 of the actuator disk simulation for entire LE series

	F_n	V_s	C_b	∇	L_{wl}	H_w	V_w
$C_{F,CFD}$	0.274117	0.334292	0.129665	0.107479	0.088504	0.179964	0.031389

The trends between the independent variables F_n, V_s, C_b, ∇, L_{wl}, and V_w and dependent variable $C_{F,CFD}$ is negative. Again, it is positive for the trend between the mean wave height and $C_{F,CFD}$.

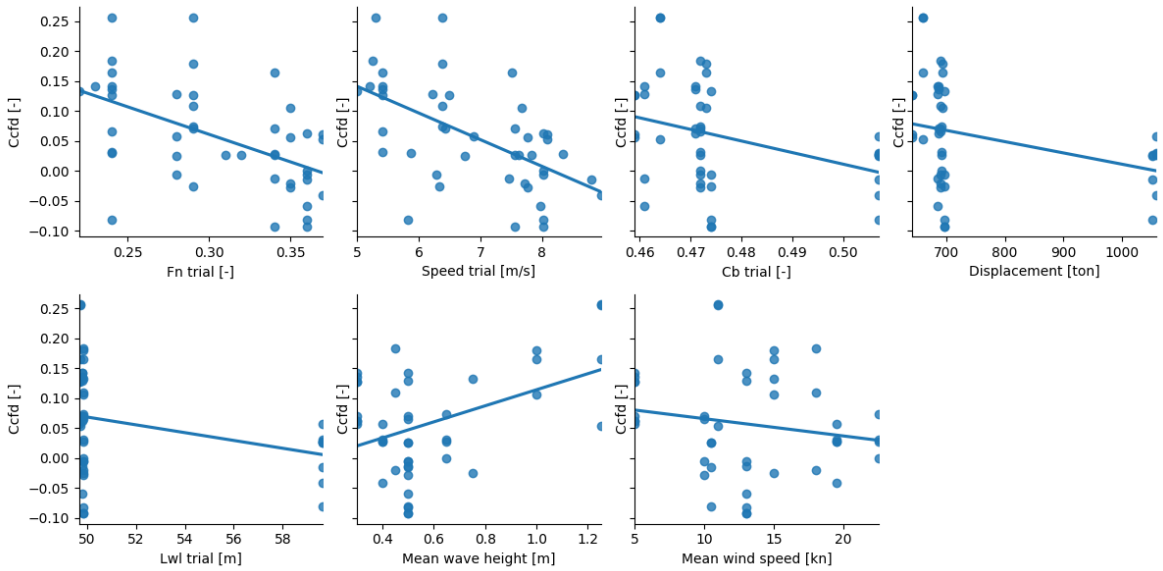

Figure 5-6: Pair plot for the actuator disk simulation for the entire LE series

5-2-7 Pair plots of the entire LE and SX series combined bare hull simulations

At last the results of the bare hull simulations for the entire LE and SX series are discussed. The pair plots are presented in figure 5-7, and the corresponding values of R^2 are presented in table 5-7. It can be seen that there is more scatter compared to the other six pair plots. This is also confirmed by the values of R^2 being smaller than of the bare hull results corresponding to the entire LE series.

Table 5-7: R^2 of the bare hull simulation for the combined LE and SX series

	F_n	V_s	C_b	∇	L_{wl}	H_w	V_w
$C_{F,\,CFD}$	0.161974	0.231458	0.091028	0.01908	0.019594	0.039959	0.042232

The trend of the relation between ship speed and $C_{F,\,CFD}$ is negative, which can also be said for the trend of the relation between $C_{F,\,CFD}$ and the hull dimensions. The relationship with mean wave height is positive while it is negative for the mean wind speed. However, both R^2 values approach zero, so the linear fit is not strong.

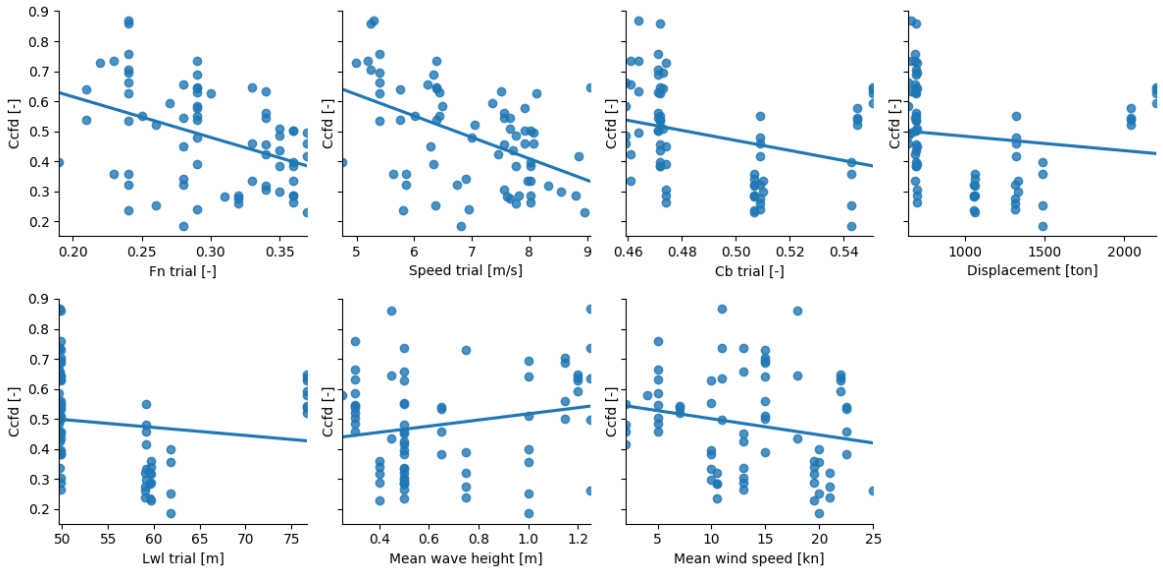

Figure 5-7: Pair plot for the bare hull simulation for the entire LE and SX series

5-3 Collinearity Matrices

In section 3-5 it was explained that the strength of collinearity between two parameters can be determined with Pearson's correlation coefficient $\rho_{a,b}$, presented in equation 3-18. Collinearity matrices are made for every dataset, and they are presented in figures C-1 through figure C-7. Strong collinearity between two parameters is indicated by $|\rho_{a,b}| > 0.7$, which is represented by "True" in collinearity matrices. There is a weak or moderate correlation between two parameters when $|\rho_{a,b}| < 0.7$, which is represented by "False" in the collinearity matrices. The collinearity between all parameters present in the databases is shown, but the parameters of interest are: "speed trial", "Fn trial", "Displacement", "Lwl trial", "Cb trial", "mean wave

height" and "mean wind speed". After inspecting figures C-1 through C-7 it was concluded that there is no collinearity between the parameters describing the three sources of variety. The F_n and C_B are chosen for the ship speed and hull differences, as these are non-dimensional, and both parameters describing the environmental conditions are selected as well. As it is expected that both are a source of the variance in $C_{F,CFD}$.

5-4 Results of the multivariate linear regression

A multivariate linear regression is performed on all seven datasets. The parameters to regress on are the F_n for the speed, the C_b for the difference in hull size ,and the H_w and the V_w for the environmental conditions. The input parameters were normalized with min/max normalization to aid interpretation of the regression coefficients. The coefficients and corresponding P-values reveal what their nature and significant statistical relationships is.

In tables 5-8, 5-9 and 5-10 the regression coefficients for the LE180 series are presented. In all three of the CFD simulations the C_B does not play a role in the variance of $C_{F,CFD}$ because the P-value exceeded the maximum significance level of 0.05. This is explained by the fact that all the hulls are comparable, which results in little spread in C_B. The ship speed represented by F_n causes the largest amount of variance in $C_{F,CFD}$ for the bare hull simulations. The impact by both the environmental conditions is comparable but opposite. The ship speed causes less variance in $C_{F,CFD}$ of the appended hull simulations compared to the bare hull simulations, while the effect of environmental conditions is comparable. For the actuator disk simulations the variance in $C_{F,CFD}$ is mostly due to the ship speed, however the impact of the mean wave height is almost as large. Now, the effect of mean wind speed is less.

Table 5-8: Bare hull

	Coefficient	P>t
R^2	0.7190	-
β_0	0.7588	0.000
F_n	-0.3581	0.000
C_b	-	-
H_w	0.1480	0.001
V_w	-0.1326	0.010

Table 5-9: Appended hull

	Coefficient	P>t
R^2	0.5900	-
β_0	0.1423	0.000
F_n	-0.1070	0.000
C_b	-	-
H_w	0.1355	0.000
V_w	-0.1375	0.000

Table 5-10: Actuator disk

	Coefficient	P>t
R^2	0.6250	-
β_0	0.1594	0.000
F_n	-0.1633	0.000
C_b	-	-
H_w	0.1412	0.000
V_w	-0.1031	0.000

The results of the multivariate linear regression for the entire LE series are presented in tables 5-11, 5-12 and 5-13. All P-values are below the maximum significance level of 0.05, except for V_w of the actuator disk simulation results. Thus, the regression on the actuator disk results was executed again without V_w. For all the bare hull and actuator disk datasets it holds that the F_n causes the largest amount of variance in $C_{F,CFD}$. While H_w is the most important in the appended hull simulations results. Because there are differences in hull size in the entire LE series, C_b has an impact on the variance of $C_{F,CFD}$ in all three simulations. Again, higher waves result in higher $C_{F,CFD}$, and stronger winds in a smaller $C_{F,CFD}$. This behavior is further elaborated in section 5-4-3.

Table 5-11: Bare hull

	Coefficient	P>t
R^2	0.5750	-
β_0	0.7307	0.000
F_n	-0.3034	0.000
C_b	-0.2203	0.000
H_w	0.2302	0.000
V_w	-0.1696	0.007

Table 5-12: Appended hull

	Coefficient	P>t
R^2	0.5950	-
β_0	0.1326	0.000
F_n	-0.0859	0.001
C_b	-0.0835	0.004
H_w	0.1157	0.000
V_w	-0.0827	0.011

Table 5-13: Actuator disk

	Coefficient	P>t
R^2	0.5200	-
β_0	0.1306	0.000
F_n	-0.1352	0.000
C_b	-0.0754	0.012
H_w	0.1025	0.004
V_w	-	-

Finally, the results of the regression on $C_{F,\,CFD}$ for the entire LE and SX series are presented in table 5-14. The F_n causes the biggest amount of scatter in $C_{F,\,CFD}$. Followed by C_B, the V_w and H_w. But the magnitude of the coefficients of the last three is comparable. Although, it stands out that the V_w has a slightly larger impact than the H_w, while this was the opposite in all other regression results.

Table 5-14: Bare hull

	Coefficient	P>t
R^2	0.4910	-
β_0	0.7788	0.000
F_n	-0.3143	0.000
C_b	-0.2147	0.000
H_w	0.1967	0.000
V_w	-0.2246	0.001

5-4-1 Dependency on the speed

In all bare hull simulations the F_n had the largest influence on the variance in $C_{F,\,CFD}$. The variance dependency of $C_{F,\,CFD}$ on F_n decreased in the appended hull simulations and then it increased slightly in the actuator disk simulations. An explanation is that the variance of $C_{F,\,CFD}$ itself decreased whilst comparing the bare hull and appended hull simulations and increased again when comparing appended hull and actuator disk simulations.

The negative dependency on speed means that $C_{F,\,CFD}$ becomes smaller as the speed increases. Two hypotheses have been developed for this negative relationship. First, it could be caused by the fact that the grid is designed for the design speed, the best results are obtained at this speed. Secondly, the trial results should be corrected with "mean of means" [3], however this can only be applied to the highest speed as for the other three ship velocities only two legs are performed while four are required to use mean of means.

5-4-2 Dependency on the hull form

The impact of C_b in the variance in $C_{F,\,CFD}$ for the LE180 series is zero because all hull shapes, and thus C_b's are almost identical. There are only minimal differences in the hulls which do not describe the variance in $C_{F,\,CFD}$. For the other cases, the relationship between C_b and $C_{F,CFD}$ is negative, a larger block coefficient leads to a smaller relative error. As explained in section 2-5-1, the added resistance due to waves only considers reflected waves.

However, this assumption only holds for typical wave heights and ship lengths which is more likely to happen for ships with a larger C_b.

The effect of C_b on $C_{F,\,CFD}$ in the bare hull simulations for the entire LE series and for the entire LE and SX series combined is approximately similar. Which makes sense because the datasets are almost similar as well. In the entire LE series the effect of C_b on the variance of $C_{F,\,CFD}$ decreases per simulation type. But including the actuator disk simulation in the comparison is unfair, because the V_w is excluded in this regression. All magnitudes of the coefficients of C_b decreased for the appended hull simulations compared to bare hull. This is explained by the fact that the total variance of $C_{F,\,CFD}$ decreased as well.

5-4-3 Dependency on the environmental conditions

The dependency on environmental conditions, although correction methods are used to compensate for them, is explained with the guidelines for Speed/Power trials by Van den Boom et al.in [32]. The paper describes the requirements and shortcomings of the correction methods.

The wind speed for the wind correction is measured with an anemometer, and the placement must be done carefully. The wind speed must be measured at a height of 10 meters above sea level, the wind speed has to be corrected if the anemometer cannot be mounted in such a way. When it's placed at the top of the wheelhouse the measured speed may have to be corrected for the velocity due to ship motions. Also, care should be taken that the anemometer is not shielded by masts, funnels or cargo. Finally, it was also recommended to use recently determined wind drag coefficient because the older coefficients are outdated due to changes in ship size and shape.

The correction method for encountered waves is a trade-off between an accurate prediction of added resistance due to waves and being practical due to the limited available input. The added resistance is composed of two components; reflected waves and motion induced waves. The first is dominant in short waves, while the latter is dominant in long waves. If the wave length is larger than the ship length they are considered as long waves. In this report, only the correction for short waves is considered, which may introduce incorrect corrections. The correction method was validated with modeltest of a panamax containership and aframax tanker. These vessels differ on hull shape and ship speeds compared to super yachts. This may also introduce less accurate correction for waves.

The relation between $C_{F,\,CFD}$ and V_W was negative. It could be explained by inspecting the equation which is used to determine the added resistance due to wind. It is a function of apparent wind speed and ship speed amongst others. The apparent wind decreases as the ship speed increases. A smaller apparent wind also leads to a smaller correction, and thus a smaller $C_{F,\,CFD}$.

5-5 Chapter Conclusion

This chapter examined the driving factors behind the variance in $C_{F,\,CFD}$, for which a multivariate linear regression was used. First, a list of possible independent parameters was compiled. Second, pair plots were used to inspect a linear relationship between the independent variables and dependent variable $C_{F,\,CFD}$ Subsequently, it was determined if the variables were actually independent by checking if the Pearson's coefficient $\rho_{a,b}$ was below 0.7, indicating the absence of collinearity. The predictor variables are normalized using min/max normalization. Finally, the regression was performed where the coefficients were evaluated not only on their magnitude but also on their statistical significance, represented by the P-value. This was all performed on the seven datasets.

The results of the regression show that the variance of $C_{F,\,CFD}$ is caused by ship speed in all seven datasets. The portion differs per dataset, which is explained by the different variance of $C_{F,\,CFD}$ itself.
The relationship between $C_{F,\,CFD}$ and F_n is negative, thus an increase in speed leads to a decrease of $C_{F,\,CFD}$. Two hypotheses are given. First, the grid is designed for the design speed of the ship. The larger the deviation from the design speed, the larger the numerical error can become. Second, sea trial results should be amassed with the "means of mean" method [3], which is only done for the highest tested ship speed.

The difference in size and shape within the LE180 series are so minimal that C_B is not responsible for causing any variance in $C_{F,\,CFD}$. The linear relationship between C_B and $C_{F,\,CFD}$ in the entire LE series, and the entire LE and SX series combined is negative. The relative error becomes smaller as C_B increases. It is explained by the application of the correction for waves, which only incorporates reflected waves. But, for this assumption to hold, a ratio between wave height and ship length may not be exceeded. Which is more likely to be true for larger ships.
As for the dependency on F_n, the dependency on C_B differs per simulation type, again it is explained by the difference in variance of $C_{F,\,CFD}$ itself.

The environmental conditions, represented by the mean wave height and mean wind speed, do play a role in the variance of $C_{F,\,CFD}$, despite the corrections for them that are applied to the resistance. The explanation is sought in the fact that the correction methods are developed for and validated against merchant vessels. Which differ in shape and size, thus the correction could be incomplete.
Next, the negative dependency on wind speed is explained with the equation for the added resistance due to wind speed. Amongst others, it depends on the apparent wind speed. Which itself may decrease as the ship speed increases. A reduction in the apparent wind speed leads to a lower added resistance But, the total resistance increases as the ship speed increases. Therefore, as the apparent wind decreases, $C_{F,\,CFD}$ can increase.

Summarizing, the driving forces behind variance in $C_{F,\,CFD}$ is always the ship speed and the environmental conditions. When multiple ship types are considered as well, a dependency on the hull shape arises.

Chapter 6

Numerical estimate of hull efficiency

This chapter presents the results of the research on the numerical estimation of the hull efficiency η_H. The aim is to answer to fourth sub-reserach question: "What is the impact of replacing experimental uncertainty by numerical uncertainty on the total uncertainty of $C_{F,CFD}$?". Numerical uncertainty is introduced by numerical errors, and experimental uncertainty by measurements errors. The experimental uncertainty is replaced by numerical uncertainty by using CFD results to computer η_H instead of sea trial measurement results. Equation 3-22 describes η_H mathematically, where thrust deduction factor t and wake fraction w can be computed with CFD or derived from sea trial measurements. To determine t and w numerically was explained in section 3-6.

6-1 Numerical estimate of thrust deduction factor t, wake factor w and hull efficiency η_H

Most of the data available is of the Amels LE180 series. Especially for the appended hull and actuator disk simulations. Hence, the numerical estimation of t, w and η_H has been made for the LE180 series only. In section 3-6 the method to determine the numerical estimates of t and w is explained. The way η_H is determined remains similar, but now it uses the numerical estimates of t and w. The numerical estimates of t, w and η_H are compared to their experimental counterparts in the following subsections.

6-1-1 Numerical estimate of t

In figure 6-1 the scatter plot and corresponding linear fitted trend lines of the numerical and experimental estimate of t are presented. For the entire LE series it is assumed by Damen that t is independent of speed and equal to 0.11. However, when looking at the results of the numerical estimates of t, the tendency is that it depends on the ship speed V_s, t increases as V_s increases. Using equation 3-20, it is concluded that with increasing ship speed V_s, required thrust T increases faster than resistance R. Which is explained by defining T as follows: $T = R_T + R_P$. R_T represent the total ship resistance, as described in section 2-2, and R_P represent the added resistance induced by the propeller. Which is caused by the change in the pressure field. The additional pressure generated by the propeller varies with the speed of the propeller inherent in the ship's speed.

Four clusters of t can be distinguished in figure 6-1, corresponding to the four ship speeds that were measured during sea trials. For the first and second it holds that the scatter is

quite large. While this the scatter in the third cluster and fourth is less. The ship speed in the third cluster corresponds to the design speed of the vessel, and, as explained in section 5-4-1, the grid is designed for the design speed. Thus, the results for that speed are the most accurate. The scatter in the fourth cluster is less because it is closer to the design speed, compared to the speed in the first two clusters.

Another aspect is that there are a few outliers, two of which stand out in particular. They are labeled as outlier in the figure. The outliers belong to the same yardnumer, and are only present in the first and fourth cluster. An explanation lies in the wave making resistance. The waves traveling over the hull of the ship can cause a wave crest or through to be located at the propeller. The wave causes the water particles to move in an orbit, so introducing a circular velocity in the water. If the direction is the same as the sailing direction it has a positive effect on the flow velocity. The inflow velocity has an influence on the delivered thrust by the propeller.

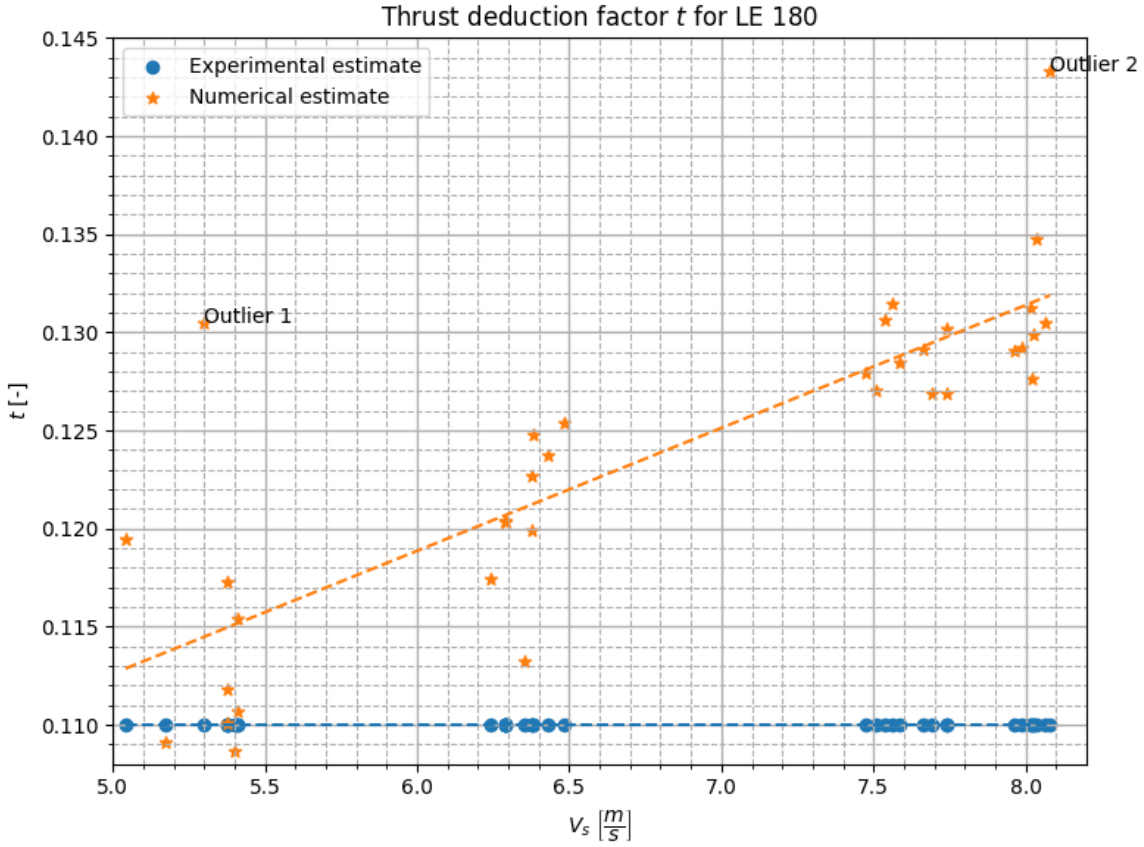

Figure 6-1: Comparison between numerical and experimental calculated t

Two major advantages of computing t with CFD are that there are not any influences of environmental conditions, and that there are no measurement errors present. But now a numerical error is introduced because a numerical model always is a simplification of reality. However, it is better to control and quantify.

6-1-2 Numerical estimate of w

The scatter plots of the numerical and experimental estimate of w are presented in figure 6-2. The trend of the linear fit of the numerical and experimental estimate differs, it is slightly positive for the first while it is slightly negative for the latter. In the book Introduction to Naval Architecture [33, p. 182] it is explained that the wake fraction is almost not affected by the velocity of the ship. Except for vessels with a large wave making component, which explains both trends.

Again, four speed clusters are distinguished, and the scatter of the numerical estimate of w is much smaller than of the experimental estimate. An explanation of the difference in scatter is that the experimental estimate is based on sea trial measurements, so it is influenced by environmental conditions, while the numerical computations are performed in calm water.

The only outlier is present in the numerical estimate of w is negative which means that the advance velocity V_a is greater than V_s. There are several phenomena that cause V_a to be greater than V_s. For example, the presence of sea currents, or the shape of the hull causes the water to accelerate. But since the numerical simulations were performed in calm water, the first explanation is not a possibility. The second explanation does not hold either, because then there should be more negative wake factors. So, it assumed that the computations of the outlier are subject to larger numerical errors. The major advantage of the numerical estimate of w compared to the experimental estimate is the lesser scatter.

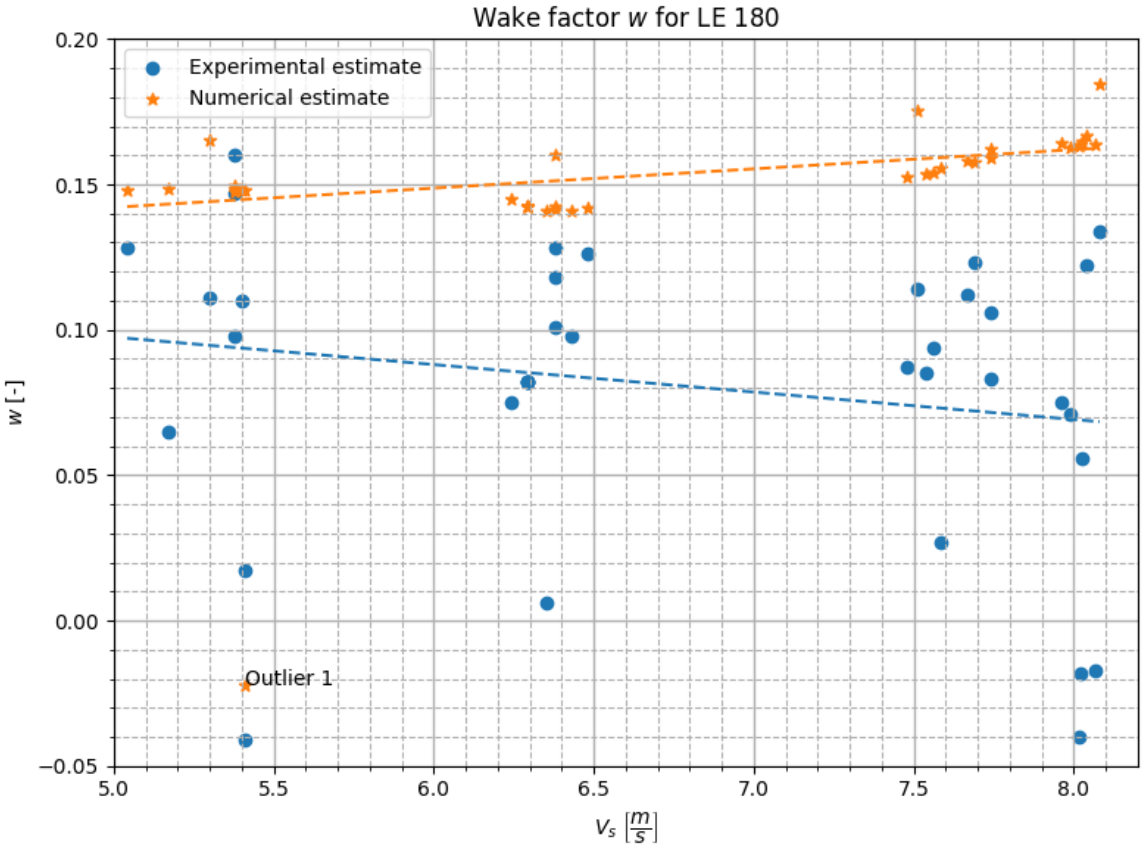

Figure 6-2: Comparison between numerical and experimental calculated w

6-1-3 Numerical estimate of η_H

Finally, the comparison between the numerical and experimental estimate of η_H is performed using a scatter diagram which is presented in figure 6-3. The hull efficiency η_H is calculated with equation 3-22, where t and w are estimated numerically, as explained in section 3-6.

First of all, there is a difference in direction of the trend. The numerical estimate of η_H increases with ship speed, while the experimental estimate decreases with ship speed. The same was seen at w, and combined with the fact that t also increases with speed, the trend of η_H is now positive. Second, the spread of the numerical estimate is smaller than of the experimental estimate, despite the fact that t is no longer constant. It is explained by the lesser scatter in the numerical estimate of w compared to the experimental estimate.

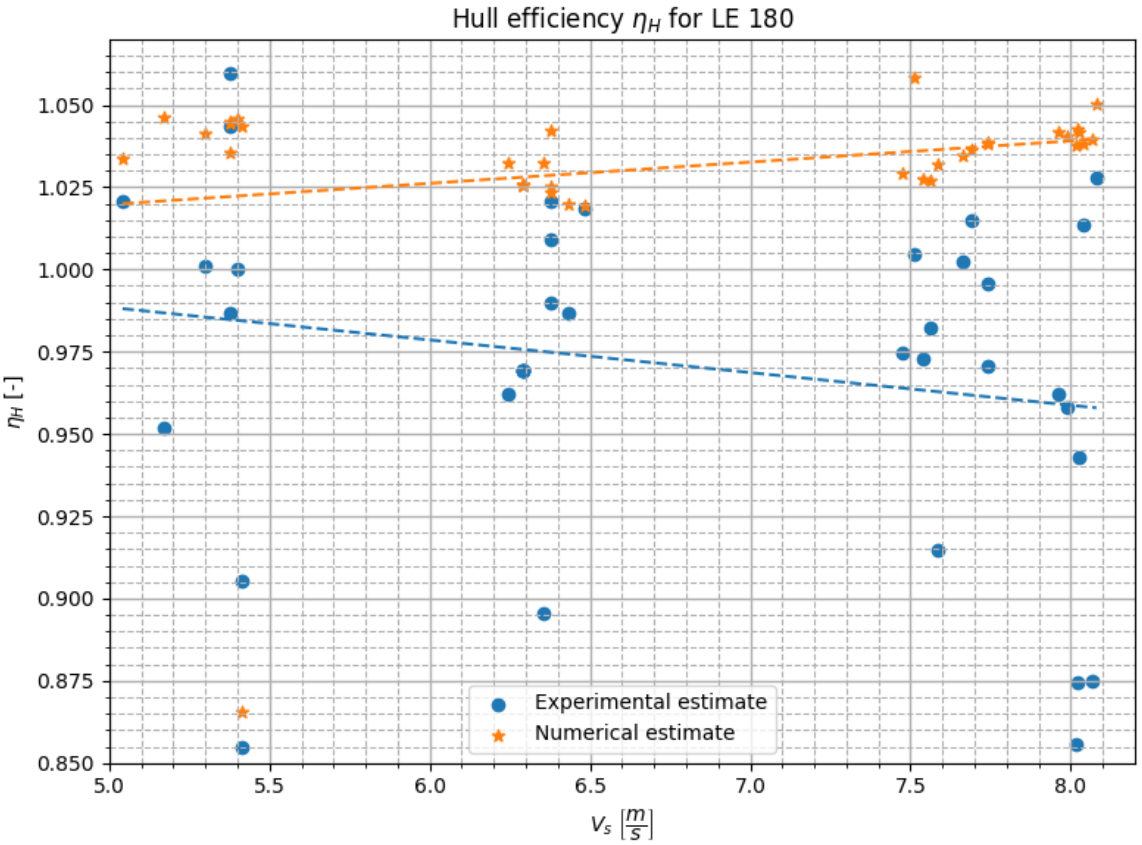

Figure 6-3: comparison between numerical and experimental calculated w

As explained in section 2-8 uncertainty is defined as a function of the accuracy and precision. μ of the dataset represents the accuracy and σ the standard deviation. However, now η_H cannot be defined as a relative error between sea trial measurement and CFD results because it is precisely these that are compared with each other. Therefore, the normalized uncertainty is used to assess the uncertainty, which is given by equation 6-1.

$$\sigma^* = \frac{\sigma}{\mu} \tag{6-1}$$

In table 6-1 μ, σ and σ^* of both the numerical and experimental η_H are presented. The normalized uncertainty of the numerical estimate is one order smaller than the uncertainty of the experimental estimate of η_H. Concluding that the numerical uncertainty is smaller.

Table 6-1: Accuracy and Precision of η_H

	Numerical estimate	Experimental estimate
μ	1.031	0.971
σ	0.009	0.051
σ^*	$8.730*10^{-3}$	$5.252*10^{-2}$

6-2 The uncertainty of $C_{F,CFD}$ based on P_B

In section 6-1 the numerical estimates of t, w and η_H are presented and compared to their experimental counterparts. Now, the effect of replacing the experimental uncertainty by numerical uncertainty on the total uncertainty of $C_{F,CFD}$ is presented. However, in this comparison, $C_{F,CFD}$ is based on break power P_B instead of resistance R. This choice was made because the resistance is derived from the break power using the TAT, which is an Damen in-house developed trial analysis tool. The time was insufficient to change the tool such that the numerical estimates of t and w can be given as input. Thus, equation 3-4 rewritten to equation 6-2. Where either the experimental or numerical estimate of η_H is incorporated in the determination of the required break power $P_{B_{CFD}}$.

$$C_{F,,CFD} = \frac{P_{B_{Trial}} - P_{B_{CFD}}}{P_{B_{CFD}}} \tag{6-2}$$

The accuracy and precision of $C_{F,,CFD}$ are presented in table 6-2. The precision of $C_{F,,CFD}$ improved with roughly 14% when comparing the numerical estimate to the experimental estimate. But the accuracy decreased with approximately 59.4%. In other words, the mean offset increased while the scatter of the offset decreased. At last the normalized uncertainty was evaluated, and the uncertainty based on the numerical estimate of η_H is roughly 3 times smaller compared tot the experimental estimate. Therefore, it can be concluded that replacing the experimental uncertainty by numerical uncertainty reduces the total uncertainty of $C_{F,,CFD}$.

Table 6-2: Accuracy and Precision of $C_{F,CFD}$ based on P_B

	Numerical estimate	Experimental estimate
μ	0.106	0.043
σ	0.114	0.130
σ^*	1.079	3.049

6-3 Conclusion

This chapter is devoted to answering the fourth sub-research question: "What is the impact of replacing experimental uncertainty by numerical uncertainty on the total uncertainty of $C_{F,\,CFD}$?". The replacement is done by computing t and w numerically instead of experimentally. Subsequently, η_H is calculated with equation 3-22. First, the numerical estimates of t, w, and η_H are compared to their experimental counterparts, and the uncertainty of the numerical and experimental η_H is assessed. Second, $C_{F,\,CFD}$ is redefined based on break power P_B. At last, the impact of the replacement on the total uncertainty of $C_{F,\,CFD}$ is evaluated.

The numerical estimate of t shows a dependency on speed. The required thrust T is a function of the total towed resistance R_T and added resistance induced by the propeller R_P. The propeller operations caused the pressure field on the hull to change. Changes in propeller RPM are inherent in changes in ship speed, an increase in RPM usually leads to in increase in ship speed. So, as the ship speed increases R_T and R_P both increase, thus T increases faster than R_T.

The scatter in the numerical estimate of w was less compared to the experimental estimate. The absence of environmental conditions in the numerical estimate explains this. Also, w is approximately constant over the speed, which is confirmed by literature.

The trend of η_H is slightly positive, which is caused by the positive trend of t, and the roughly constant value of w. Also, the scatter of the numerical estimate is much less compared to the experimental estimate. The uncertainty of η_H is assessed by means of the normalized uncertainty. It shows that the numerical uncertainty an order ten smaller compared to experimental uncertainty.

Finally, the impact of replacing experimental uncertainty by numerical uncertainty on the total uncertainty of $C_{F,\,CFD}$ is determined, which was done by comparing the accuracy and precision. It was seen that the accuracy of $C_{F,\,CFD}$ computed with an experimental estimate of η_H is greater, and that the precision of $C_{F,\,CFD}$ based on the numerical estimate is higher. To be conclusive, the normalized uncertainty is compared. The normalized uncertainty of the numerical estimate was three times smaller than that of the experimental estimate. Therefore, it was concluded that the impact of replacing the experimental uncertainty by numerical uncertainty on the total uncertainty is positive.

Chapter 7

CFD based power-speed prediction method with a statistical correction factor

The fifth sub-research question "To what extent can a statistical $C_{F,CFD}$ be used to predict the power-speed relationship?" is answered in this chapter. First, it was investigated if $C_{F,CFD}$ could be described by a normal distribution, and it was said that this is reasonable. Subsequently, the untreated CFD results were investigated and it was discovered that the error between CFD and sea trials changes with the ship speed. So, it was decided to distinguish four speed clusters in the CFD and sea trial results, and a $C_{F,CFD}$ was calculated for every speed cluster. Two correction factors were investigated for a power prediction method. The first was based on the mean of $C_{F,CFD}$ and the second on the value read from a CDF at 95% probability. At last, the two methods were compared on how they perform in predicting the required break power.

7-1 The pre-investigation to the distribution of the data

Before a statistical prediction method could be developed for the CFD correction factor $C_{F,CFD}$, it was investigated if $C_{F,CFD}$ is normally distributed. Before developing a statistical model for the CFD correction factor $C_{F,CFD}$, it was investigated if $C_{F,CFD}$ is normally distributed. The procedure is explained in section 3-4-1, and in this section the results are presented. A Gaussian KDE curve is plotted next to a bell curve based on μ and σ, for both hold that a wider curve represent a larger σ. Additionally, histograms are used to explain deviations the Gaussian KDE plot has from the bell curve. This is executed per simulation type for the LE180 series, the entire LE series and the LE and SX series combined.

Figures 7-1 through 7-3 are used to investigate whether $C_{F,CFD}$ of the LE180 series is normally distributed. The histograms are normalized: the area under the graph sums to one. Figure 7-1 shows the $C_{F,CFD}$ based on bare hull simulations. The Gaussian KDE curve follows the theoretical bell curve well, except that it is more flat. Which is explained with the histogram, the data is somewhat more located to the left of the center. But the distribution approaches the normal distribution. Subsequently, the histogram plot for $C_{F,CFD}$ based on appended hull simulations can be found in figure 7-2. Unfortunately, the data for the appended hull

seems less normally distributed than for bare hull simulation. The Gaussian KDE curve shows a deviation from the bell curve at the center. Using the histogram, it can be concluded that this is because the peak of the data is to the right of the center. Which may be due to the fact that fewer data points are present. However, for the appended hull simulations a normal distribution can be assumed as well. At last, it can be seen that the Gaussian KDE curve of $C_{F,CFD}$ follows the bell curve reasonably. Only the center of de KDE curve is located slightly to the left of the theoretical center. Which is caused by more data being located left of the center. It can be said $C_{F,CFD}$ of the LE180 series of the actuator disk simulations is normally distributed.

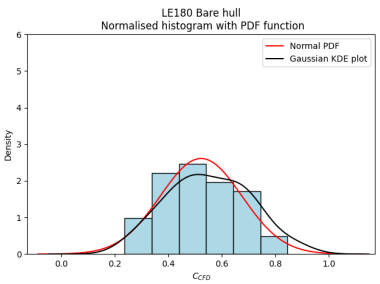

Figure 7-1: Bare hull

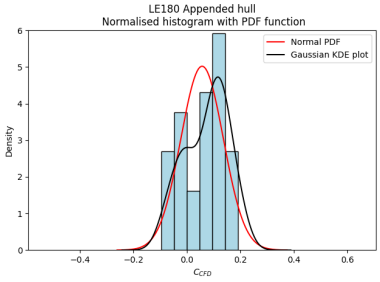

Figure 7-2: Appended hull

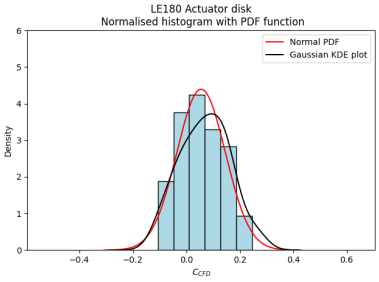

Figure 7-3: Actuator disk

Figures 7-4, 7-5 and 7-6 are used to determine the distribution of $C_{F,CFD}$ for the entire LE series. Figure 7-4 shows the results for the bare hull simulations, the Gaussian KDE curve shows again that it is flattened compared to the theoretical bell curve. With the aid of the histogram it can be seen that it is due to the peak of the data located to the left of the center. Nevertheless, a normal distribution can be assumed. Then, the appended hull simulations presented in figure 7-5 shows that there are two peaks. One left from the center and the other to the right from the center. This is also reflected in the Gaussian KDE plot. It could be caused by the size of the dataset, Despite these observations a normal distribution for was assumed for $C_{F,CFD}$. The plots for $C_{F,CFD}$ corresponding to the actuator disk simulations are presented in figure 7-6. The Gaussian KDE curve follows the bell curve, except that the center is slightly located towards the left.Which is confirmed by the histogram. However, a normal distribution is still acceptable.

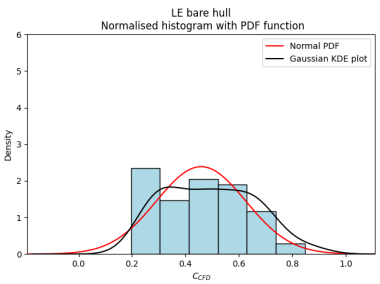

Figure 7-4: Bare hull

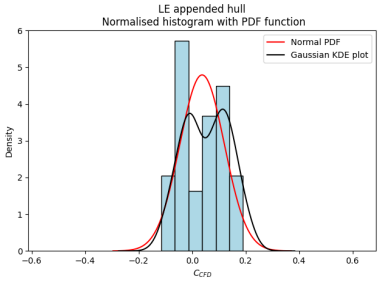

Figure 7-5: Appended hull

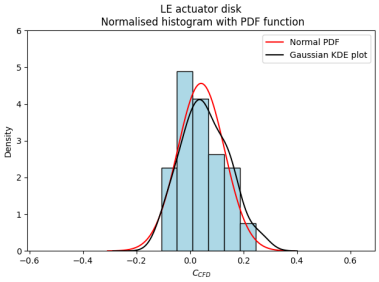

Figure 7-6: Actuator disk

For the Amels SX series only bare hull simulation data was available. Figure 7-7 shows the plots used to investigate the distribution of $C_{F,CFD}$. The left-hand side is less normally distributed than the right-hand side. Due to this the Gaussian KDE curve is flattened compared to the bell curve. However, it is still acceptable to state that the $C_{F,CFD}$ is normally distributed.

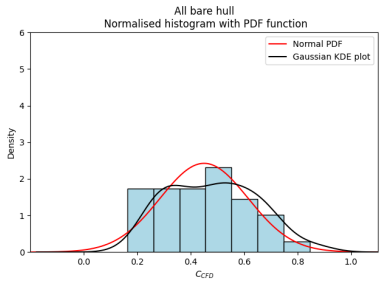

Figure 7-7: Bare hull

As explained in the introduction of this section, the width of a bell curve is the characteristic of the standard deviation. The wider, the higher the standard deviation. In chapter 4 the means and standard deviations of all $C_{F,CFD}$'s were given. For all it holds that the standard deviation of $C_{F,CFD}$ based on the bare hull simulations was the largest, it decreased for appended hull simulations, and then increased again for the actuator disk simulations. This tendency is also seen in figures 7-1 through 7-7.

7-1-1 Conclusion

The distributions of $C_{F,CFD}$ of the bare hull, appended hull and actuator disk simulations were presented in figures 7-1 through 7-7. First, this investigation was performed for $C_{F,CFD}$ of the LE180 series. Because this data set has the least variation in ship main dimensions. Second, the distribution of $C_{F,CFD}$ of the entire LE series was investigated. This was of interested because the effect of more variety in the main dimensions of the ships could be investigated. Third, data of the SX series was combined with the entire LE series to be able to investigate the effect of having even more variety. Now, not only in the main dimensions, but also in the hull form. The investigation led to the conclusion that for all the distributions of $C_{F,CFD}$ it was acceptable to assume a normal distribution.

7-2 Comparing untreated CFD based power to sea trial measured and Holtrop-Mennen based power

In this section the predicted required break power P_B based on the uncorrected resistance computed with CFD simulations is compared to the actual measured P_B during sea trial and to the required P_B based on the Holtrop-Mennen resistance. The power-speed relationships are presented in figure 7-8 for the LE180 series, in figure 7-9 for the entire LE series, and in figure 7-10 for the entire LE and SX series combined. A polynomial curve is fitted over the data so that interpreting the trend is easier. From the figures it is learned that $C_{F,CFD}$ is speed dependent, and in every figure four speed clusters are distinguished. The clusters are explained by sea trial measurements being performed on four different engine settings.

In figure 7-8 the P_B-V_s curves are shown, it can be seen that all three CFD simulations underpredict P_B, especially for lower speeds. This was expected after the analysis of $C_{F,CFD}$ in chapter 4 and section 7-1. The following four speed clusters were distinguished. The first speed cluster is between 5 and 5.5 [m/s], the second between 5.5 and 6.5 [m/s], the third between 6.5 and 7.8 [m/s] and the fourth above 7.8 [m/s]. The trend of the P_B-V_s curve based on the bare hull, appended hull and actuator disk simulations is similar. P_B is always underpredicted based on the bare hull simulations, however, the steepness of the P_B-V_s curve increases after the third cluster for the bare hull simulations. Considering the prediction based on the appended hull and actuator disk simulations, P_B is underpredicted in the first two speed clusters and an overprediction starts to arise after the third speed cluster. The increase in steepness causes the trends to deviate from the sea trial measurement based P_B-V_s curve. The power-speed curve corresponding to the untreated Holtrop-Mennen resistance prediction also underpredicts P_B, but the trend of the curve is more like the sea trial measurement based power-speed curve, automatically deviating from the P_B-V_s curves based on the CFD simulations. Compared to the bare hull simulations, it performs better as it is closer to the sea trial measurements. The performance in the first two speed clusters is comparable to the appended hull and actuator disk simulations, after which the steepness of the CFD simulations increases more sharply and a larger difference emerges.

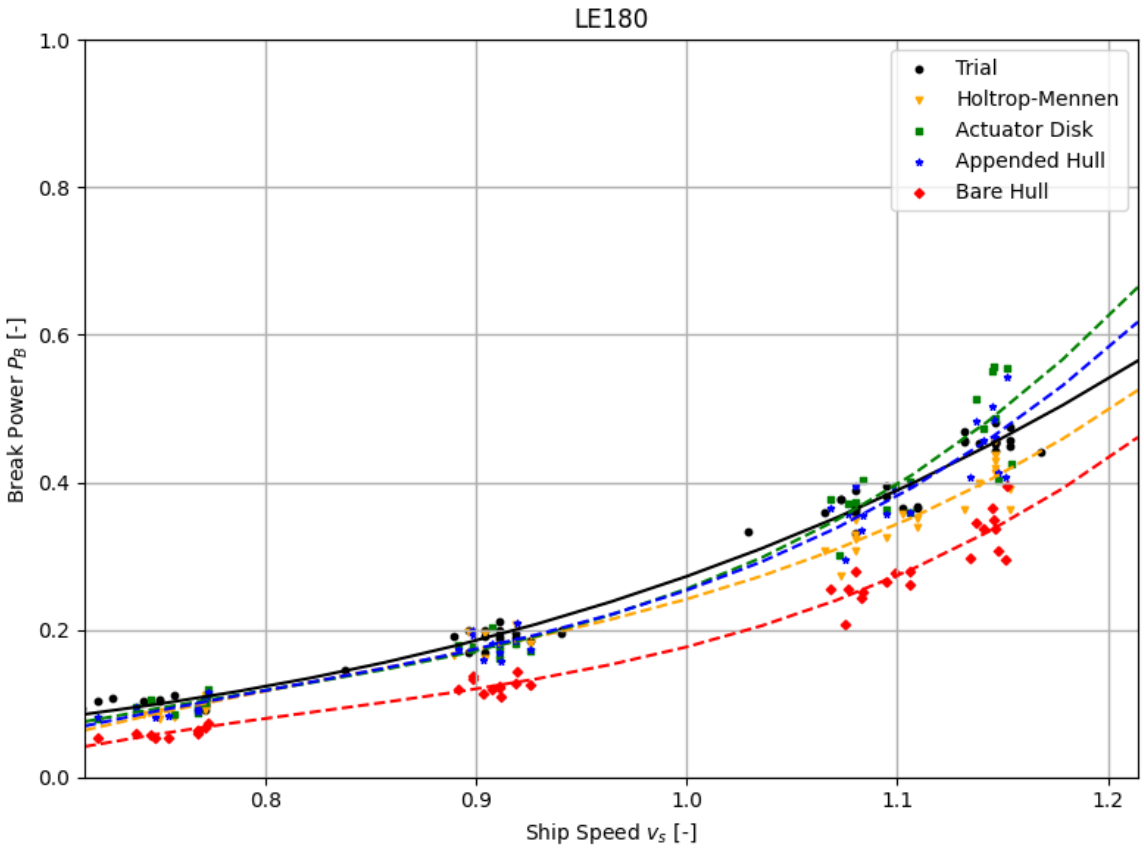

Figure 7-8: P_B-V_s diagrams with untreated CFD

In figure 7-9 the results for the entire LE series are presented. Unfortunately, there are fewer data points for the CFD results present in the speed zone above 7 [m/s] and together with the larger spread of the data, the analysis is more difficult. Still, it can be seen that the power is underpredicted for the entire speed range. Now, the first speed cluster is between 5 and 6 [m/s], the second between 6 and 7 [m/s], the third between 7 and 7.8 [m/s] and the last above 7.8 [m/s]. For all CFD based P_B-V_s curves it can be said that they underpredict the power measured during trial. The trend of the P_B-V_s curves of the bare hull and appended hull simulations follows the trend of sea trial measurement curve. While this cannot be said for the actuator disk simulations, where the trend deviates from the sea trial measurements after the third speed cluster. In all CFD-based curves, a wobbly behavior can be seen between the first and the second cluster. It is expected that this is caused by the absence of data points below 5 [m/s]. The power-speed curve based on Holtrop-Mennen resistance also underpredicts P_B compared to the sea trial measurements. The trend is comparable to the appended and bare hull simulations, and thus also deviates from the actuator disk simulations.

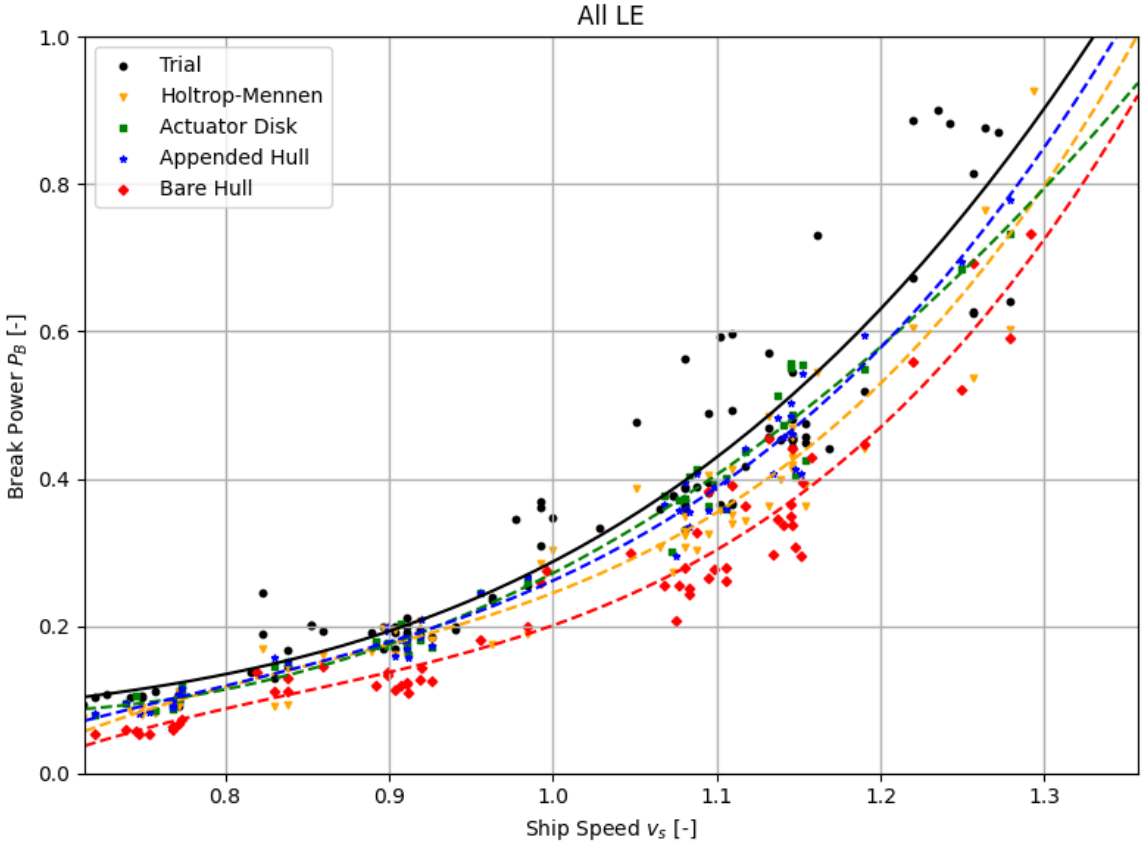

Figure 7-9: P_B-V_s diagrams with untreated CFD

The power-speed curves for the entire LE and SX series combined are presented in figure 7-10. Only bare hull simulations were available for the SX series. The same four speed clusters as for the entire LE series were used in this analysis. It can be seen that the P_B-V_s curve of the bare hull simulations always underpredicts P_B compared to the sea trial measurements.

The underprediction is less in the first two speed clusters, and increases at the third cluster and then decreases again in the fourth. As with the entire LE series, wobbly behavior can be seen between the first and the second cluster, which is due to the same cause. The P_B-V_s curve based on the Holtrop-Mennen calculation also underpredicts P_B compared to the sea trial measurements, but it performs better compared to the bare hull simulations. Also, the trend of the Holtrop-Mennen curve is more comparable to the sea trial measurements as for the bare hull simulations.

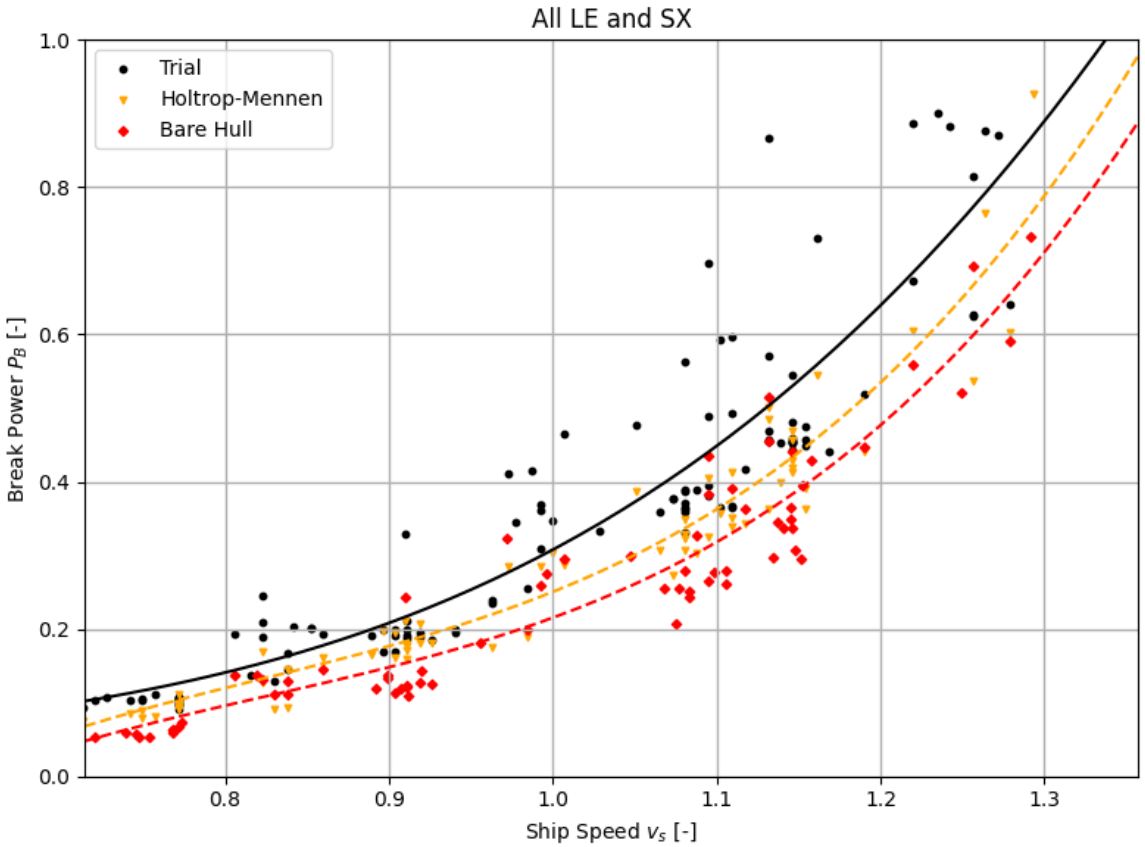

Figure 7-10: P_B-V_s diagrams with untreated CFD

7-3 Power-Speed curves with speed-dependent mean correction on CFD computed resistance

Power-speed curves based on corrected resistance predictions are presented in this section. The results of the LE180 series, the entire LE series and the entire LE and SX series are discussed separately. The speed clusters derived in section 7-2 are used. The $C_{F,CFD}$ is determined per speed cluster, and now it is based on the sample mean $\overline{X}$ instead of the population mean σ because every cluster is a sample of the entire population. The CFD simulations based predictions, consisting of bare hull, appended hull and actuator disk simulations, are compared to the measured P_B and to the Holtrop-Mennen based power prediction. The Holtrop-Mennen based power-prediction results are corrected according to the Damen standards: 12% increase of resistance and 5% decreases on the ship speed.

In table 7-1 the sample means of $C_{F,CFD}$ per speed cluster are presented. It shows that for all simulation types $\overline{X}$ decreases per speed cluster step. This was expected after the analysis in section 7-2. The positive values of $\overline{X}$ indicate an underprediction of the measured power by the CFD simulations. The negative $\overline{X}$ of the fourth speed cluster of the actuator disk simulations implies an overprediction.

Table 7-1: Speed dependent $\overline{X}$ of $C_{F,CFD}$ for the LE180

	Bare	Appended	Actuator
$\overline{X}$ of $C_{F,CFD}$ speed cluster 1	0.7177	0.1162	0.1380
$\overline{X}$ of $C_{F,CFD}$ speed cluster 2	0.5925	0.1040	0.1011
$\overline{X}$ of $C_{F,CFD}$ speed cluster 3	0.4743	0.0485	0.0300
$\overline{X}$ of $C_{F,CFD}$ speed cluster 4	0.4030	0.0185	-0.0079

The P_B-V_s curves for the LE180 series are presented in figure 7-11. The trend of the bare hull, appended hull and actuator disk simulations follows the trend of the sea trial measurements. Except that a small overprediction arises at the fourth speed cluster. The break power is always overpredicted by the Holtrop-Mennen method with Damen standard corrections. Also, the trend deviates more from the sea trial measured trend than the CFD simulations do.

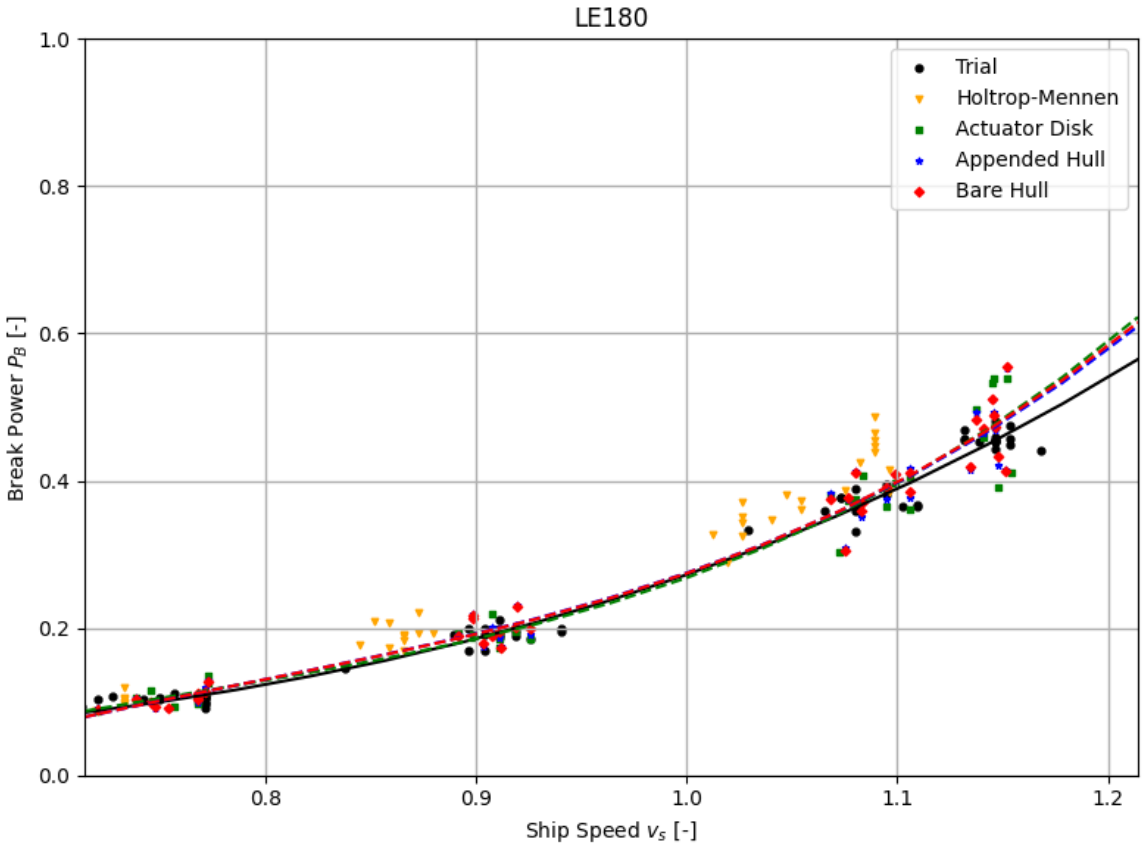

Figure 7-11: P_B-V_s diagrams with $\overline{X}$ based $C_{F,CFD}$

The $\overline{X}$ of $C_{F,\,CFD}$ per speed cluster for the entire LE series are presented in table 7-2. It shows that per speed cluster the required correction becomes less, which is in line with results presented in section 7-2. Again, the required correction in the fourth speed cluster for the actuator disk simulations is negative.

Table 7-2: Speed dependent $\overline{X}$ of $C_{F,\,CFD}$ for the entire LE series

	Bare	Appended	Actuator
$\overline{X}$ of $C_{F,\,CFD}$ speed cluster 1	0.7177	0.1162	0.1380
$\overline{X}$ of $C_{F,\,CFD}$ speed cluster 2	0.5390	0.0787	0.0781
$\overline{X}$ of $C_{F,\,CFD}$ speed cluster 3	0.4189	0.0380	0.0316
$\overline{X}$ of $C_{F,\,CFD}$ speed cluster 4	0.3964	0.0038	-0.0053

The power-speed relationships for the sea trial measurements, the three CFD simulations and the Holtrop-Mennen prediction for the entire LE series are presented in figure 7-12. What strikes first is that the predictions based on the CFD simulations of the entire LE series are less accurate compared to the LE180 series. It is caused by a larger variance in ship main dimensions, and fewer data available on the other ship types than on the LE180. The trend of the bare hull, appended hull and actuator disk simulations deviates from the sea trial measurements on various aspects. For all three, there is wobbly behavior around the first two clusters, which does not appear in the data from the sea trials. It is due to the absence of data below the speed of 5 [m/s], causing the polynomial fit to be incorrect in that region. The P_B-V_s curve of the bare hull simulations is overpredicted compared to the sea trial measurements at the second cluster, then the overprediction shrinks at the third cluster and starts to grow again at the fourth. The appended hull and actuator disk simulation based P_B-V_s curves are close to the sea trial based curve between the first two clusters, but starts to underpredict the required P_B afterwards. Then, the trend of the power speed curve based on the appended hull simulations roughly follows the sea trial based trend. While the trend based on the actuator disc simulations deviates even further. The Holtrop-Mennen based P_B is always overpredicted compared to sea trial results and CFD simulations. The trend also differs from both.

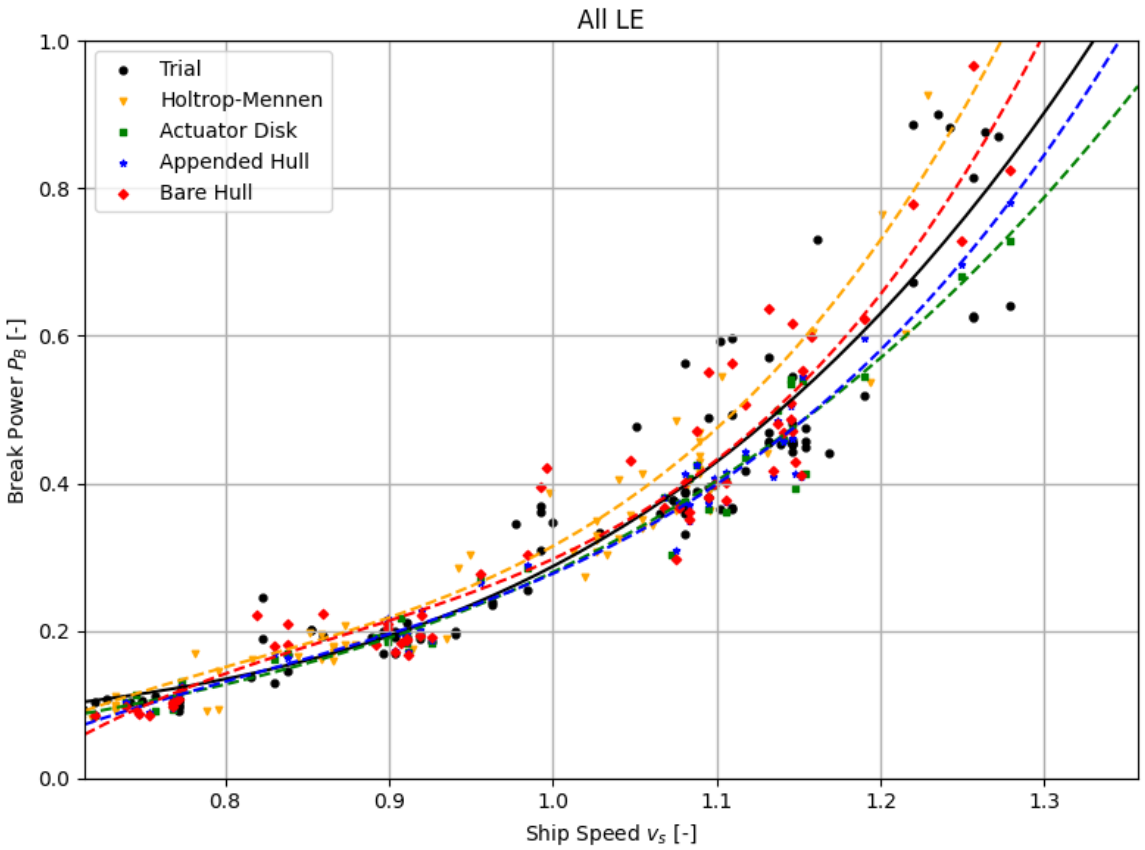

Figure 7-12: P_B-V_s diagrams with $\overline{X}$ based $C_{F,\,CFD}$

Finally, the results of the entire LE and SX series are discussed. As said, only the bare hull simulations were available for the SX series. The sample means per speed cluster are presented in table 7-3. Again, the required correction decreased per speed cluster step.

Table 7-3: Speed dependent $\overline{X}$ of $C_{F,\,CFD}$ for the entire LE and SX series

	Bare	Appended	Actuator
$\overline{X}$ of $C_{F,\,CFD}$ speed cluster 1	0.6887	-	-
$\overline{X}$ of $C_{F,\,CFD}$ speed cluster 2	0.5150	-	-
$\overline{X}$ of $C_{F,\,CFD}$ speed cluster 3	0.4187	-	-
$\overline{X}$ of $C_{F,\,CFD}$ speed cluster 4	0.4057	-	-

In figure 7-13 the P_B-V_s curves are presented. The inclusion of the SX series leads to even more spread in the data. A similar trend in the bare hull simulations as in figure 7-12 is seen, there is wobbly behavior between the first and second cluster. After which the prediction comes closer to the measured curve. But then, the steepness increases again, and the trend deviates more. The Holtrop-Mennen based curve shows comparable behavior as the curve based on CFD. Although, it deviates even more from the sea trial based curve after the third cluster. The fact that both curves deviate so much from the sea trial measurement curve is explained by the absence of data that represent the other vessel types than LE180 series.

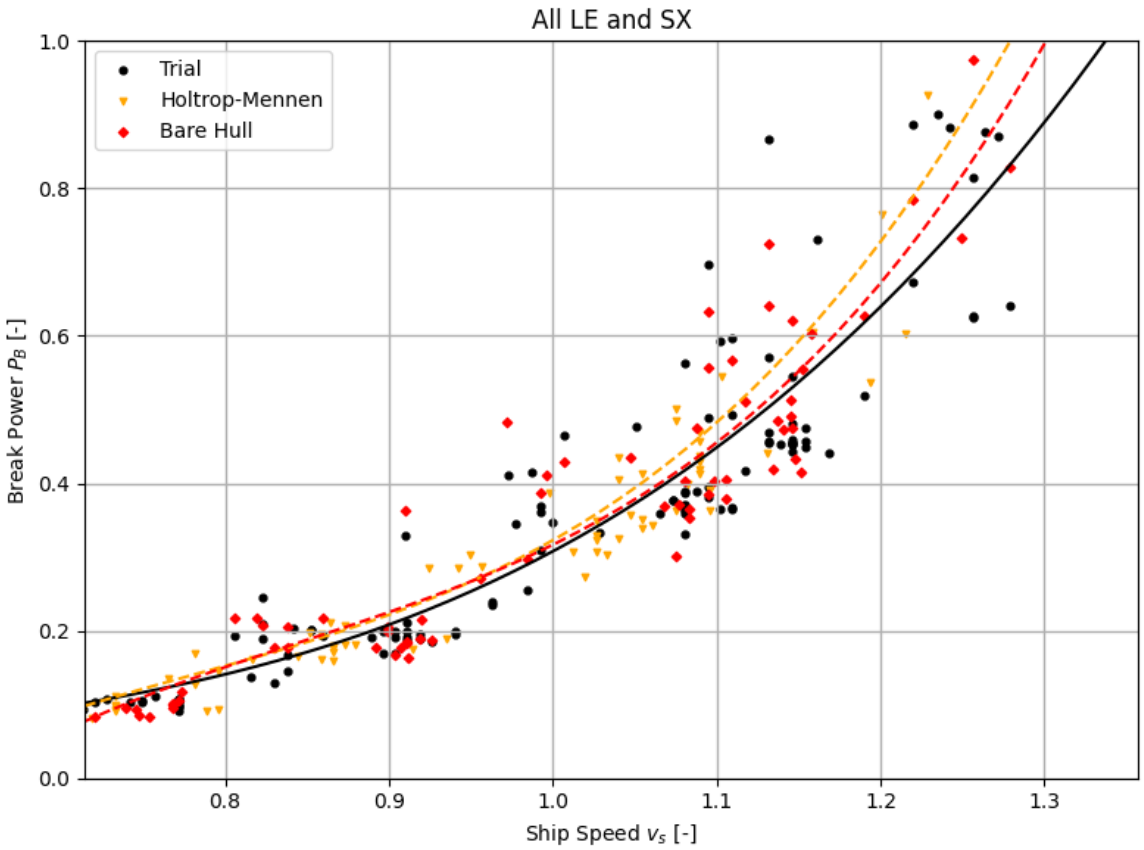

Figure 7-13: P_B-V_s diagrams with $\overline{X}$ based $C_{F,\,CFD}$

7-3-1 Conclusion

The strength of the CFD based power-speed prediction with a speed dependent $C_{F,\,CFD}$ depends on the dataset. The CFD simulations for the LE180 can predict the P_B-V_s relationship accurately. While this is true to a lesser extent for the entire LE series, and the entire LE and SX series. The reason behind this is that the scatter in the plots was larger compared to the plots of the LE180 series, which in place is caused by the absence of available data describing the greater variance in ship main dimensions and ship speeds. Thus, more data from ship types other than the LE180 series are required to improve power speed predictions.

7-4 Power-Speed curves with a speed-dependent correction factor derived from a CDF

In this section the performance of the second correction factor is discussed. Now, $C_{F,\,CFD}$ is determined using a cumulative density function (CDF). In section 7-1 it was concluded that a normal distribution can be assumed for all $C_{F,\,CFD}$. Thus, the CDF's are also normally distributed, as explained in section 3-4. As $C_{F,\,CFD}$ was divided into four speed clusters, they became subsets of the entire distribution. Therefore, the Student's t-distribution is used to describe the CDF's per speed cluster. $C_{F,\,CFD}$ is determined by reading the value at 95%

probability on the CDF plot. This was explained in further detail in section 3-4. A probability of 95% means that for 95% of the cases the correction ensures no underprediction, in other words it can be said that the risk of underpredicting the power-speed curve is equal to 5%. For all three of the series, the bare hull, appended hull and actuator disk simulation based power-speed curve predictions are compared to the curve measured during sea trial, and to the curve determined with the Holtrop-Mennen method. First the CDF's and corresponding $C_{F,\,CFD}$ are presented, and subsequently the power-speed diagrams are shown.

The CDF's per speed cluster corresponding to the LE180 series are presented in figure 7-14. The location of a CDF corresponds to the accuracy of $C_{F,\,CFD}$, the closer towards zero, the higher the accuracy. The precision is represented by the steepness of the CDF, the steeper, the more precise. The accuracy and precision of the bare hull simulations are worse at every speed cluster compared with the appended hull and actuator disk simulations. The accuracy and precision of the appended hull and actuator disk simulations are comparable.

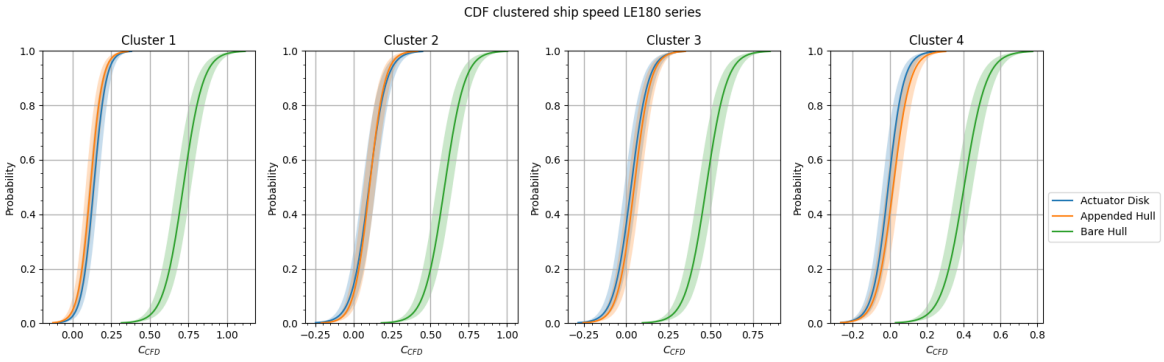

Figure 7-14: CDF's per speed cluster corresponding to the LE180 series

The $C_{F,\,CFD}$'s derived using the CDF's are presented in table 7-4. As for the $\overline{X}$ based $C_{F,\,CFD}$, it decreases every speed cluster. As expected, the largest correction is needed on the bare hull simulations, and the correction on the appended hull and actuator disk simulation is comparable. What stands out is that $C_{F,\,CFD}$ increases at the second speed cluster for the appended hull and actuator disk simulations. Which was not directly expected based on figure 7-8. The mean of $C_{F,\,CFD}$ in the second speed cluster is comparable to that of the first cluster, but the variance is larger. Resulting in a less steep CDF and a wider uncertainty band. Which leads to an increase in the correction factor.

Table 7-4: Speed dependent $C_{F,\,CFD}$ derived from a CDF for the LE180 series

	Bare	Appended	Actuator
CDF based $C_{F,\,CFD}$ speed cluster 1	0.9288	0.2441	0.2667
CDF based $C_{F,\,CFD}$ speed cluster 2	0.8097	0.2689	0.2853
CDF based $C_{F,\,CFD}$ speed cluster 3	0.6736	0.2081	0.1950
CDF based $C_{F,\,CFD}$ speed cluster 4	0.5994	0.1685	0.1272

In figure 7-15 the power-speed diagrams corresponding to the LE180 are presented. The power is overpredicted in all four speed clusters for all three of the CFD simulation types. The trend

of all three of the CFD simulations types follows the P_B-V_s curve based on the sea trial results up until the second speed cluster, after which they start to deviate. In order to reduce the overprediction, two solutions are present. The first is to reduce the standard deviation of $C_{F,CFD}$, which causes a steeper CDF. Secondly, accept a larger risk of underprediction. A lower value of $C_{F,CFD}$ corresponds to a larger risk. The Holtrop-Mennen based power-speed prediction is equal to which was seen in figure 7-11, and is almost identical to the three CFD simulation based P_B-V_s curves.

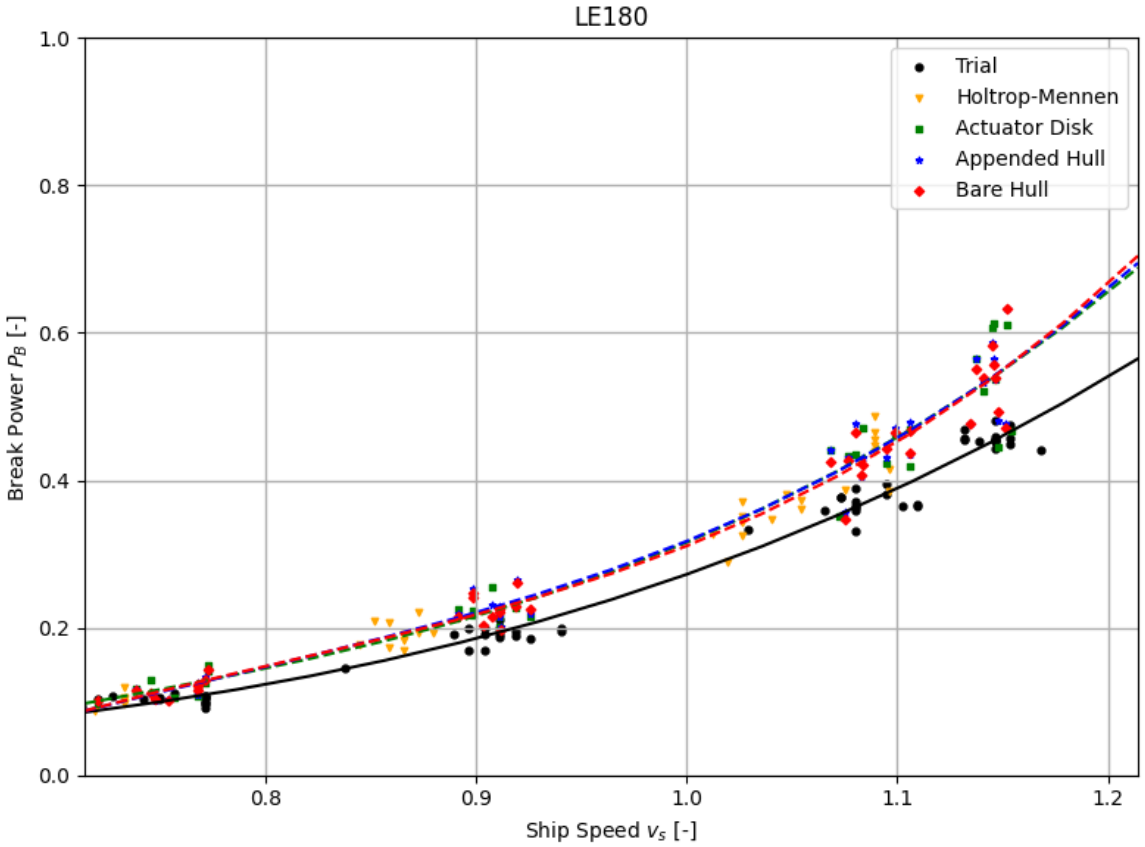

Figure 7-15: P_B-V_s diagrams with CDF based $C_{F,CFD}$

Figure 7-16 shows the CDF's per speed cluster of the entire LE series. The investigation to the accuracy and precision of $C_{F,CFD}$ presented in chapter 4 showed that especially the precision worsened as more different ship types were included. This is confirmed by comparing figure 7-16 to figure 7-14 where the CDF's corresponding to the LE180 series are showed. Considering the entire LE series, it is clear to see that the accuracy and precision of the bare hull simulations is the least and that the appended hull and actuator disk simulations perform similarly.

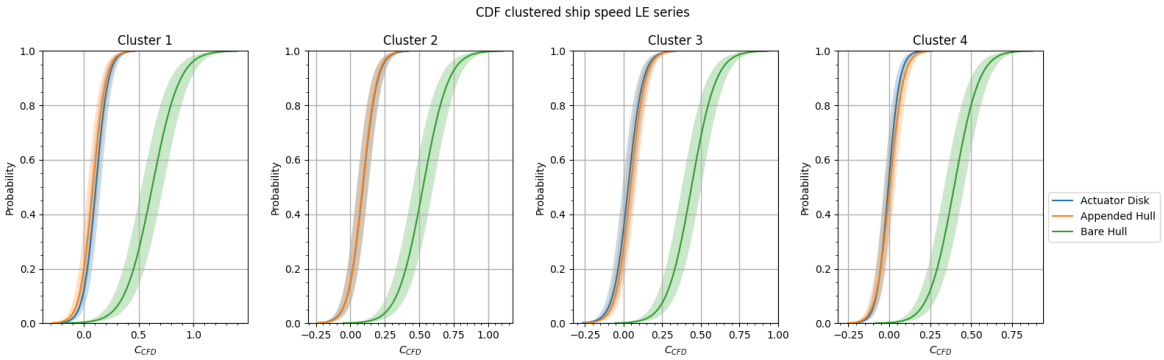

Figure 7-16: CDF's per speed cluster corresponding to the entire LE series

Table 7-5 shows the $C_{F,CFD}$'s derived from the CDF's corresponding to the entire LE series. The increase of $C_{F,CFD}$ at the second speed cluster, that was seen for the LE180 series, is not present in the entire LE series dataset.

Table 7-5: Speed dependent $C_{F,CFD}$ derived from a CDF for all the LE series

	Bare	Appended	Actuator
95% probability $C_{F,CFD}$ speed cluster 1	1.0344	0.2779	0.2960
95% probability $C_{F,CFD}$ speed cluster 2	0.8324	0.2600	0.2635
95% probability $C_{F,CFD}$ speed cluster 3	0.7006	0.1978	0.1850
95% probability $C_{F,CFD}$ speed cluster 4	0.6508	0.1388	0.1095

The power-speed diagrams corresponding to the entire LE series dataset are presented in figure 7-17. It can be seen that the P_B-V_s relationship is well predicted in the first speed cluster for all three of the CFD simulations, subsequently an overprediction arises at the second speed cluster. Then the overprediction slightly reduces between the second and the beginning of the third cluster. From there the trends of the three CFD simulation types differ. The trend of the P_B-V_s curve moves further away from the measured P_B-V_s curve in terms of a greater overprediction. The overprediction by the appended hull and actuator disk based simulations decreases up until the fourth speed cluster. Then even an underprediction of P_B occurs based on the actuator disk simulations. The Holtrop-Mennen based power-speed curves does not follow the trend of the trial measurements either. Initially, it follows the trend of the appended hull and actuator disk simulation, but at the second cluster it starts to follow the trend of the bare hull simulations. The number of data points that were used for fitting the polynomials of all thee the CFD simulations and the Holtrop-Mennen based prediction is half as much as was used for the sea trial measurements. This may be a reason for the fact that the trends do not follow the trend of the measurements accurately.

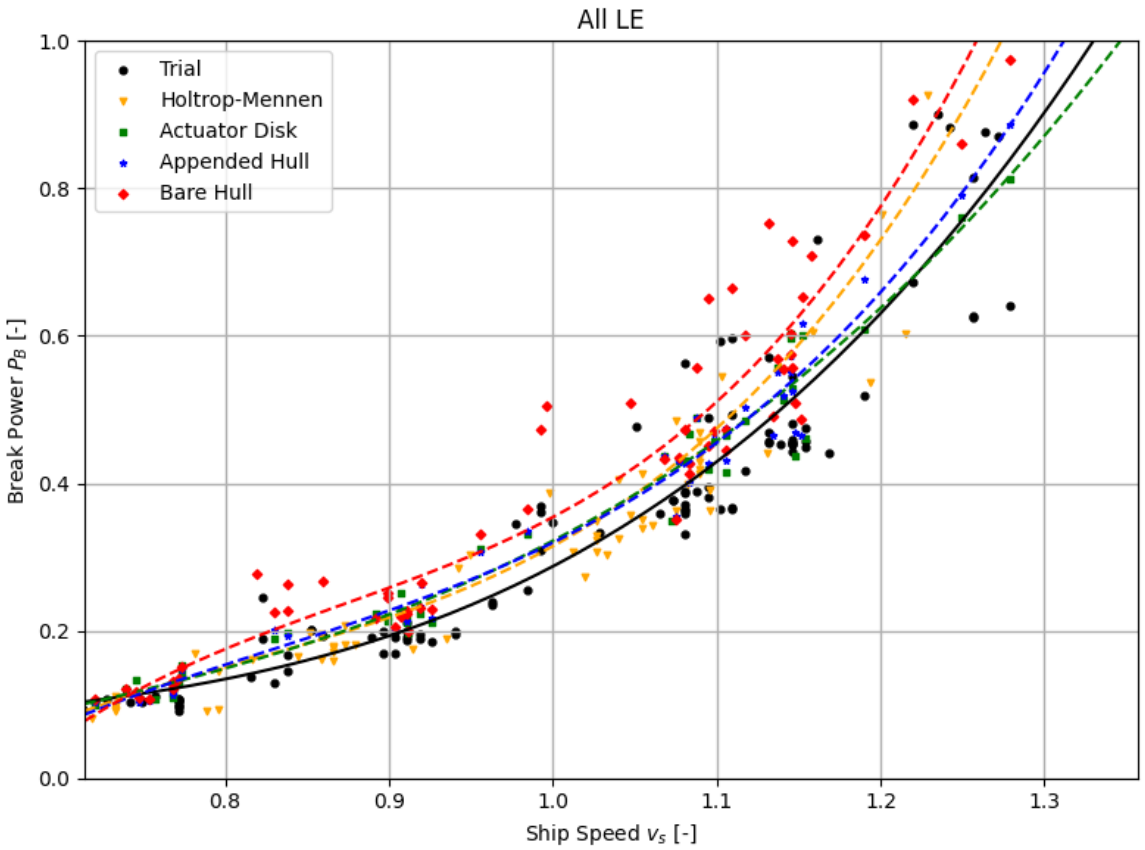

Figure 7-17: P_B-V_s diagrams with CDF based $C_{F,\,CFD}$

At last, the power-prediction for the entire LE and SX series are discussed. The CDF's per speed cluster are presented in figure 7-18. The accuracy and precision is comparable as to that of the bare hull simulations for the entire LE series, presented in figure 7-16.

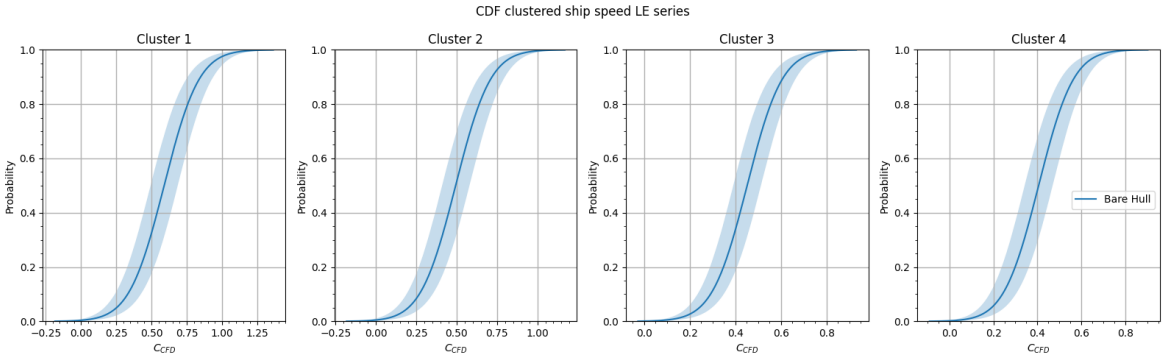

Figure 7-18: CDF's per speed cluster corresponding to the entire LE and SX series

The $C_{F,\,CFD}$'s derived from the CDF's are shown in table 7-6. It can be seen clearly that $C_{F,\,CFD}$ decreases every speed cluster step. This is caused by the fact that the accuracy and precision becomes larger at higher speeds.

Table 7-6: Speed dependent CDF based $C_{F,\,CFD}$ for all the LE and SX series

	Bare	Appended	Actuator
95% probability $C_{F,\,CFD}$ speed cluster 1	0.9971	-	-
95% probability $C_{F,\,CFD}$ speed cluster 2	0.8501	-	-
95% probability $C_{F,\,CFD}$ speed cluster 3	0.7042	-	-
95% probability $C_{F,\,CFD}$ speed cluster 4	0.6661	-	-

Figure 7-19 shows the P_B-V_s curves based on the sea trial measurements, the bare hull simulation and the Holtrop-Mennen method. Both the trend of the bare hull simulation and Holtrop-Mennen based curve deviate from the measured curve, especially after the third cluster. Also, they both overpredict the required break power. This can be explained by the same cause as earlier given for the entire LE series. The number of data points of the bare hull simulation and Holtrop-Mennen method is much less compared to the sea trial measurements.

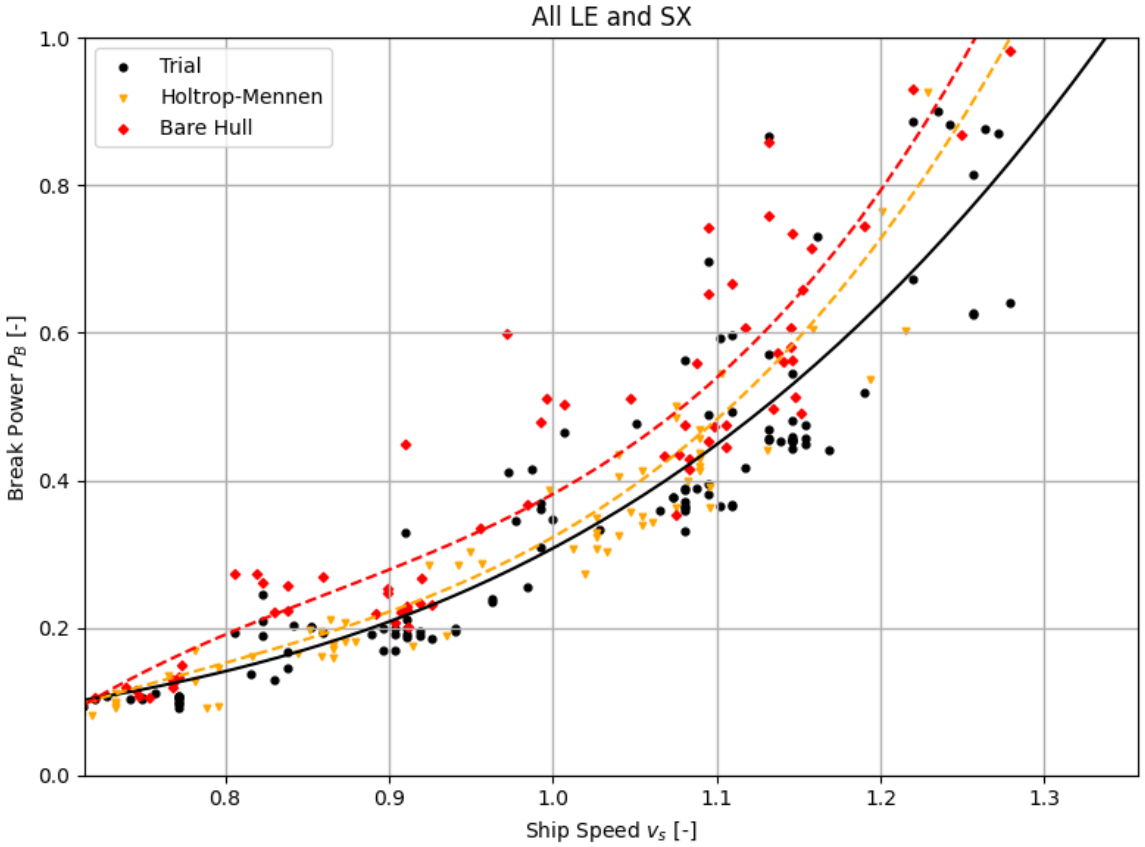

Figure 7-19: P_B-V_s diagrams with CDF based $C_{F,\,CFD}$

7-4-1 Conclusion

Overall it was seen that the power-speed relation based on CFD with $C_{F,\,CFD}$ derived from CDF overpredicts the sea trial measurements. Only the trend of both the Holtrop-Mennen and CFD simulations based prediction for the LE180 series follows the trend of the sea trial measurements. The trends of the other two series do not follow the trend of the sea trial measurements. It was explained by the fact that number of data points was too little for an accurate prediction. It can be concluded that a correction factor drawn from the current CDF's at 95% probability is too conservative. If the accuracy and precision of $C_{F,\,CFD}$ is increased, it may lead to a better prediction of the power-speed relation.

7-5 Comparison of two statistical correction factors

The performance of two statistical corrections factors for CFD based power speed predictions were investigated. The correction factor is the relative difference between the resistance measured during sea trial and the resistance calculated with the CFD. This is mathematically described with equation 3-4. Section 7-3 shows the performance of $C_{F,\,CFD}$ based on the sample mean $\overline{X}$, and section 7-4 shows it of a $C_{F,\,CFD}$ derived from a CDF. In this section both statistical $C_{F,\,CFD}$'s are compared on the accuracy and precision of the predicted P_B. The relative error between the measured and predicted P_B is computed, and μ represent the accuracy and σ the precision.

Table 7-7 presents μ and σ of both the statistical correction methods for the LE180 series. As expected, the precision of both methods is the same. The statistical correction is constant per speed cluster, thus it does not affect the variance of the data. The accuracy of the $\overline{X}$ based $C_{F,\,CFD}$ is comparable for all three of the CFD simulations types. Which is also true for the accuracy of the $C_{F,\,CFD}$ derived from a CDF. The accuracy of the bare hull simulations of the $\overline{X}$ based $C_{F,\,CFD}$ is approximately 6.8 times better compared to the accuracy of the $C_{F,\,CFD}$ derived from CDF, the accuracy of the appended hull simulations roughly 7.2 times better, and of the actuator disk simulations almost 6 times better.

Table 7-7: Comparison of accuracy and precision between the two correction factors

	Bare Hull	Appended Hull	Actuator Disk
μ of $\overline{X}$ based $C_{F,\,CFD}$	-0.0198	-0.0199	-0.0246
μ of $C_{F,\,CFD}$ derived from CDF	-0.1352	-0.1412	-0.1469
σ of $\overline{X}$ based $C_{F,\,CFD}$	0.1019	0.1065	0.0976
σ of $C_{F,\,CFD}$ derived from CDF	0.1019	0.1065	0.0976

The scatter diagrams of the relative error between measured and calculated P_B corresponding to the LE180 series are presented in figures 7-20, 7-21 and 7-22. The plots confirm that the accuracy of $C_{F,\,CFD}$ is greater, and also that the variance of both correction factors is equal.

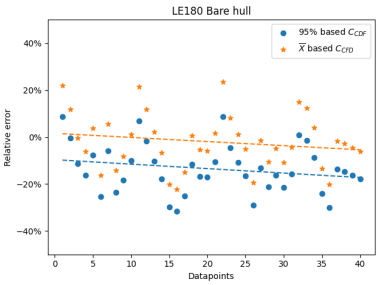

Figure 7-20: Bare hull LE180

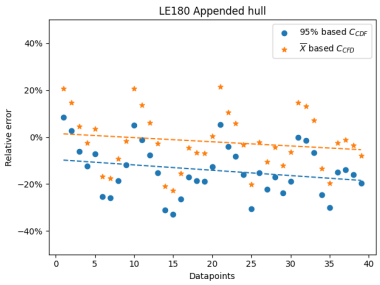

Figure 7-21: Appended hull LE180

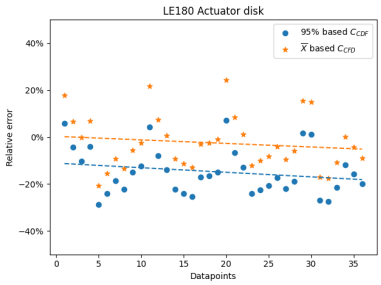

Figure 7-22: Actuator disk LE180

In table 7-8 the accuracy and precision of the statistical correction methods are presented for the entire LE series. As for the LE180 series, the precision of both correction factors is equal, and the accuracy of the predicted P_B with a correction based on the $\overline{X}$ of $C_{F,CFD}$ is greater. Both the accuracy of bare hull and appended hull simulations is roughly 5.6 times better, and the accuracy of the actuator disk approximately 4.6 times.

Table 7-8: Comparison of accuracy and precision between the two correction factors

	Bare Hull	Appended Hull	Actuator Disk
μ of $\overline{X}$ based $C_{F,CFD}$	-0.0345	-0.0280	-0.0340
μ of $C_{F,CFD}$ derived from CDF	-0.1966	-0.1575	-0.1581
σ of $\overline{X}$ based $C_{F,CFD}$	0.1104	0.1059	0.0951
σ of $C_{F,CFD}$ derived from CDF	0.1104	0.1059	0.0951

The scatter diagrams for the entire LE series are presented in figures 7-23, 7-24 and 7-25. In the diagrams it can be seen that the variance in the relative error of both prediction of P_B is similar, and that P_B is heavier overpredicted by the method with a correction factor derived from the CDF.

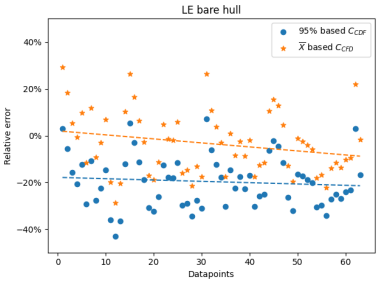

Figure 7-23: Bare hull all LE

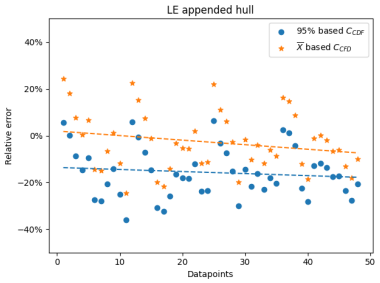

Figure 7-24: Appended hull all LE

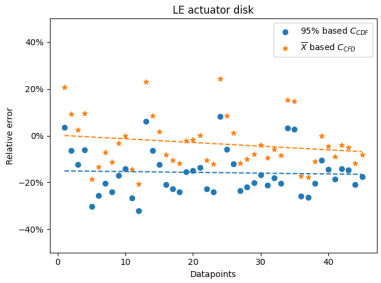

Figure 7-25: Actuator disk all LE

At last, the performance of the entire LE and SX series is discussed. Table 7-9 presents μ and σ. The accuracy of the predicted P_B with a $C_{F,CFD}$ based on $\overline{X}$ is about 7.8 times greater than with a $C_{F,CFD}$ derived from the CDF, and the precision of both predictions is identical.

Table 7-9: Comparison of accuracy and precision between the two correction factors

	Bare Hull	Appended Hull	Actuator Disk
μ of $\overline{X}$ based $C_{F,CFD}$	-0.0252	-	-
μ of $C_{F,CFD}$ derived from CDF	-0.1961	-	-
σ of $\overline{X}$ based $C_{F,CFD}$	0.1114	-	-
σ of $C_{F,CFD}$ derived from CDF	0.1114	-	-

Figure 7-26 shows the scatter diagrams with the predicted break power of the bare hull simulations of the entire LE and SX series. Again, the scatter plot confirms what is presented in table 7-9.

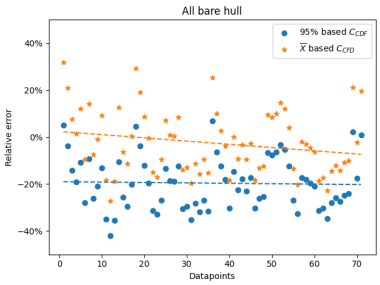

Figure 7-26: Bare hull all LE/SX

Summarizing, the precision of both predicted P_B is equivalent, while the accuracy differs. The accuracy of P_B computed with a $C_{F,CFD}$ based on $\overline{X}$ is greater than with a $C_{F,CFD}$ derived from a CDF. How much greater the accuracy is, depends on the simulation type and vessel series.

7-6 Chapter Conclusion

In this chapter the results of the investigation on the performance of a power prediction method based on full-scale RANSe CFD with a statistical $C_{F,\,CFD}$ are presented. First, it was investigated if $C_{F,\,CFD}$ could be described with a normal distribution. Second, the uncorrected CFD results were presented and inspected. Third, the power-speed relationship was predicted based on CFD results with a sample mean $\overline{X}$ based $C_{F,\,CFD}$. Afterwards, the same analysis was performed but then for a $C_{F,\,CFD}$ derived from a CDF. Finally, the two power-prediction methods were compared by inspecting the relative error between the predicted and measured break power P_B.

A histogram plot combined with a Gaussian KDE plot and theoretical bell curve were used to evaluate if $C_{F,\,CFD}$ is normally distributed. In general, all $C_{F,\,CFD}$ followed the bell curve, although some deviations were seen. Nevertheless, it was concluded that it is reasonable to state that all $C_{F,\,CFD}$ can be described with a normal distribution.

From the analysis of the uncorrected CFD based power-speed relations, it was discovered that the error between predictions and measurements was speed dependent. The error was larger for lower ship speeds, then decreased as the ship speed increased. Which was explained earlier in section 5-4-1; the grid is designed for the design speed of the vessel, so larger numerical errors may arise at other ship speeds. The $C_{F,\,CFD}$ can be divided into four speed clusters, corresponding to the four engine speeds tested during sea trial measurements. For every cluster, a separate $C_{F,\,CFD}$ was computed. Now, $C_{F,\,CFD}$ is a subset of the entire dataset. Thus, the sample mean $\overline{X}$ is used as correction factor, and the Students-t distribution to compute the CDF's.

It was concluded that the strength of the predicted the power-speed relationship with a $\overline{X}$ based $C_{F,\,CFD}$ depends on the dataset. For the LE180 series the predictions are accurate for all three of the CFD simulation types. While it is less accurate for the entire LE series, and the entire LE and SX series. The power-speed relationship is overpredicted by the method with a correction factor derived from a CDF. Due to this, it is concluded that the risk of 5% is too conservative for accurate predictions. Subsequently, both discussed predictions methods are compared on the performance of accuracy and precision. This is done by computing the relative error between the measured and calculated P_B. The accuracy is represented by μ and the precision by σ. It is concluded that the precision of both methods is identical, due to the constant correction per speed cluster. This also results in the trend of both prediction methods being similar. However, the accuracy of the prediction method with $C_{F,\,CFD}$ based on $\overline{X}$ is greater than that of the method with $C_{F,\,CFD}$ derived from a CDF, which confirms what was seen in the prediction of the power-speed relationships.

Concluding, a statistical correction factor based on $\overline{X}$ can be used to predict the power-speed relationship accurately. While, this is not the case for a statistical correction factor derived from a CDF with a risk of 5%. For both it holds that the predictions are not very precise. In order to improve the precision, the variance in the data must be reduced. It is believed that it can be reduced most easily by improving the corrections for environmental conditions in the sea trial measurements.

Chapter 8

Conclusions

The uncertainty of a statistical correction between CFD and sea trial measurements is investigated. In this research Amels LE and SX yachts were investigated, and sea trial and CFD databases were provided by Damen. The uniqueness of the CFD datasets is that the simulations were run after sea trial at the same speeds that were measured. Three CFD simulation types were run: bare hull, appended hull and actuator disk. The resistance computed with CFD is compared to the resistance measured during sea trial using the relative error between them: $C_{F,\,CFD}$. The relative error is the statistical correction between CFD and sea trial measurements. By developing this statistical correction factor the resistance predictions based on CFD can be improved, and with them the power-speed predictions. The uncertainty of $C_{F,\,CFD}$ is defined as a function of accuracy and precision. Where mean μ represent the accuracy, and standard deviation σ the precision. Further, two types of uncertainty are distinguished: computational and experimental. Computational uncertainty is present in the CFD results, and is caused by modeling or numerical errors. As Damen uses a commercial CFD code, the modeling errors are difficult to change. The numerical errors consist of discretization, convergence and round-off errors, and are simulations dependent. Experimental uncertainty is present in the sea trial measurement data set, and is due to the measuring of the data. The problem is captured with the following the main research question: "How can the uncertainty of the statistical $C_{F,\,CFD}$ be quantified and reduced, and to what extent can it be used to predict the required installed power?". The main-research question was divided into five sub-research questions, to facilitate in answering it.

1. What is the impact of including more physical effects in the simulations on the uncertainty of $C_{F,\,CFD}$?

The first sub-research question is answered by investigating the changes in mean μ and standard deviation σ, representing the accuracy and precision, of $C_{F,\,CFD}$ based on the three simulation types. Also, the effect of roughness was investigated by including it via Townsins equation. The accuracy improved the most between bare hull and appended hull simulations, and improved only a little between appended hull and actuator disk simulations. For the precision it as seen that it improved between the simulations of bare hull and appended hull, but it decreased between appended hull and actuator disk. Clearly, the uncertainty reduced between the bare hull and the appended hull simulations. While the impact on the uncertainty between the appended hull and actuator disk simulations is more difficult to assess. But, a high precision is favored over a high accuracy. Therefore, the uncertainty decreased between

the appended hull and actuator disk simulations. Three possible causes for the deterioration of the uncertainty are proposed. First, the actuator disk is a simplification and apparently not leading to a better simulation of the flow. But, an advantage of actuator disk simulations is that the thrust force can be computed. Second, t is assumed constant which may introduce an incorrect derivation of the resistance, and thus an incorrect $C_{F,\,CFD}$ based on the bare hull and appended hull simulations. Third, the corrections for environmental conditions are executed on the resistance rather than the thrust, thus the gap between CFD and sea trial results is bigger. The Townsin roughness resulted in a higher accuracy but lower precision. Therefore, it was said that it was unnecessary to include it in the roughness. Finally, it was concluded that including more physical effects can reduce the uncertainty of $C_{F,\,CFD}$, and the usage of the actuator disk model should be revised.

2. What is the effect of increasing variety in ship dimensions on the uncertainty of $C_{F,\,CFD}$?

Five Amels LE and SX types are considered to investigate the effect of variety in the main dimensions of a ship on the total uncertainty of $C_{F,\,CFD}$. The hull shape of all five of the LE types is comparable, but they differ in size. The size and shape of the LE and SX types differ both. The changes of mean μ and standard deviation σ between the vessel series are evaluated per simulations type. The accuracy increased as the variety in ship dimensions increased. It was explained by the way correction for waves are executed. Namely, only reflected waves and not motion-induced waves are considered. This assumption only holds to a certain extent where a ratio between wave height and ship length is not exceeded. The ships other than the LE180 are larger, thus the chance the assumption holds is greater. In general, the precision decreased as the variety in ship main dimensions increased. This was expected because σ is a measure of the variety in a dataset. However, it did improve slightly in two cases, which was explained by the mathematical definition of σ. It depends on the μ amongst others, and a change in μ can introduce a change in σ. It was concluded that the effect of the variety in ship main dimensions was negative on the uncertainty of $C_{F,\,CFD}$, because the accuracy improved, but the precision decreases as the variety increased.

3. What are the driving factors behind the variance in $C_{F,\,CFD}$?

A multivariate linear regression was used to determine the driving factors behind the variance. It is a linear regression technique where multiple variables are considered. In a multivariate linear regression the predictor variables must be not collinear. The regression was performed for all seven datasets separately. First, a list with possible predictor variables was set up. Then, by using pair plots the size of the list was reduced. At last, the Pearson's coefficient was used to assess the collinearity between two predictor variables. It was concludes that the following parameters are independent: F_n, C_B, H_W, and V_W. Second, the independent variables are normalized using a min/max-normalization, to aid the interpretation of the magnitudes of the regression coefficients. Finally, the regression coefficients are not only assessed on the magnitude, which explains the portion of the total variance of $C_{F,\,CFD}$ is caused by it, but also on the statistical significance represented by the P-value.

The variance in all three of the datasets corresponding to the LE180 series is caused by F_n, H_W, and V_W. While, in the other four datasets it is caused by F_n, C_B, H_W, and V_W. Except, for the dataset corresponding to the actuator disk simulations for the entire LE series, where V_W is excluded because the statistical significance is insufficient.

The linear relationship between $C_{F,\,CFD}$ and F_n is always negative, thus $C_{F,\,CFD}$ decreases as F_n increases. Two explanations are given. First, the grid is built for the design speed, the closer the ship speed to the design speed the smaller the numerical errors. Second, the "means of mean" method [3] should be applied to the sea trial measurement results, which was only done for the highest tested ship speed.

The absence of dependency of $C_{F,\,CFD}$ on C_B in the LE180 series is explained by the fact that the hull sizes and shapes are roughly equal. For the other series the relationship is negative again. This is explained by method of correction for environmental conditions. Which uses the ship main dimensions as input, amongst others. There is only a correction for reflected waves applied, and not for motion induced waves. For this assumption to hold, a ratio between wave height and ship length may not be exceeded. Which is more likely to stand for ships with a larger block coefficient.

At last, the dependency on environmental conditions itself is explained by the fact that the correction methods are developed for and validated against merchant vessels instead of super yachts. These vessel types differ in size and shape, which could introduce incomplete corrections.

Concluding, the variance in the datasets is always caused by the ship speed (F_n) and environmental conditions (H_W and V_W). When ships are considered that differ in size and shape are considered as well, the C_B starts to become important too.

4. What is the impact of reducing the experimental uncertainty on the uncertainty of $C_{F,\,CFD}$?

The experimental uncertainty is caused by parameters that are determined during sea trial. One of these parameters is the hull efficiency η_H. Which is a function of the thrust deduction factor t and wake factor w. The experimental uncertainty is replaced by numerical uncertainty by computing the t and w with CFD instead of with sea trial data.

In the investigation, the numerical estimates of t, w, and η_H are compared to the experimental estimates. After which the uncertainty of the numerical and experimental estimate of η_H is assessed by means of the normalized uncertainty. At last, the impact of the total uncertainty on the total uncertainty of $C_{F,\,CFD}$ is evaluated. Now, $C_{F,\,CFD}$ is based on P_B instead of R because R is derived using a Damen in-house developed tool, for which it was not possible to change the t and w inputs.

The numerical results show that t depends on speed, while it is assumed to be constant. The thrust deduction factor is given by equation 3-20. Where T represent the required thrust and R the total towed resistance. T in place, is a function of R and R_P. R_P is the added resistance due to propeller operations. It increases as the propeller RPM increases, which is inherent in an increasing ship speed. Concluding, the T increases sharper than R as the ship speed increases, which explained the speed dependency of t.

The main difference between the numerical and experimental estimate of w is the scatter. As there are no environmental conditions present in CFD, the scatter in the numerical estimate of w is less compared to the experimental estimate. Also w, is now only slightly positive instead of slightly negative. In literature, it was also seen that w is roughly independent of speed.

The trend of the numerical estimate of η_H is positive while the trend of the experimental estimate is negative, which is explained by the trend of t and w. This also explained the lesser scatter in the numerical estimate. The uncertainty of η_H is compared using the normalized uncertainty, it was concluded that the uncertainty of the numerical estimate is of a order ten smaller compared to the experimental estimate.

The impact on the total uncertainty of $C_{F,\,CFD}$ was assessed by comparing the accuracy, precision, and the normalized uncertainty. The accuracy of the experimental estimate is higher, while the precision of the numerical estimate is higher. Therefore, the normalized uncertainty is evaluated. The numerical estimate shows a normalized uncertainty that is three times smaller than the experimental estimate. Therefore, it is concluded that replacing experimental uncertainty by numerical uncertainty leads to a reduction of the total uncertainty. Thus, the impact of it is positive on the total uncertainty.

5. To what extent can a statistical $C_{F,\,CFD}$ be used to predict the required installed power PB?

To answer the final sub-research question, the P_B calculated based on CFD is compared with the P_B measured during sea trials. The resistance computed with CFD is adjusted with $C_{F,\,CFD}$, after which P_B is calculated. First, it is assessed whether $C_{F,\,CFD}$ is normally distributed. Subsequently, the untreated CFD is compared to the sea trial measurements. Where four speed clusters of $C_{F,\,CFD}$ are derived. Third, two statistical correction factors are presented and evaluated. At last, the two are compared to each other in terms of accuracy and precision.

The underlying distribution of $C_{F,\,CFD}$ is examined. A Gaussian KDE plot is compared to the theoretical bell curve to assess if the distribution is normal. Any deviations are explained using histogram plots. Despite the presence of some deviations, it is concluded that for the seven datasets it is reasonable to assume a normal distribution for $C_{F,\,CFD}$.

The untreated CFD based P_B's are compared to P_B measured during sea trial. It showed that the difference between CFD and trial changes over speed. The speed dependency was said to be related to the grid, which is designed for the design speed. Four speed clusters are distinguished, corresponding to the four engine speeds that were tested during sea trial measurements. Now, every speed cluster is a subset of the entire dataset.

The performance of two statistical correction factors is evaluated. This is done by determining the reliability of the predicted power-speed relationship, and also by comparing the uncertainty of the relative error between predicted and measured P_B. The first correction factor is the sample mean $\overline{X}$ of $C_{F,\,CFD}$, the second is derived from a CDF with a 95% confidence band. It is read at the upper bound of the confidence band at 95% probability, which corresponds to a risk of 5%.

It is concluded that the power-speed relationship can be predicted accurately with the $\overline{X}$ based $C_{F,\,CFD}$ when the LE180 series is considered. When considering the entire LE series, and the entire LE and SX series combined the predicted relationship is less accurate. Next, the power-speed relationship is well overpredicted with the $C_{F,\,CFD}$ derived from a CDF, for all three of the vessel series. Therefore, it is concluded that a risk of 5% is too conservative.

The two correction factors are analyzed by computing the relative error between the predicted and measured P_B on the accuracy and precision. The correction factors are constant per speed

cluster, thus the variance remains equal. Thus resulting in an equal precision. The accuracy, however, is affected by the correction factors. It is higher for the $\overline{X}$ based $C_{F,\,CFD}$. Which confirms the conclusion presented in the previous paragraph.

Finally, as the $C_{F,\,CFD}$ based on the $\overline{X}$ can predict the power-speed relationship accurate but not precise, and the $C_{F,\,CFD}$ derived from the CDF cannot do either of them, it is concluded that the precision must be improved and that the risk of 5% is too conservative for accurate predictions.

How can the uncertainty of the statistical $C_{F,\,CFD}$ be quantified and reduced, and to what extent can it be used to predict the required installed power?

By answering all five sub-research questions the main-research question is answered. The uncertainty of $C_{F,\,CFD}$ can be quantified by treating it as a function of the mean μ and standard deviation σ of $C_{F,\,CFD}$.

The uncertainty can be reduced by including more physics in the CFD simulations. It was seen that both the accuracy and precision improved whilst comparing the bare hull and appended hull simulations. But, whilst comparing appended hull and actuator disk simulations, no improvement is seen. The usage of an actuator disk does not lead to a more realistic simulation of the flow. A major advantage, however, is that the thrust force can be computed. Another method of reducing the total uncertainty is by replacing a part of the experimental uncertainty by numerical uncertainty.

At last, it is concluded that the quality of the predicted power-speed relationship depends on multiple aspects. First of all, the performance of the prediction strongly depends on the vessel series. Two types of $C_{F,\,CFD}$ are investigated on the reliability of their predicted power-speed relationship. The first being $C_{F,\,CFD}$ based on $\overline{X}$, and the second derived from a CDF. For the LE180 series it holds that $\overline{X}$ based $C_{F,\,CFD}$ can predict the relationship accurately, but less precise. While the predicted power-speed relationship of the other two series is not accurate and precise. The prediction of the power-speed relationship by the $C_{F,\,CFD}$ derived from the CDF is not accurate and precise for all series, thus the risk of 5% is too conservative. Therefore, it is concluded that only the $C_{F,\,CFD}$ based on the $\overline{X}$ can be used to predict the power-speed relationship accurately. However, the precision must be improved in order to make reliable predictions. Concluding that the quality also depends on the type of $C_{F,\,CFD}$. At last, by inspecting the untreated CFD data it is discovered that $C_{F,\,CFD}$ is speed dependent. Therefore, the quality also depends on the speed cluster.

Chapter 9

Recommendations

With this investigation, the research on the topic is not finalized. This chapter presents several recommendations based on the research that was conducted. They are divided into four categories: explanations and other approaches, possible improvements, increasing the database and possible research paths.

1. Explanations and other approaches:
    - It was seen that the uncertainty of $C_{F,\,CFD}$ did not improve whilst comparing appended hull simulations to actuator disk simulations. Thus, it was concluded that the actuator disk does not provide a more realistic simulation of the flow. However, the simulation are useful in determining the required thrust T, the thrust deduction factor t, and the wake fraction w. Namely, it was concluded that the total uncertainty can be receded by replacing experimental uncertainty by numerical uncertainty by means of the η_H.
    - Another approach of assessing the precision of the power-speed relationship, is by also inspecting the R^2 value of the fitted trend line. As it is a measure of the deviation of the data points from the trend line. The accuracy cannot be evaluated with it.
    - In this research the CFD simulations were run after the sea trials were conducted. Resulting in very minimal the differences in displacement and speed. Normally, CFD is used to predict the sea trial results, leading to larger deviations between speed and displacement amongst others. This results in that matching CFD to sea trial is more difficult. It is suggested to match by first making a resistance-speed diagram. With this diagram $C_{F,\,CFD}$ can be determined over a range. However, the interpolation of the resistance over speed introduces extra numerical uncertainties.
2. Possible improvements:
    - It was concluded that the precision of $C_{F,\,CFD}$ must be reduced in order to make more reliable power-speed relationship predictions. Most of the gains can be made in improving the corrections for environmental conditions. First, it was mentioned that the currently used method only considers reflected waves, which may lead to incomplete corrections. It is believed that it is worth it to implement the correction

for motion induced waves to improve the method to compute the added resistance due to waves. However, this required real-time data gathering during sea trial measurements which may be too expensive. Second, The currently used corrections methods are developed for and validated against merchant vessels. They differ a lot in shape compared to super yachts. To improve the corrections, a method for more slender ships has to be developed. Third, another method of reducing the impact of environmental conditions is by restricting the usage of sea trial data. If a sea state is too heavy, the results should not be used in the comparison between calm water CFD simulations and sea trial results. At last, the precision of $C_{F,\,CFD}$ can possibly be improved by simulating the encountered environmental condition in CFD , instead of correcting the sea trial results for them.

- Currently, the trial analysis tool used by Damen, does not consider the numerically determined t and w. If so, the measured sea trial resistance can be derived more accurately and precisely. As was seen that the total uncertainty can be reduced by replacing experimental uncertainty by numerical uncertainty.
- The actuator disk combined with open water propeller data is used to determine t and w. However, there are more advanced propeller models available where the usage of open water propeller data is not required. It is worth it to investigate if using such models leads to more accurate and precise predictions of t and w.

3. Increasing the size of the databases:

   - Two aspects of the databases have to be increased. First, check if it is possible to add more data of other vessels than the LE180 to the sea trial database to enable investigating the effect of variety in more detail. Second, the amount of appended hull and actuator disk simulations corresponding to vessels other than the LE180 must be increased. Such that, more t and w can be computed in order to investigate the numerical estimate of η_H in more detail.

4. Possible new research paths:

   - In this research a linear regression was used to investigate which parameters cause variance. However, interaction between some predictor variables is expected. For example, the wave height and wind speed. In order to explore this, a higher order regression can be used.
   - Now, only the numerical estimate of η_H is investigated. But, as advanced numerical propeller models are present, the interaction between propeller and hull can be determined.
   - By comparing the untreated CFD results to the sea trial results it discovered that $C_{F,\,CFD}$ is speed dependent, and four different speed clusters were distinguished. However, when considering the entire LE, and entire LE and SX series combined the clustering was less convenient, due to different speeds and sizes of the vessels. The F_n can provide the solution, as it not only includes speed but also the ship length. As the vessels within the LE series are comparable, it is expected that the range of F_n is comparable too.
   - The risk of 5% taken in deriving $C_{F,\,CFD}$ from a CDF is considered as too conservative because predicted the power-speed relationship was not accurate enough. Therefore, the threshold of the allowed taken risk must be found.

Appendix A

Actuator Disk Body Drag Parameters

In the equations below C_T and K_T represent the thrust and torque coefficient respectively, J is the advance ratio, n is the number in rps, Ω is the rotation speed, R_p is the propeller radius, R_H is the hub radius, Δ is the actuator disk thickness.

$$A_x = \frac{C_T}{\Delta} \frac{105}{16(4+3r_h^{'})(1-r_h^{'})} \tag{A-1}$$

$$A_\theta = \frac{K_Q}{\Delta J^2} \frac{105}{\pi(4+3r_h^{'})(1-r_h^{'})} \tag{A-2}$$

$$r^* = \frac{r^{'} - r_h^{'}}{1-r_h^{'}} \tag{A-3}$$

$$r_h^{'} = \frac{R_H}{R_P} \tag{A-4}$$

$$r^{'} = \frac{r}{R_P} \tag{A-5}$$

$$J = \frac{U}{nD_p} \tag{A-6}$$

$$D_p = 2R_p \tag{A-7}$$

$$n = \frac{\Omega}{2\pi} \tag{A-8}$$

$$C_T = \frac{2T}{\rho U^2 \pi R_p^2} \tag{A-9}$$

$$K_T = \frac{T}{\rho n D_p^4} \tag{A-10}$$

$$K_Q = \frac{Q}{\rho n D_p^5} \tag{A-11}$$

$$\tag{A-12}$$

Appendix B

Convergence Error

The resistance-speed graphs from CFD are presented in figure B-1. It can be seen that there is first an overshoot afterwards is slowly converges, as concluded by van Dijk [2]. As explained in section 2-8-1 the resistance is determined as a mean over the last 250 time steps, with a standard deviation of less than 1%, which means that the convergence error is less than 1%.

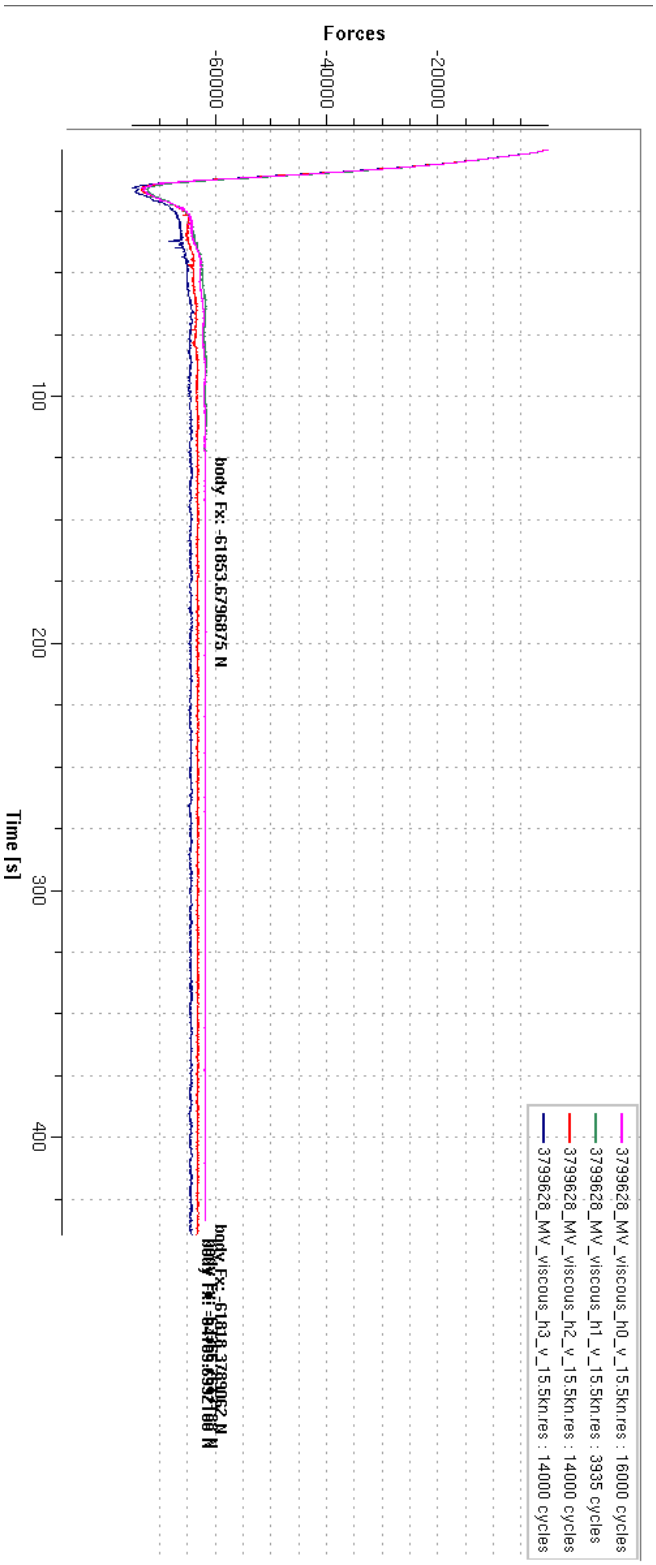

Figure B-1: Convergence Error computed by van Dijk [2]

Appendix C

Collinearity matrices

	Yard Number	Speed trial [m/s]	Speed CFD [m/s]	Fn trial [-]	Fn CFD [-]	Delta Fn [-]	Re CFD [-]	Aws [m^2]	Aws [-]	Lwl cfd [m]	Displacement [ton]	Volume cfd [m^3]	Lwl trial [m]	Bwl trial [m]	Dwl trial [m]	Cb trial [-]	Cb CFD [-]	Delta Cb [-]	L/B trial [-]	Cc/d [-]	Mean keel clearance [-]	Mean wave height [m]	Mean wind speed [kn]
Yard Number	TRUE	FALSE	FALSE	FALSE	FALSE	FALSE	FALSE	FALSE	FALSE	FALSE	FALSE	FALSE	FALSE	FALSE	FALSE	FALSE	FALSE	FALSE	FALSE	FALSE	FALSE	FALSE	FALSE
Speed trial [m/s]	FALSE	TRUE	TRUE	TRUE	TRUE	FALSE	TRUE	TRUE	TRUE	FALSE	FALSE	FALSE	FALSE	FALSE	FALSE	FALSE	FALSE	FALSE	FALSE	TRUE	FALSE	FALSE	FALSE
Speed CFD [m/s]	FALSE	TRUE	TRUE	TRUE	TRUE	FALSE	TRUE	TRUE	TRUE	FALSE	FALSE	FALSE	FALSE	FALSE	FALSE	FALSE	FALSE	FALSE	FALSE	TRUE	FALSE	FALSE	FALSE
Fn trial [-]	FALSE	TRUE	TRUE	TRUE	TRUE	FALSE	TRUE	TRUE	TRUE	FALSE	FALSE	FALSE	FALSE	FALSE	FALSE	FALSE	FALSE	FALSE	FALSE	TRUE	FALSE	FALSE	FALSE
Fn CFD [-]	FALSE	TRUE	TRUE	TRUE	TRUE	FALSE	TRUE	TRUE	TRUE	FALSE	FALSE	FALSE	FALSE	FALSE	FALSE	FALSE	FALSE	FALSE	FALSE	TRUE	FALSE	FALSE	FALSE
Delta Fn [-]	FALSE	FALSE	FALSE	FALSE	FALSE	TRUE	FALSE	FALSE	FALSE	FALSE	FALSE	FALSE	FALSE	FALSE	FALSE	FALSE	FALSE	FALSE	FALSE	FALSE	FALSE	FALSE	FALSE
Re CFD [-]	FALSE	TRUE	TRUE	TRUE	TRUE	FALSE	TRUE	TRUE	TRUE	FALSE	FALSE	FALSE	FALSE	FALSE	FALSE	FALSE	FALSE	FALSE	FALSE	TRUE	FALSE	FALSE	FALSE
Aws [m^2]	FALSE	TRUE	TRUE	TRUE	TRUE	FALSE	TRUE	TRUE	TRUE	FALSE	FALSE	FALSE	FALSE	FALSE	FALSE	FALSE	FALSE	FALSE	FALSE	TRUE	FALSE	FALSE	FALSE
Aws [-]	FALSE	TRUE	TRUE	TRUE	TRUE	FALSE	TRUE	TRUE	TRUE	FALSE	FALSE	FALSE	FALSE	FALSE	FALSE	FALSE	FALSE	FALSE	FALSE	TRUE	FALSE	FALSE	FALSE
Lwl cfd [m]	FALSE	FALSE	FALSE	FALSE	FALSE	FALSE	FALSE	FALSE	FALSE	FALSE	TRUE	FALSE	TRUE	FALSE	TRUE	FALSE	TRUE	TRUE	FALSE	FALSE	FALSE	FALSE	FALSE
Displacement [ton]	FALSE	FALSE	FALSE	FALSE	FALSE	FALSE	FALSE	FALSE	FALSE	TRUE	FALSE	TRUE	FALSE	FALSE	TRUE	FALSE	TRUE	TRUE	FALSE	FALSE	FALSE	FALSE	FALSE
Volume cfd [m^3]	FALSE	FALSE	FALSE	FALSE	FALSE	FALSE	FALSE	FALSE	FALSE	TRUE	FALSE	TRUE	FALSE	FALSE	TRUE	FALSE	TRUE	TRUE	FALSE	FALSE	FALSE	FALSE	FALSE
Lwl trial [m]	FALSE	FALSE	FALSE	FALSE	FALSE	FALSE	FALSE	FALSE	FALSE	TRUE	FALSE	TRUE	FALSE	FALSE	TRUE	FALSE	TRUE	TRUE	FALSE	FALSE	FALSE	FALSE	FALSE
Bwl trial [m]	FALSE	FALSE	FALSE	FALSE	FALSE	FALSE	FALSE	FALSE	FALSE	FALSE	FALSE	FALSE	FALSE	FALSE	FALSE	FALSE	FALSE	FALSE	FALSE	FALSE	FALSE	FALSE	FALSE
Dwl trial [m]	FALSE	FALSE	FALSE	FALSE	FALSE	FALSE	FALSE	FALSE	FALSE	TRUE	FALSE	TRUE	FALSE	FALSE	TRUE	FALSE	TRUE	TRUE	FALSE	FALSE	FALSE	FALSE	FALSE
Cb trial [-]	FALSE	FALSE	FALSE	FALSE	FALSE	FALSE	FALSE	FALSE	FALSE	TRUE	TRUE	TRUE	TRUE	FALSE	TRUE	TRUE	TRUE	TRUE	FALSE	FALSE	FALSE	FALSE	FALSE
Cb CFD [-]	FALSE	FALSE	FALSE	FALSE	FALSE	FALSE	FALSE	FALSE	FALSE	FALSE	FALSE	FALSE	FALSE	FALSE	FALSE	FALSE	FALSE	FALSE	FALSE	FALSE	FALSE	FALSE	FALSE
Delta Cb [-]	FALSE	FALSE	FALSE	FALSE	FALSE	FALSE	FALSE	FALSE	FALSE	TRUE	TRUE	TRUE	TRUE	FALSE	TRUE	TRUE	TRUE	TRUE	FALSE	FALSE	FALSE	FALSE	FALSE
L/B trial [-]	FALSE	FALSE	FALSE	FALSE	FALSE	FALSE	FALSE	FALSE	FALSE	TRUE	TRUE	TRUE	TRUE	FALSE	TRUE	TRUE	TRUE	TRUE	FALSE	FALSE	FALSE	FALSE	FALSE
Cc/d [-]	FALSE	TRUE	TRUE	TRUE	TRUE	FALSE	TRUE	TRUE	TRUE	FALSE	FALSE	FALSE	FALSE	FALSE	FALSE	FALSE	FALSE	FALSE	FALSE	TRUE	FALSE	FALSE	FALSE
Mean keel clearance [-]	FALSE	FALSE	FALSE	FALSE	FALSE	FALSE	FALSE	FALSE	FALSE	FALSE	FALSE	FALSE	FALSE	FALSE	FALSE	FALSE	FALSE	FALSE	FALSE	FALSE	TRUE	FALSE	FALSE
Mean wave height [m]	FALSE	FALSE	FALSE	FALSE	FALSE	FALSE	FALSE	FALSE	FALSE	FALSE	FALSE	FALSE	FALSE	FALSE	FALSE	FALSE	FALSE	FALSE	FALSE	FALSE	FALSE	TRUE	FALSE
Mean wind speed [kn]	FALSE	FALSE	FALSE	FALSE	FALSE	FALSE	FALSE	FALSE	FALSE	FALSE	FALSE	FALSE	FALSE	FALSE	FALSE	FALSE	FALSE	FALSE	FALSE	FALSE	FALSE	FALSE	TRUE

Figure C-1: Collinearity matrix bare hull simulation of the LE180

	Yard Number	Speed trial [m/s]	Speed CFD [m/s]	Fn trial [-]	Fn CFD [-]	Delta Fn [-]	Re CFD [-]	Aws [m^2]	Aws [-]	Lwl cfd [m]	Displacement [ton]	Volume cfd [m^3]	Lwl trial [m]	Bwl trial [m]	Dwl trial [m]	Cb trial [-]	Cb CFD [-]	Delta Cb [-]	L/B trial [-]	Cc/d [-]	Mean keel clearance [-]	Mean wave height [m]	Mean wind speed [kn]
Yard Number	TRUE	FALSE	FALSE	FALSE	FALSE	FALSE	FALSE	FALSE	FALSE	FALSE	FALSE	FALSE	FALSE	FALSE	FALSE	FALSE	FALSE	FALSE	FALSE	FALSE	FALSE	FALSE	FALSE
Speed trial [m/s]	FALSE	TRUE	TRUE	TRUE	TRUE	FALSE	TRUE	TRUE	TRUE	FALSE	FALSE	FALSE	FALSE	FALSE	FALSE	FALSE	FALSE	FALSE	FALSE	FALSE	FALSE	FALSE	FALSE
Speed CFD [m/s]	FALSE	TRUE	TRUE	TRUE	TRUE	FALSE	TRUE	TRUE	TRUE	FALSE	FALSE	FALSE	FALSE	FALSE	FALSE	FALSE	FALSE	FALSE	FALSE	FALSE	FALSE	FALSE	FALSE
Fn trial [-]	FALSE	TRUE	TRUE	TRUE	TRUE	FALSE	TRUE	TRUE	TRUE	FALSE	FALSE	FALSE	FALSE	FALSE	FALSE	FALSE	FALSE	FALSE	FALSE	FALSE	FALSE	FALSE	FALSE
Fn CFD [-]	FALSE	TRUE	TRUE	TRUE	TRUE	FALSE	TRUE	TRUE	TRUE	FALSE	FALSE	FALSE	FALSE	FALSE	FALSE	FALSE	FALSE	FALSE	FALSE	FALSE	FALSE	FALSE	FALSE
Delta Fn [-]	FALSE	FALSE	FALSE	FALSE	FALSE	TRUE	FALSE	FALSE	FALSE	FALSE	FALSE	FALSE	FALSE	FALSE	FALSE	FALSE	FALSE	FALSE	FALSE	FALSE	FALSE	FALSE	FALSE
Re CFD [-]	FALSE	TRUE	TRUE	TRUE	TRUE	FALSE	TRUE	TRUE	TRUE	FALSE	FALSE	FALSE	FALSE	FALSE	FALSE	FALSE	FALSE	FALSE	FALSE	FALSE	FALSE	FALSE	FALSE
Aws [m^2]	FALSE	TRUE	TRUE	TRUE	TRUE	FALSE	TRUE	TRUE	TRUE	FALSE	FALSE	FALSE	FALSE	FALSE	FALSE	FALSE	FALSE	FALSE	FALSE	FALSE	FALSE	FALSE	FALSE
Aws [-]	FALSE	TRUE	TRUE	TRUE	TRUE	FALSE	TRUE	TRUE	TRUE	FALSE	FALSE	FALSE	FALSE	FALSE	FALSE	FALSE	FALSE	FALSE	FALSE	FALSE	FALSE	FALSE	FALSE
Lwl cfd [m]	FALSE	FALSE	FALSE	FALSE	FALSE	FALSE	FALSE	FALSE	FALSE	FALSE	TRUE	FALSE	TRUE	FALSE	TRUE	TRUE	FALSE	TRUE	TRUE	FALSE	FALSE	FALSE	FALSE
Displacement [ton]	FALSE	FALSE	FALSE	FALSE	FALSE	FALSE	FALSE	FALSE	FALSE	TRUE	FALSE	TRUE	FALSE	FALSE	FALSE	FALSE	FALSE	FALSE	FALSE	FALSE	FALSE	FALSE	FALSE
Volume cfd [m^3]	FALSE	FALSE	FALSE	FALSE	FALSE	FALSE	FALSE	FALSE	FALSE	FALSE	TRUE	FALSE	TRUE	FALSE	TRUE	TRUE	FALSE	TRUE	TRUE	FALSE	FALSE	FALSE	FALSE
Lwl trial [m]	FALSE	FALSE	FALSE	FALSE	FALSE	FALSE	FALSE	FALSE	FALSE	TRUE	FALSE	TRUE	FALSE	FALSE	FALSE	FALSE	FALSE	FALSE	FALSE	FALSE	FALSE	FALSE	FALSE
Bwl trial [m]	FALSE	FALSE	FALSE	FALSE	FALSE	FALSE	FALSE	FALSE	FALSE	FALSE	FALSE	FALSE	FALSE	FALSE	FALSE	FALSE	FALSE	FALSE	FALSE	FALSE	FALSE	FALSE	FALSE
Dwl trial [m]	FALSE	FALSE	FALSE	FALSE	FALSE	FALSE	FALSE	FALSE	FALSE	TRUE	FALSE	TRUE	FALSE	FALSE	FALSE	FALSE	FALSE	FALSE	FALSE	FALSE	FALSE	FALSE	FALSE
Cb trial [-]	FALSE	FALSE	FALSE	FALSE	FALSE	FALSE	FALSE	FALSE	FALSE	TRUE	FALSE	TRUE	FALSE	FALSE	FALSE	FALSE	FALSE	FALSE	FALSE	FALSE	FALSE	FALSE	FALSE
Cb CFD [-]	FALSE	FALSE	FALSE	FALSE	FALSE	FALSE	FALSE	FALSE	FALSE	FALSE	TRUE	FALSE	TRUE	FALSE	TRUE	TRUE	FALSE	TRUE	TRUE	FALSE	FALSE	FALSE	FALSE
Delta Cb [-]	FALSE	FALSE	FALSE	FALSE	FALSE	FALSE	FALSE	FALSE	FALSE	FALSE	TRUE	FALSE	TRUE	FALSE	TRUE	TRUE	FALSE	TRUE	TRUE	FALSE	FALSE	FALSE	FALSE
L/B trial [-]	FALSE	FALSE	FALSE	FALSE	FALSE	FALSE	FALSE	FALSE	FALSE	FALSE	TRUE	FALSE	TRUE	FALSE	TRUE	TRUE	FALSE	TRUE	TRUE	FALSE	FALSE	FALSE	FALSE
Cc/d [-]	FALSE	FALSE	FALSE	FALSE	FALSE	FALSE	FALSE	FALSE	FALSE	FALSE	FALSE	FALSE	FALSE	FALSE	FALSE	FALSE	FALSE	FALSE	FALSE	TRUE	FALSE	FALSE	FALSE
Mean keel clearance [-]	FALSE	FALSE	FALSE	FALSE	FALSE	FALSE	FALSE	FALSE	FALSE	FALSE	FALSE	FALSE	FALSE	FALSE	FALSE	FALSE	FALSE	FALSE	FALSE	FALSE	TRUE	FALSE	FALSE
Mean wave height [m]	FALSE	FALSE	FALSE	FALSE	FALSE	FALSE	FALSE	FALSE	FALSE	FALSE	FALSE	FALSE	FALSE	FALSE	FALSE	FALSE	FALSE	FALSE	FALSE	FALSE	FALSE	TRUE	FALSE
Mean wind speed [kn]	FALSE	FALSE	FALSE	FALSE	FALSE	FALSE	FALSE	FALSE	FALSE	FALSE	FALSE	FALSE	FALSE	FALSE	FALSE	FALSE	FALSE	FALSE	FALSE	FALSE	FALSE	FALSE	TRUE

Figure C-2: Collinearity matrix appended hull simulation of the LE180

	Yard Number	Speed trial [m/s]	Speed CFD [m/s]	Fn trial [-]	Fn CFD [-]	Delta Fn [-]	Re CFD [-]	Aws [m^2]	Aws [-]	Lwl cfd [m]	Displacement [ton]	Volume cfd [m^3]	Lwl trial [m]	Bwl trial [m]	Dwl trial [m]	Cb trial [-]	Cb CFD [-]	Delta Cb [-]	L/B trial [-]	Cc/d [-]	Mean keel clearance [-]	Mean wave height [m]	Mean wind speed [kn]
Yard Number	TRUE	FALSE	FALSE	FALSE	FALSE	FALSE	FALSE	FALSE	FALSE	FALSE	FALSE	FALSE	FALSE	FALSE	FALSE	FALSE	FALSE	FALSE	FALSE	FALSE	FALSE	FALSE	FALSE
Speed trial [m/s]	FALSE	TRUE	TRUE	TRUE	TRUE	FALSE	TRUE	TRUE	TRUE	FALSE	FALSE	FALSE	FALSE	FALSE	FALSE	FALSE	FALSE	FALSE	FALSE	FALSE	FALSE	FALSE	FALSE
Speed CFD [m/s]	FALSE	TRUE	TRUE	TRUE	TRUE	FALSE	TRUE	TRUE	TRUE	FALSE	FALSE	FALSE	FALSE	FALSE	FALSE	FALSE	FALSE	FALSE	FALSE	FALSE	FALSE	FALSE	FALSE
Fn trial [-]	FALSE	TRUE	TRUE	TRUE	TRUE	FALSE	TRUE	TRUE	TRUE	FALSE	FALSE	FALSE	FALSE	FALSE	FALSE	FALSE	FALSE	FALSE	FALSE	FALSE	FALSE	FALSE	FALSE
Fn CFD [-]	FALSE	TRUE	TRUE	TRUE	TRUE	FALSE	TRUE	TRUE	TRUE	FALSE	FALSE	FALSE	FALSE	FALSE	FALSE	FALSE	FALSE	FALSE	FALSE	FALSE	FALSE	FALSE	FALSE
Delta Fn [-]	FALSE	FALSE	FALSE	FALSE	FALSE	TRUE	FALSE	FALSE	FALSE	FALSE	FALSE	FALSE	FALSE	FALSE	FALSE	FALSE	FALSE	FALSE	FALSE	FALSE	FALSE	FALSE	FALSE
Re CFD [-]	FALSE	TRUE	TRUE	TRUE	TRUE	FALSE	TRUE	TRUE	TRUE	FALSE	FALSE	FALSE	FALSE	FALSE	FALSE	FALSE	FALSE	FALSE	FALSE	FALSE	FALSE	FALSE	FALSE
Aws [m^2]	FALSE	TRUE	TRUE	TRUE	TRUE	FALSE	TRUE	TRUE	TRUE	FALSE	FALSE	FALSE	FALSE	FALSE	FALSE	FALSE	FALSE	FALSE	FALSE	TRUE	FALSE	FALSE	FALSE
Aws [-]	FALSE	TRUE	TRUE	TRUE	TRUE	FALSE	TRUE	TRUE	TRUE	FALSE	FALSE	FALSE	FALSE	FALSE	FALSE	FALSE	FALSE	FALSE	FALSE	FALSE	FALSE	FALSE	FALSE
Lwl cfd [m]	FALSE	FALSE	FALSE	FALSE	FALSE	FALSE	FALSE	FALSE	FALSE	FALSE	TRUE	FALSE	FALSE	FALSE	FALSE	FALSE	FALSE	FALSE	FALSE	FALSE	FALSE	FALSE	FALSE
Displacement [ton]	FALSE	FALSE	FALSE	FALSE	FALSE	FALSE	FALSE	FALSE	FALSE	TRUE	FALSE	FALSE	FALSE	FALSE	FALSE	FALSE	FALSE	FALSE	FALSE	FALSE	FALSE	FALSE	FALSE
Volume cfd [m^3]	FALSE	FALSE	FALSE	FALSE	FALSE	FALSE	FALSE	FALSE	FALSE	FALSE	FALSE	FALSE	FALSE	FALSE	FALSE	FALSE	FALSE	FALSE	FALSE	FALSE	FALSE	FALSE	FALSE
Lwl trial [m]	FALSE	FALSE	FALSE	FALSE	FALSE	FALSE	FALSE	FALSE	FALSE	TRUE	FALSE	FALSE	FALSE	FALSE	FALSE	FALSE	FALSE	FALSE	FALSE	FALSE	FALSE	FALSE	FALSE
Bwl trial [m]	FALSE	FALSE	FALSE	FALSE	FALSE	FALSE	FALSE	FALSE	FALSE	TRUE	FALSE	FALSE	FALSE	FALSE	FALSE	FALSE	FALSE	FALSE	FALSE	FALSE	FALSE	FALSE	FALSE
Dwl trial [m]	FALSE	FALSE	FALSE	FALSE	FALSE	FALSE	FALSE	FALSE	FALSE	TRUE	FALSE	FALSE	FALSE	FALSE	FALSE	FALSE	FALSE	FALSE	FALSE	FALSE	FALSE	FALSE	FALSE
Cb trial [-]	FALSE	FALSE	FALSE	FALSE	FALSE	FALSE	FALSE	FALSE	FALSE	TRUE	FALSE	FALSE	FALSE	FALSE	FALSE	FALSE	FALSE	FALSE	FALSE	FALSE	FALSE	FALSE	FALSE
Cb CFD [-]	FALSE	FALSE	FALSE	FALSE	FALSE	FALSE	FALSE	FALSE	FALSE	TRUE	FALSE	FALSE	FALSE	FALSE	FALSE	FALSE	FALSE	FALSE	FALSE	FALSE	FALSE	FALSE	FALSE
Delta Cb [-]	FALSE	FALSE	FALSE	FALSE	FALSE	FALSE	FALSE	FALSE	FALSE	TRUE	FALSE	FALSE	FALSE	FALSE	FALSE	FALSE	FALSE	FALSE	FALSE	FALSE	FALSE	FALSE	FALSE
L/B trial [-]	FALSE	FALSE	FALSE	FALSE	FALSE	FALSE	FALSE	FALSE	FALSE	TRUE	FALSE	FALSE	FALSE	FALSE	FALSE	FALSE	FALSE	FALSE	FALSE	FALSE	FALSE	FALSE	FALSE
Cc/d [-]	FALSE	FALSE	FALSE	FALSE	FALSE	FALSE	FALSE	TRUE	FALSE	FALSE	FALSE	FALSE	FALSE	FALSE	FALSE	FALSE	FALSE	FALSE	FALSE	FALSE	FALSE	FALSE	FALSE
Mean keel clearance [-]	FALSE	FALSE	FALSE	FALSE	FALSE	FALSE	FALSE	FALSE	FALSE	FALSE	FALSE	FALSE	FALSE	FALSE	FALSE	FALSE	FALSE	FALSE	FALSE	FALSE	TRUE	FALSE	FALSE
Mean wave height [m]	FALSE	FALSE	FALSE	FALSE	FALSE	FALSE	FALSE	FALSE	FALSE	FALSE	FALSE	FALSE	FALSE	FALSE	FALSE	FALSE	FALSE	FALSE	FALSE	FALSE	FALSE	TRUE	FALSE
Mean wind speed [kn]	FALSE	FALSE	FALSE	FALSE	FALSE	FALSE	FALSE	FALSE	FALSE	FALSE	FALSE	FALSE	FALSE	FALSE	FALSE	FALSE	FALSE	FALSE	FALSE	FALSE	FALSE	FALSE	TRUE

Figure C-3: Collinearity matrix actuator disk simulation of the LE180

	Yard Number	Speed trial [m/s]	Speed CFD [m/s]	Fn trial [-]	Fn CFD [-]	Delta Fn [-]	Re CFD [-]	Aws [m^2]	Aws [-]	Lwl cfd [m]	Displacement [ton]	Volume cfd [m^3]	Lwl trial [m]	Bwl trial [m]	Dwl trial [m]	Cb trial [-]	Cb CFD [-]	Delta Cb [-]	L/B trial [-]	Cc/d [-]	Mean keel clearance [-]	Mean wave height [m]	Mean wind speed [kn]
Yard Number	TRUE	FALSE	FALSE	FALSE	FALSE	FALSE	TRUE	TRUE	FALSE	TRUE	TRUE	TRUE	TRUE	TRUE	TRUE	TRUE	TRUE	TRUE	FALSE	FALSE	FALSE	FALSE	FALSE
Speed trial [m/s]	FALSE	TRUE	TRUE	TRUE	TRUE	FALSE	TRUE	FALSE	FALSE	FALSE	FALSE	FALSE	FALSE	FALSE	FALSE	FALSE	FALSE	FALSE	FALSE	FALSE	FALSE	FALSE	FALSE
Speed CFD [m/s]	FALSE	TRUE	TRUE	TRUE	TRUE	FALSE	TRUE	FALSE	FALSE	FALSE	FALSE	FALSE	FALSE	FALSE	FALSE	FALSE	FALSE	FALSE	FALSE	FALSE	FALSE	FALSE	FALSE
Fn trial [-]	FALSE	TRUE	TRUE	TRUE	TRUE	FALSE	TRUE	FALSE	FALSE	FALSE	FALSE	FALSE	FALSE	FALSE	FALSE	FALSE	FALSE	FALSE	FALSE	FALSE	FALSE	FALSE	FALSE
Fn CFD [-]	FALSE	TRUE	TRUE	TRUE	TRUE	FALSE	TRUE	FALSE	FALSE	FALSE	FALSE	FALSE	FALSE	FALSE	FALSE	FALSE	FALSE	FALSE	FALSE	FALSE	FALSE	FALSE	FALSE
Delta Fn [-]	FALSE	FALSE	FALSE	FALSE	FALSE	TRUE	FALSE	FALSE	FALSE	FALSE	FALSE	FALSE	FALSE	FALSE	FALSE	FALSE	FALSE	FALSE	FALSE	FALSE	FALSE	FALSE	FALSE
Re CFD [-]	TRUE	TRUE	TRUE	FALSE	FALSE	FALSE	TRUE	TRUE	FALSE	TRUE	TRUE	TRUE	TRUE	TRUE	FALSE	TRUE	TRUE	TRUE	FALSE	FALSE	FALSE	FALSE	FALSE
Aws [m^2]	TRUE	FALSE	FALSE	FALSE	FALSE	FALSE	TRUE	TRUE	FALSE	TRUE	TRUE	TRUE	TRUE	TRUE	TRUE	TRUE	TRUE	TRUE	FALSE	FALSE	FALSE	FALSE	FALSE
Aws [-]	FALSE	FALSE	FALSE	FALSE	FALSE	FALSE	FALSE	FALSE	TRUE	FALSE	FALSE	FALSE	FALSE	FALSE	FALSE	TRUE	FALSE	FALSE	TRUE	FALSE	FALSE	FALSE	FALSE
Lwl cfd [m]	TRUE	FALSE	FALSE	FALSE	FALSE	FALSE	TRUE	TRUE	FALSE	TRUE	TRUE	TRUE	TRUE	TRUE	TRUE	TRUE	TRUE	TRUE	FALSE	FALSE	FALSE	FALSE	FALSE
Displacement [ton]	TRUE	FALSE	FALSE	FALSE	FALSE	FALSE	TRUE	TRUE	FALSE	TRUE	TRUE	TRUE	TRUE	TRUE	TRUE	TRUE	TRUE	TRUE	FALSE	FALSE	FALSE	FALSE	FALSE
Volume cfd [m^3]	TRUE	FALSE	FALSE	FALSE	FALSE	FALSE	TRUE	TRUE	FALSE	TRUE	TRUE	TRUE	TRUE	TRUE	TRUE	TRUE	TRUE	TRUE	FALSE	FALSE	FALSE	FALSE	FALSE
Lwl trial [m]	TRUE	FALSE	FALSE	FALSE	FALSE	FALSE	TRUE	TRUE	FALSE	TRUE	TRUE	TRUE	TRUE	TRUE	TRUE	TRUE	TRUE	TRUE	FALSE	FALSE	FALSE	FALSE	FALSE
Bwl trial [m]	TRUE	FALSE	FALSE	FALSE	FALSE	FALSE	TRUE	TRUE	FALSE	TRUE	TRUE	TRUE	TRUE	TRUE	TRUE	TRUE	TRUE	TRUE	FALSE	FALSE	FALSE	FALSE	FALSE
Dwl trial [m]	TRUE	FALSE	FALSE	FALSE	FALSE	FALSE	FALSE	TRUE	FALSE	TRUE	TRUE	TRUE	TRUE	TRUE	TRUE	TRUE	TRUE	TRUE	FALSE	FALSE	FALSE	FALSE	FALSE
Cb trial [-]	TRUE	FALSE	FALSE	FALSE	FALSE	FALSE	TRUE	TRUE	FALSE	TRUE	TRUE	TRUE	TRUE	TRUE	TRUE	TRUE	TRUE	TRUE	FALSE	FALSE	FALSE	FALSE	FALSE
Cb CFD [-]	TRUE	FALSE	FALSE	FALSE	FALSE	FALSE	TRUE	TRUE	FALSE	TRUE	TRUE	TRUE	TRUE	TRUE	TRUE	TRUE	TRUE	TRUE	FALSE	FALSE	FALSE	FALSE	FALSE
Delta Cb [-]	TRUE	FALSE	FALSE	FALSE	FALSE	FALSE	FALSE	FALSE	FALSE	FALSE	FALSE	FALSE	FALSE	FALSE	FALSE	TRUE	TRUE	FALSE	FALSE	FALSE	FALSE	FALSE	FALSE
L/B trial [-]	FALSE	FALSE	FALSE	FALSE	FALSE	FALSE	FALSE	FALSE	TRUE	FALSE	FALSE	FALSE	FALSE	FALSE	FALSE	FALSE	FALSE	FALSE	TRUE	FALSE	FALSE	FALSE	FALSE
Cc/d [-]	FALSE	FALSE	FALSE	FALSE	FALSE	FALSE	FALSE	FALSE	FALSE	FALSE	FALSE	FALSE	FALSE	FALSE	FALSE	FALSE	FALSE	FALSE	FALSE	TRUE	FALSE	FALSE	FALSE
Mean keel clearance [-]	FALSE	FALSE	FALSE	FALSE	FALSE	FALSE	FALSE	FALSE	FALSE	FALSE	FALSE	FALSE	FALSE	FALSE	FALSE	FALSE	FALSE	FALSE	FALSE	FALSE	TRUE	FALSE	FALSE
Mean wave height [m]	FALSE	FALSE	FALSE	FALSE	FALSE	FALSE	FALSE	FALSE	FALSE	FALSE	FALSE	FALSE	FALSE	FALSE	FALSE	FALSE	FALSE	FALSE	FALSE	FALSE	FALSE	TRUE	FALSE
Mean wind speed [kn]	FALSE	FALSE	FALSE	FALSE	FALSE	FALSE	FALSE	FALSE	FALSE	FALSE	FALSE	FALSE	FALSE	FALSE	FALSE	FALSE	FALSE	FALSE	FALSE	FALSE	FALSE	FALSE	TRUE

Figure C-4: Collinearity matrix bare hull simulation of all LE series

	Yard Number	Speed trial [m/s]	Speed CFD [m/s]	Fn trial [-]	Fn CFD [-]	Delta Fn [-]	Re CFD [-]	Aws [m^2]	Aws [-]	Lwl cfd [m]	Displacement [ton]	Volume cfd [m^3]	Lwl trial [m]	Bwl trial [m]	Dwl trial [m]	Cb trial [-]	Cb CFD [-]	Delta Cb [-]	L/B trial [-]	Cc/d [-]	Mean keel clearance [-]	Mean wave height [m]	Mean wind speed [kn]
Yard Number	TRUE	FALSE	FALSE	FALSE	FALSE	FALSE	FALSE	TRUE	TRUE	TRUE	TRUE	TRUE	TRUE	TRUE	TRUE	TRUE	TRUE	TRUE	TRUE	FALSE	FALSE	FALSE	FALSE
Speed trial [m/s]	FALSE	TRUE	TRUE	TRUE	TRUE	FALSE	TRUE	FALSE	FALSE	FALSE	FALSE	FALSE	FALSE	FALSE	FALSE	FALSE	FALSE	FALSE	FALSE	FALSE	FALSE	FALSE	FALSE
Speed CFD [m/s]	FALSE	TRUE	TRUE	TRUE	TRUE	FALSE	TRUE	FALSE	FALSE	FALSE	FALSE	FALSE	FALSE	FALSE	FALSE	FALSE	FALSE	FALSE	FALSE	FALSE	FALSE	FALSE	FALSE
Fn trial [-]	FALSE	TRUE	TRUE	TRUE	TRUE	FALSE	TRUE	FALSE	FALSE	FALSE	FALSE	FALSE	FALSE	FALSE	FALSE	FALSE	FALSE	FALSE	FALSE	FALSE	FALSE	FALSE	FALSE
Fn CFD [-]	FALSE	TRUE	TRUE	TRUE	TRUE	FALSE	TRUE	FALSE	FALSE	FALSE	FALSE	FALSE	FALSE	FALSE	FALSE	FALSE	FALSE	FALSE	FALSE	FALSE	FALSE	FALSE	FALSE
Delta Fn [-]	FALSE	FALSE	FALSE	FALSE	FALSE	TRUE	FALSE	FALSE	FALSE	FALSE	FALSE	FALSE	FALSE	FALSE	FALSE	FALSE	FALSE	FALSE	FALSE	FALSE	FALSE	FALSE	FALSE
Re CFD [-]	FALSE	TRUE	TRUE	TRUE	TRUE	FALSE	TRUE	FALSE	FALSE	FALSE	FALSE	FALSE	FALSE	FALSE	FALSE	FALSE	FALSE	FALSE	FALSE	FALSE	FALSE	FALSE	FALSE
Aws [m^2]	TRUE	FALSE	FALSE	FALSE	FALSE	FALSE	FALSE	TRUE	TRUE	TRUE	TRUE	TRUE	TRUE	TRUE	TRUE	TRUE	TRUE	TRUE	TRUE	FALSE	FALSE	FALSE	FALSE
Aws [-]	TRUE	FALSE	FALSE	FALSE	FALSE	FALSE	FALSE	TRUE	TRUE	TRUE	TRUE	TRUE	TRUE	TRUE	FALSE	TRUE	TRUE	TRUE	TRUE	FALSE	FALSE	FALSE	FALSE
Lwl cfd [m]	TRUE	FALSE	FALSE	FALSE	FALSE	FALSE	FALSE	TRUE	TRUE	TRUE	TRUE	TRUE	TRUE	TRUE	TRUE	TRUE	TRUE	TRUE	TRUE	FALSE	FALSE	FALSE	FALSE
Displacement [ton]	TRUE	FALSE	FALSE	FALSE	FALSE	FALSE	FALSE	TRUE	TRUE	TRUE	TRUE	TRUE	TRUE	TRUE	TRUE	TRUE	TRUE	TRUE	TRUE	FALSE	FALSE	FALSE	FALSE
Volume cfd [m^3]	TRUE	FALSE	FALSE	FALSE	FALSE	FALSE	FALSE	TRUE	TRUE	TRUE	TRUE	TRUE	TRUE	TRUE	TRUE	TRUE	TRUE	TRUE	TRUE	FALSE	FALSE	FALSE	FALSE
Lwl trial [m]	TRUE	FALSE	FALSE	FALSE	FALSE	FALSE	FALSE	TRUE	TRUE	TRUE	TRUE	TRUE	TRUE	TRUE	TRUE	TRUE	TRUE	TRUE	TRUE	FALSE	FALSE	FALSE	FALSE
Bwl trial [m]	TRUE	FALSE	FALSE	FALSE	FALSE	FALSE	FALSE	TRUE	TRUE	TRUE	TRUE	TRUE	TRUE	TRUE	TRUE	TRUE	TRUE	TRUE	TRUE	FALSE	FALSE	FALSE	FALSE
Dwl trial [m]	TRUE	FALSE	FALSE	FALSE	FALSE	FALSE	FALSE	TRUE	FALSE	TRUE	TRUE	TRUE	TRUE	TRUE	TRUE	TRUE	TRUE	TRUE	TRUE	FALSE	FALSE	FALSE	FALSE
Cb trial [-]	TRUE	FALSE	FALSE	FALSE	FALSE	FALSE	FALSE	TRUE	TRUE	TRUE	TRUE	TRUE	TRUE	TRUE	TRUE	TRUE	TRUE	TRUE	TRUE	FALSE	FALSE	FALSE	FALSE
Cb CFD [-]	TRUE	FALSE	FALSE	FALSE	FALSE	FALSE	FALSE	TRUE	TRUE	TRUE	TRUE	TRUE	TRUE	TRUE	TRUE	TRUE	TRUE	TRUE	TRUE	FALSE	FALSE	FALSE	FALSE
Delta Cb [-]	TRUE	FALSE	FALSE	FALSE	FALSE	FALSE	FALSE	TRUE	TRUE	TRUE	TRUE	TRUE	TRUE	TRUE	TRUE	TRUE	TRUE	TRUE	TRUE	FALSE	FALSE	FALSE	FALSE
L/B trial [-]	TRUE	FALSE	FALSE	FALSE	FALSE	FALSE	FALSE	TRUE	TRUE	TRUE	TRUE	TRUE	TRUE	TRUE	TRUE	TRUE	TRUE	TRUE	TRUE	FALSE	FALSE	FALSE	FALSE
Cc/d [-]	FALSE	FALSE	FALSE	FALSE	FALSE	FALSE	FALSE	FALSE	FALSE	FALSE	FALSE	FALSE	FALSE	FALSE	FALSE	FALSE	FALSE	FALSE	FALSE	TRUE	FALSE	FALSE	FALSE
Mean keel clearance [-]	FALSE	FALSE	FALSE	FALSE	FALSE	FALSE	FALSE	FALSE	FALSE	FALSE	FALSE	FALSE	FALSE	FALSE	FALSE	FALSE	FALSE	FALSE	FALSE	FALSE	TRUE	FALSE	FALSE
Mean wave height [m]	FALSE	FALSE	FALSE	FALSE	FALSE	FALSE	FALSE	FALSE	FALSE	FALSE	FALSE	FALSE	FALSE	FALSE	FALSE	FALSE	FALSE	FALSE	FALSE	FALSE	FALSE	TRUE	FALSE
Mean wind speed [kn]	FALSE	FALSE	FALSE	FALSE	FALSE	FALSE	FALSE	FALSE	FALSE	FALSE	FALSE	FALSE	FALSE	FALSE	FALSE	FALSE	FALSE	FALSE	FALSE	FALSE	FALSE	FALSE	TRUE

Figure C-5: Collinearity matrix appended hull simulation of all LE series

	Yard Number	Speed trial [m/s]	Speed CFD [m/s]	Fn trial [-]	Fn CFD [-]	Delta Fn [-]	Re CFD [-]	Aws [m^2]	Aws [-]	Lwl cfd [m]	Displacement [ton]	Volume cfd [m^3]	Lwl trial [m]	Bwl trial [m]	Dwl trial [m]	Cb trial [-]	Cb CFD [-]	Delta Cb [-]	L/B trial [-]	Cc/d [-]	Mean keel clearance [-]	Mean wave height [m]	Mean wind speed [kn]
Yard Number	TRUE	FALSE	FALSE	FALSE	FALSE	FALSE	FALSE	TRUE	TRUE	TRUE	TRUE	TRUE	TRUE	TRUE	TRUE	TRUE	TRUE	TRUE	TRUE	FALSE	FALSE	FALSE	FALSE
Speed trial [m/s]	FALSE	TRUE	TRUE	TRUE	TRUE	FALSE	TRUE	FALSE	FALSE	FALSE	FALSE	FALSE	FALSE	FALSE	FALSE	FALSE	FALSE	FALSE	FALSE	FALSE	FALSE	FALSE	FALSE
Speed CFD [m/s]	FALSE	TRUE	TRUE	TRUE	TRUE	FALSE	TRUE	FALSE	FALSE	FALSE	FALSE	FALSE	FALSE	FALSE	FALSE	FALSE	FALSE	FALSE	FALSE	FALSE	FALSE	FALSE	FALSE
Fn trial [-]	FALSE	TRUE	TRUE	TRUE	TRUE	FALSE	TRUE	FALSE	FALSE	FALSE	FALSE	FALSE	FALSE	FALSE	FALSE	FALSE	FALSE	FALSE	FALSE	FALSE	FALSE	FALSE	FALSE
Fn CFD [-]	FALSE	TRUE	TRUE	TRUE	TRUE	FALSE	TRUE	FALSE	FALSE	FALSE	FALSE	FALSE	FALSE	FALSE	FALSE	FALSE	FALSE	FALSE	FALSE	FALSE	FALSE	FALSE	FALSE
Delta Fn [-]	FALSE	FALSE	FALSE	FALSE	FALSE	TRUE	FALSE	FALSE	FALSE	FALSE	FALSE	FALSE	FALSE	FALSE	FALSE	FALSE	FALSE	FALSE	FALSE	FALSE	FALSE	FALSE	FALSE
Re CFD [-]	FALSE	TRUE	TRUE	TRUE	TRUE	FALSE	TRUE	FALSE	FALSE	FALSE	FALSE	FALSE	FALSE	FALSE	FALSE	FALSE	FALSE	FALSE	FALSE	FALSE	FALSE	FALSE	FALSE
Aws [m^2]	TRUE	FALSE	FALSE	FALSE	FALSE	FALSE	FALSE	TRUE	TRUE	TRUE	TRUE	TRUE	TRUE	TRUE	TRUE	TRUE	TRUE	TRUE	TRUE	FALSE	FALSE	FALSE	FALSE
Aws [-]	TRUE	FALSE	FALSE	FALSE	FALSE	FALSE	FALSE	TRUE	TRUE	TRUE	TRUE	TRUE	TRUE	TRUE	TRUE	TRUE	TRUE	TRUE	TRUE	FALSE	FALSE	FALSE	FALSE
Lwl cfd [m]	TRUE	FALSE	FALSE	FALSE	FALSE	FALSE	FALSE	TRUE	TRUE	TRUE	TRUE	TRUE	TRUE	TRUE	TRUE	TRUE	TRUE	TRUE	TRUE	FALSE	FALSE	FALSE	FALSE
Displacement [ton]	TRUE	FALSE	FALSE	FALSE	FALSE	FALSE	FALSE	TRUE	TRUE	TRUE	TRUE	TRUE	TRUE	TRUE	TRUE	TRUE	TRUE	TRUE	TRUE	FALSE	FALSE	FALSE	FALSE
Volume cfd [m^3]	TRUE	FALSE	FALSE	FALSE	FALSE	FALSE	FALSE	TRUE	TRUE	TRUE	TRUE	TRUE	TRUE	TRUE	TRUE	TRUE	TRUE	TRUE	TRUE	FALSE	FALSE	FALSE	FALSE
Lwl trial [m]	TRUE	FALSE	FALSE	FALSE	FALSE	FALSE	FALSE	TRUE	TRUE	TRUE	TRUE	TRUE	TRUE	TRUE	TRUE	TRUE	TRUE	TRUE	TRUE	FALSE	FALSE	FALSE	FALSE
Bwl trial [m]	TRUE	FALSE	FALSE	FALSE	FALSE	FALSE	FALSE	TRUE	TRUE	TRUE	TRUE	TRUE	TRUE	TRUE	TRUE	TRUE	TRUE	TRUE	TRUE	FALSE	FALSE	FALSE	FALSE
Dwl trial [m]	TRUE	FALSE	FALSE	FALSE	FALSE	FALSE	FALSE	TRUE	FALSE	TRUE	TRUE	TRUE	TRUE	TRUE	TRUE	TRUE	TRUE	TRUE	TRUE	FALSE	FALSE	FALSE	FALSE
Cb trial [-]	TRUE	FALSE	FALSE	FALSE	FALSE	FALSE	FALSE	TRUE	TRUE	TRUE	TRUE	TRUE	TRUE	TRUE	TRUE	TRUE	TRUE	TRUE	TRUE	FALSE	FALSE	FALSE	FALSE
Cb CFD [-]	TRUE	FALSE	FALSE	FALSE	FALSE	FALSE	FALSE	TRUE	TRUE	TRUE	TRUE	TRUE	TRUE	TRUE	TRUE	TRUE	TRUE	TRUE	TRUE	FALSE	FALSE	FALSE	FALSE
Delta Cb [-]	TRUE	FALSE	FALSE	FALSE	FALSE	FALSE	FALSE	TRUE	TRUE	TRUE	TRUE	TRUE	TRUE	TRUE	TRUE	TRUE	TRUE	TRUE	TRUE	FALSE	FALSE	FALSE	FALSE
L/B trial [-]	TRUE	FALSE	FALSE	FALSE	FALSE	FALSE	FALSE	TRUE	TRUE	TRUE	TRUE	TRUE	TRUE	TRUE	TRUE	TRUE	TRUE	TRUE	TRUE	FALSE	FALSE	FALSE	FALSE
Cc/d [-]	FALSE	FALSE	FALSE	FALSE	FALSE	FALSE	FALSE	FALSE	FALSE	FALSE	FALSE	FALSE	FALSE	FALSE	FALSE	FALSE	FALSE	FALSE	FALSE	TRUE	FALSE	FALSE	FALSE
Mean keel clearance [-]	FALSE	FALSE	FALSE	FALSE	FALSE	FALSE	FALSE	FALSE	FALSE	FALSE	FALSE	FALSE	FALSE	FALSE	FALSE	FALSE	FALSE	FALSE	FALSE	FALSE	TRUE	FALSE	FALSE
Mean wave height [m]	FALSE	FALSE	FALSE	FALSE	FALSE	FALSE	FALSE	FALSE	FALSE	FALSE	FALSE	FALSE	FALSE	FALSE	FALSE	FALSE	FALSE	FALSE	FALSE	FALSE	FALSE	TRUE	FALSE
Mean wind speed [kn]	FALSE	FALSE	FALSE	FALSE	FALSE	FALSE	FALSE	FALSE	FALSE	FALSE	FALSE	FALSE	FALSE	FALSE	FALSE	FALSE	FALSE	FALSE	FALSE	FALSE	FALSE	FALSE	TRUE

Figure C-6: Collinearity matrix actuator disk simulation of all LE series

	Yard Number	Speed trial [m/s]	Speed CFD [m/s]	Fn trial [-]	Fn CFD [-]	Delta Fn [-]	Re CFD [-]	Aws [m^2]	Aws [-]	Lwl cfd [m]	Displacement [ton]	Volume cfd [m^3]	Lwl trial [m]	Bwl trial [m]	Dwl trial [m]	Cb trial [-]	Cb CFD [-]	Delta Cb [-]	L/B trial [-]	Cc/cfd [-]	Mean keel clearance [-]	Mean wave height [m]	Mean wind speed [kn]
Yard Number	TRUE	FALSE	FALSE	FALSE	FALSE	FALSE	FALSE	FALSE	FALSE	FALSE	FALSE	FALSE	FALSE	FALSE	FALSE	FALSE	FALSE	FALSE	FALSE	FALSE	FALSE	FALSE	FALSE
Speed trial [m/s]	FALSE	TRUE	TRUE	TRUE	TRUE	FALSE	TRUE	FALSE	FALSE	FALSE	FALSE	FALSE	FALSE	FALSE	FALSE	FALSE	FALSE	FALSE	FALSE	FALSE	FALSE	FALSE	FALSE
Speed CFD [m/s]	FALSE	TRUE	TRUE	TRUE	TRUE	FALSE	TRUE	FALSE	FALSE	FALSE	FALSE	FALSE	FALSE	FALSE	FALSE	FALSE	FALSE	FALSE	FALSE	FALSE	FALSE	FALSE	FALSE
Fn trial [-]	FALSE	TRUE	TRUE	TRUE	TRUE	FALSE	TRUE	FALSE	FALSE	FALSE	FALSE	FALSE	FALSE	FALSE	FALSE	FALSE	FALSE	FALSE	FALSE	FALSE	FALSE	FALSE	FALSE
Fn CFD [-]	FALSE	TRUE	TRUE	TRUE	TRUE	FALSE	TRUE	FALSE	FALSE	FALSE	FALSE	FALSE	FALSE	FALSE	FALSE	FALSE	FALSE	FALSE	FALSE	FALSE	FALSE	FALSE	FALSE
Delta Fn [-]	FALSE	FALSE	FALSE	FALSE	FALSE	TRUE	FALSE	FALSE	FALSE	FALSE	FALSE	FALSE	FALSE	FALSE	FALSE	FALSE	FALSE	FALSE	FALSE	FALSE	FALSE	FALSE	FALSE
Re CFD [-]	FALSE	TRUE	TRUE	TRUE	TRUE	FALSE	TRUE	FALSE	FALSE	FALSE	FALSE	FALSE	FALSE	FALSE	FALSE	FALSE	FALSE	FALSE	FALSE	FALSE	FALSE	FALSE	FALSE
Aws [m^2]	FALSE	FALSE	FALSE	FALSE	FALSE	FALSE	TRUE	TRUE	FALSE	FALSE	FALSE	FALSE	FALSE	FALSE	FALSE	FALSE	FALSE	FALSE	FALSE	FALSE	FALSE	FALSE	FALSE
Aws [-]	FALSE	FALSE	FALSE	FALSE	FALSE	FALSE	FALSE	FALSE	TRUE	FALSE	FALSE	FALSE	FALSE	FALSE	FALSE	FALSE	FALSE	FALSE	FALSE	FALSE	FALSE	FALSE	FALSE
Lwl cfd [m]	FALSE	FALSE	FALSE	FALSE	FALSE	FALSE	TRUE	TRUE	FALSE	TRUE	TRUE	TRUE	TRUE	TRUE	TRUE	TRUE	TRUE	TRUE	TRUE	FALSE	FALSE	FALSE	FALSE
Displacement [ton]	FALSE	FALSE	FALSE	FALSE	FALSE	FALSE	TRUE	TRUE	FALSE	TRUE	TRUE	TRUE	TRUE	TRUE	TRUE	TRUE	TRUE	TRUE	TRUE	FALSE	FALSE	FALSE	FALSE
Volume cfd [m^3]	FALSE	FALSE	FALSE	FALSE	FALSE	FALSE	TRUE	TRUE	FALSE	TRUE	TRUE	TRUE	TRUE	TRUE	TRUE	TRUE	TRUE	TRUE	TRUE	FALSE	FALSE	FALSE	FALSE
Lwl trial [m]	FALSE	FALSE	FALSE	FALSE	FALSE	FALSE	TRUE	TRUE	FALSE	TRUE	TRUE	TRUE	TRUE	TRUE	TRUE	TRUE	TRUE	TRUE	TRUE	FALSE	FALSE	FALSE	FALSE
Bwl trial [m]	FALSE	FALSE	FALSE	FALSE	FALSE	FALSE	TRUE	TRUE	FALSE	TRUE	TRUE	TRUE	TRUE	TRUE	TRUE	TRUE	TRUE	TRUE	TRUE	FALSE	FALSE	FALSE	FALSE
Dwl trial [m]	FALSE	FALSE	FALSE	FALSE	FALSE	FALSE	TRUE	TRUE	FALSE	TRUE	TRUE	TRUE	TRUE	TRUE	TRUE	TRUE	TRUE	TRUE	TRUE	FALSE	FALSE	FALSE	FALSE
Cb trial [-]	FALSE	FALSE	FALSE	FALSE	FALSE	FALSE	TRUE	TRUE	FALSE	TRUE	TRUE	TRUE	TRUE	TRUE	TRUE	TRUE	TRUE	TRUE	TRUE	FALSE	FALSE	FALSE	FALSE
Cb CFD [-]	FALSE	FALSE	FALSE	FALSE	FALSE	FALSE	TRUE	TRUE	FALSE	TRUE	TRUE	TRUE	TRUE	TRUE	TRUE	TRUE	TRUE	TRUE	TRUE	FALSE	FALSE	FALSE	FALSE
Delta Cb [-]	FALSE	FALSE	FALSE	FALSE	FALSE	FALSE	TRUE	TRUE	FALSE	TRUE	TRUE	TRUE	TRUE	TRUE	TRUE	TRUE	TRUE	TRUE	TRUE	FALSE	FALSE	FALSE	FALSE
L/B trial [-]	FALSE	FALSE	FALSE	FALSE	FALSE	FALSE	TRUE	TRUE	FALSE	TRUE	TRUE	TRUE	TRUE	TRUE	TRUE	TRUE	TRUE	TRUE	TRUE	FALSE	FALSE	FALSE	FALSE
Cc/cfd [-]	FALSE	FALSE	FALSE	FALSE	FALSE	FALSE	TRUE	TRUE	FALSE	TRUE	TRUE	TRUE	TRUE	TRUE	TRUE	TRUE	TRUE	TRUE	TRUE	TRUE	FALSE	FALSE	FALSE
Mean keel clearance [-]	FALSE	FALSE	FALSE	FALSE	FALSE	FALSE	FALSE	FALSE	FALSE	FALSE	FALSE	FALSE	FALSE	FALSE	FALSE	FALSE	FALSE	FALSE	FALSE	FALSE	TRUE	FALSE	FALSE
Mean wave height [m]	FALSE	FALSE	FALSE	FALSE	FALSE	FALSE	FALSE	FALSE	FALSE	FALSE	FALSE	FALSE	FALSE	FALSE	FALSE	FALSE	FALSE	FALSE	FALSE	FALSE	FALSE	TRUE	FALSE
Mean wind speed [kn]	FALSE	FALSE	FALSE	FALSE	FALSE	FALSE	FALSE	FALSE	FALSE	FALSE	FALSE	FALSE	FALSE	FALSE	FALSE	FALSE	FALSE	FALSE	FALSE	FALSE	FALSE	FALSE	TRUE

Figure C-7: Collinearity matrix bare hull simulation of all LE and SX series

Appendix D

Sea Trial Parameters

Table D-1: Parameters measured during each run [3]

	Acceptable measurement devices	Unit
Ship's position	DGPS	Lat., Lon., °
Speed over ground	DGPS (for information purpose only)	knots
Shaft torque or Shaft power	Torsion meter with calibrated torque sensor or strain gauges. Power calculated from torque and propeller shaft speed	kNm kW
Propeller shaft speed	Pick-up, optical sensor, ship's revolutions counter	min^{-1}
Propeller pitch	Bridge replicator, indicator on shaft	°or mm
Time	GPS Time	hh:mm:ss or UTC
Water depth	Ship echo sounder & nautical charts	m
Ship's heading	Gyro compass, or compass- DGPS	°
Relative wind velocity and direction	Ship's anemometer, however if not available, a dedicated trial anemometer	m/s, °
Wave height, period and direction Swell height, period, and direction	Wave measuring device such as wave buoy, wave radar, or lidar. Observation by multiple mariners. The average observed wave height derived from observations by multiple mariners is assumed to be equal to the significant wave height over the run length.	m, s, °
Bow acceleration (STAWAVE- 1)	Acceleration meter	m/s^2
Date	Calendar	yyyy-mm-dd

Table D-2: Parameters measured at the speed trial site [3]

Water density	Salinity sensor, Conductivity Density Temperature (CDT) sensor	kg/m^3
Water temperature	Thermometer, CDT sensor	°C
Air temperature	Thermometer	°C
Air pressure	Barometer	hPa, mb
Torsion meter zero setting	Torsion meter with calibrated torque sensor or strain gauges	kNm
Trial area	Geographical position (Lat-Long) by DGPS	dddd-mm
Vertical position of anemometer	General arrangement plan of the ship	m
Drafts	Physical observation and / or calibrated draft gauges	m

Bibliography

[1] L. Larsson and H. C. Raven, *Principles of Naval Architecture Series - Ship Resistance and Flow*. Society of Naval Architects and Marine Engineers (SNAME), 2010.

[2] J. M. van Dijk, "A computational fluid dynamics based prediction method for full-scale ship resistance and propulsion," p. 50, 2019.

[3] ISO and ITTC, "ISO 15016:2015," Internation Towing Tank Conference, Tech. Rep., 2015.

[4] J. Holtrop and G. G. J. Mennen, "AN APPROXIMATE POWER PREDICTION METHOD," TU Delft, Tech. Rep., 1982.

[5] J. Holtrop, "A statistical re-analysis of resistance and propulsion data," *International Shipbuilding Progress*, vol. 31, pp. 272–276, 1984.

[6] V. Bertram, "Resistance and Propulsion," in *Practical Ship Hydrodynamics*, 2012, ch. 3, pp. 73–141.

[7] H. C. Raven, A. Van Der Ploeg, and A. R. Starke, "TOWARDS A CFD-BASED PREDICTION OF SHIP PERFORMANCE-PROGRESS IN PREDICTING FULL-SCALE RESISTANCE AND SCALE EFFECTS," Instituto Superior Técnico (IST), Portugal, Tech. Rep., 2008.

[8] M. Terziev, T. Tezdogan, and A. Incecik, "A geosim analysis of ship resistance decomposition and scale effects with the aid of CFD," *Applied Ocean Research*, vol. 92, no. March, p. 101930, 2019.

[9] A. M. Castro, P. M. Carrica, and F. Stern, "Full scale self-propulsion computations using discretized propeller for the KRISO container ship KCS," *Computers and Fluids*, vol. 51, no. 1, pp. 35–47, 12 2011.

[10] D. Ponkratov and C. Zegos, "Validation of Ship Scale CFD Self-Propulsion Simulation by the Direct Comparison with Sea Trials Results," *RINA, Royal Institution of Naval Architects - International Conference on Computational and Experimental Marine Hydrodynamics, MARHY 2014*, no. June, pp. 143–150, 2014.

[11] H. Jasak, V. Vukčević, I. Gatin, and I. Lalović, "CFD validation and grid sensitivity studies of full scale ship self propulsion," *International Journal of Naval Architecture and Ocean Engineering*, vol. 11, no. 1, pp. 33–43, 2018.

[12] H. Mikkelsen, M. L. Steffensen, C. Ciortan, and J. H. Walther, "Ship scale validation of CFD model of self-propelled ship," *MARINE 2019 Computational Methods in Marine Engineering VIII*, pp. 718–729, 2019.

[13] K. Niklas and H. Pruszko, "Full-scale CFD simulations for the determination of ship resistance as a rational, alternative method to towing tank experiments," *Ocean Engineering*, vol. 190, no. April, p. 106435, 2019.

[14] W. Sun, Q. Hu, S. Hu, J. Su, J. Xu, J. Wei, and G. Huang, "Numerical analysis of full-scale ship self-propulsion performance with direct comparison to statistical sea trail results," *Journal of Marine Science and Engineering*, vol. 8, no. 1, 2020.

[15] D. Ponkratov, "Proceedings 2016 workshop on ship scale hydrodynamic computer simulation," in *Lloyd's Register*, no. February, 2017, p. 225.

[16] D. Ponkratov and G. D. Struijk, "Jores Jip a Unique Joint Industry Project To Close the Knowledge Gap on Ship Hydrodynamics," *Full Scale Ship Performance*, no. October, 2018.

[17] Damen, "Amels LE." [Online]. Available: https://www.damenyachting.com/portfolio/limited-editions/

[18] ——, "SeaXplorer." [Online]. Available: https://www.damenyachting.com/portfolio/seaxplorer/

[19] Numeca, "FINEMarine-Theory-guide."

[20] MIT, "Performance of Propellers." [Online]. Available: https://web.mit.edu/16.unified/www/FALL/thermodynamics/notes/node86.html

[21] H. Klein Woud and D. Stapersma, *Design of Propulsion and Electric Power Generation Systems*, 2008th ed. IMarEST, 2002.

[22] V. Bertram, "Introduction," in *Practical Ship Hydrodynamics*, 2012, ch. 1, pp. 1–39.

[23] BIPM, "International vocabulary of metrology - Basic and general concepts and associated terms," Bureau International international des Poids et Mesures, Tech. Rep., 2008.

[24] C. Eckert and O. Isaksson, "Safety Margins and Design Margins: A Differentiation between Interconnected Concepts," in *Procedia CIRP*, vol. 60. Elsevier B.V., 2017, pp. 267–272.

[25] ITTC, "1978 ITTC Performance Prediction Method," Internation Towing Tank Conference, Tech. Rep., 1978.

[26] "Accuracy-Precision." [Online]. Available: http://www.antarcticglaciers.org/glacial-geology/dating-glacial-sediments-2/precision-and-accuracy-glacial-geology/

[27] A. Vrijdag, "Estimation of uncertainty in ship performance predictions," *Journal of Marine Engineering and Technology*, vol. 13, no. 3, pp. 45–55, 2014.

[28] F. Dekkiing, C. Kraaikamp, H. Lopuhaä, and L. Meester, *A Modern Introduction to Probability and Statistics*. Springer, 2005.

[29] H. A. Sturges, "The Choice of a Class Interval," *Journal of the American Statistical Association*, vol. 21, no. 153, pp. 65–66, 1926.

[30] G. James, D. Witten, T. Hastie, and R. Tibshirani, *An Introduction to Statistical Learning - with Applications in R*. Springer, 2013.

[31] E. Weisstein, "Statistical Correlation." [Online]. Available: https://mathworld.wolfram.com/StatisticalCorrelation.html

[32] H. van den Boom, H. Huisman, and F. Mennen, "New Guidelines for Speed/Power Trials," *SWZ Maritime*, pp. 1–11, 2013.

[33] E. C. Tupper, "Propulsion," in *Introduction to Naval Architecture*. Elsevier Ltd, 2013, ch. Chapter 8., pp. 161–204. [Online]. Available: http://dx.doi.org/10.1016/B978-0-08-098237-3.00008-4